Developing Peptide-Based Receptors to Study Molecular Recognition in Water

Author: Azade S. Hosseini

Developing Peptide-Based Receptors to Study Molecular Recognition in Water

AZADE S. HOSSEINI

A Dissertation

Submitted to the Faculty of Chemistry

in Partial Fulfillment

of the Requirements for the Degree of

Doctor of Philosophy

Boston College
Morissey College of Arts and Sciences
Graduate School

September 2016

Developing Peptide-Based Receptors to Study Molecular Recognition in Water

Azade S. Hosseini **Professor Jianmin Gao**

September 23rd, 2016 Research Advisor

Abstract

My graduate research career has focused on studying the principles that underlie molecular recognition, which include protein folding, protein-membrane interactions, structural preoranization for target binding and non-covalent interactions. This thesis will present an overview of this work through three different projects.

I) Synthetic receptors for target binding in water

Molecular interactions in water provide the foundation for life. More specifically, the interactions between one or more molecules, through hydrogen bonding, π-effects, hydrophobic interactions and electrostatic interactions, all play a significant role essential to biological processes. This chapter will present an overview of supramolecular chemistry in water, with a focus on small molecule receptor "warheads" that target biomolecules of interest. The discussion will then move towards the ability to preorganize these "warheads" on a scaffold to improve their potency towards a target. The fundamental principles discussed in this section will provide a foundation for the following chapter in this thesis.

II) Understanding Phosphatidylserine Recognition Using the Model cLac Peptide

The plasma membrane serves as a defining feature of the cell membrane, acting as a barrier for material exchange between a cell and its local environment. More importantly, membrane lipids are involved in mediating numerous cell-signaling events and acting as receptors to recruit proteins that carry out a specific function. Due to the important role that lipids play, it is highly desirable to develop affinity ligands for the diverse range of lipid headgroup structures on a cell membrane. Although prevalent, proteins have intrinsic limitations due to their size, low stabilities and slow clearance rates. This chapter will focus on the model peptide, cLac, which was previously developed as an affinity ligand for phosphatidylserine recognition. We will focus on understanding the key properties that contribute to PS selectivity and affinity, then attempt to improve this scaffold through structural preorganization.

III) A prolinomycin-based scaffold for developing functional peptides

Nature has evolved proteins to bind cell-signaling molecules with exquisite affinity and specificity, making molecular recognition an essential part of biology. It has been a highly sought after goal within the chemistry field to be able to mimic the structure and function of certain proteins with smaller molecules, such as peptides. Specifically, cyclic peptides are showing promise as therapeutic agents due to their high proteolytic stabilities, faster clearance rates and ease of synthesis compared to proteins. One challenge, however, is that peptides generally do not possess the ability to properly fold and display their side chains for target binding, as proteins do. In this chapter, I will present a prolinomycin-based scaffold, which can fold in the presence of K^+ ions to preorganize its side chains for target binding. Moreover, the focus will be on the

structural aspects of this cyclic peptide, along with proof-of-concept studies demonstrating its ability to recognize a target under physiological conditions. The findings in this study will be useful in developing peptide-based tools that recognize various targets.

IV) Dissecting the energetic consequences of fluorinating a protein core

Proteins have emerged as a powerful class of therapeutic agents due to their superior properties over small molecules in the clinic. Some of the key advantages include their large surface areas and highly defined structures, which allow them to perform very specific functions that are generally not reproducible with traditional small molecule scaffolds. In addition, proteins possess the ability to properly fold under physiological conditions through precise, noncovalent interactions between their side chain residues. Perhaps the most relevant interactions arise from aromatic side chains, which can interact in a variety of ways to help proteins fold. In this chapter, we will focus on the model protein, VHP35, which contains a hydrophobic core of three interacting Phe residues, to study the effects of fluorination on an edge-face interaction.

Acknowledgements

I want to thank the members of my PhD thesis committee, Professor Mary Roberts, Professor Eranthie Weerapana and Professor Abhishek Chatterjee for carefully reviewing my thesis and providing valuable feedback during this process. I would like to especially thank Professor Mary Roberts for her constant support over the past five years—thank you for the countless conversations and discussions about research and career related decisions.

I am also thankful to my research advisor, Professor Jianmin Gao, for his supervision during my time here at BC. The knowledge and skills I've learned under his guidance will be useful for the rest of my career.

More importantly, I want to thank my parents for their constant love and support throughout my entire life. You have both set and incredible example for me, which helped me to set and achieve goals that I could never imagine in life. I love you both with all of my heart.

To my sister, my best friend—thank you for supporting me and always being there. My friends, especially those I've made during my time at BC—thank you for the great memories and all of the laughter.

Finally, to Sebastian, thank you for your constant love, encouragement and patience. You have been the most supportive person in my life on a daily basis. We have made incredible memories over the past few years and I feel lucky to have you by my side.

Table of Contents

Table of Abbreviations

5-IAF	Fluorescein 5-Iodocacetamide
Bip	Biphenylalanine
cLac	Cyclic lactadherin-mimicking peptide
cLac-wt	Cyclic lactadherin-mimicking peptide via native chemical ligation
CD	Circular Dichroism
Dbz	Diaminobenzoyl
DMF	Dimethylformamide
DMSO	Dimethyl sulfoxide
FITC	Fluorescein isothiocyanate
FRET	Fluorescence Resonance Energy Transfer
GFP	Green Fluorescent Protein
GdmCl	Guanidinium chloride
LysoPS	1-oleoyl-2-hydroxy-sn-glycero-3-phospho-L-serine
MSQ	Macrocyclic squaramide-containing receptor
Nbz	N-acyl-benzimidazolinone
NCL	Native Chemical Ligation
NMR	Nuclear Magnetic Resonance
PC	Phosphatidylcholine
PEG	Polyethylene glycol
PG	Phosphatiylglycerol
POPC	1-palmitoyl-2-oleoyle-sn-glycero-3-phosphocholine
POPS	1-palmitoyl-2-oleoyle-sn-glycero-3-phospho-L-serine

POPG	1-palmitoyl-2-oleoyle-sn-glycero-3-phospohlycerol
PS	Phosphatidylserine
SUV	Small unilamellar vesicle
TCEP	(tris(2-carboxyethyl)phosphine)
TFA	Trifluoroacetic acid
tPro	Thioproline
VHP35	Villin Headpiece

List of Figures

List of Tables

List of Schemes

Chapter 1. Synthetic receptors for target binding in water

1.1 Introduction

Molecular interactions in water provide the foundation for life. More specifically, the interactions between one or more molecules, through hydrogen bonding, π-effects, hydrophobic interactions, van der Waals forces and electrostatic interactions, play a significant role in all essential biological processes. The field of supramolecular chemistry embodies these fundamental principles by focusing on systems that incorporate weak and reversible non-covalent interactions between two or more chemical entities. These types of molecular recognition elements include, but are not limited to, self-assembly, host-guest complexes and folding, all of which are processes that have inspired the synthetic design of functional molecules in water. This chapter will focus on the development of synthetic receptors and molecular scaffolds that can exhibit these fundamental properties in water.

The field of supramolecular chemistry in water has rapidly expanded in recent years due to the need for developing functional molecules that possess activity in biological environments. The main challenges in using water as a reaction medium include competition from the bulk solvent, which renders otherwise strong interactions, such as hydrogen bonding and polar interactions relatively ineffective. Hydrophobic interactions can be used to overcome these drawbacks, but they also present their own unique challenges, since solubility and selectivity are generally not optimal under these conditions.

To overcome these challenges, one must study natural receptors, such as proteins and DNA, which complex other functional molecules through several weak, non-covalent interactions in water. For example, large, three-dimensional molecules, such as proteins, rely on these critical contacts to either maintain their fold, or to selectively recognize a binding partner and perform a specific function. These natural systems have inspired the rational design of synthetic receptors, which seek to mimic the potent and selective binding behaviors of biomolecules that can function through several non-covalent interactions in aqueous medium.

1.2 From chemical warheads to synthetic receptors

This section presents some key examples of small molecule host receptors that can recognize a variety of guest molecules through fundamental molecular interactions, which include hydrogen bonding, electrostatic interactions and covalent chemistry. These synthetic receptors derive from designed chemical "warheads" that recognize a specific functional group that is presented on a biomolecule of interest. In addition to showcasing their unique chemical reactivity of the warheads, I will also demonstrate through specific examples, how one can take advantage of the cooperative display of these chemical "warheads" to gain high specificity and affinity towards a target. The design of such receptors will highlight the integration of a range of interactions to successfully target a guest molecule.

1.2.1 Guanidine-based designs to target carboxylates

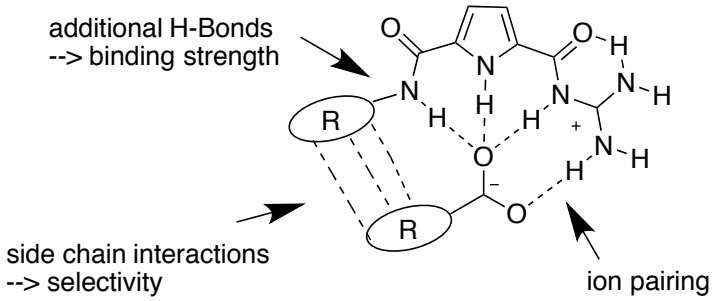

Figure 1-1. Interaction between guanidinocarbonylpyrrole receptor with a guest carboxylate. Figure adopted from reference [1].

In 1999, Schmuck and co-workers introduced a de novo designed carboxylate binding motif, which combines electrostatic interactions with multiple hydrogen bonds to efficiently target carboxylate motifs [1]. Compared to simple guanidinium cations, which can only form stable ion pairs in low dielectric environments, these guanidinocarbonylpyrrole receptors contain highly acidic guanidinium species as a result of the adjacent acyl group on the scaffold, which in combination with the additional hydrogen bonds, help the receptor to form very stable complexes in water (**Figure 1-1**). More specifically, the strong binding to carboxylates in water can be attributed to the pyrrole NH group, which acts as a hydrogen bond donor during complexation. To test this hypothesis, the binding properties of systematically varied receptors were measured by NMR analysis in a 40% water/DMSO mixture to determine association constants (K) with N-acetyl alanyl carboxylate (Ac-L-Ala-O^-) as the substrate [2]. The structures can be found in **Figure 1-2**.

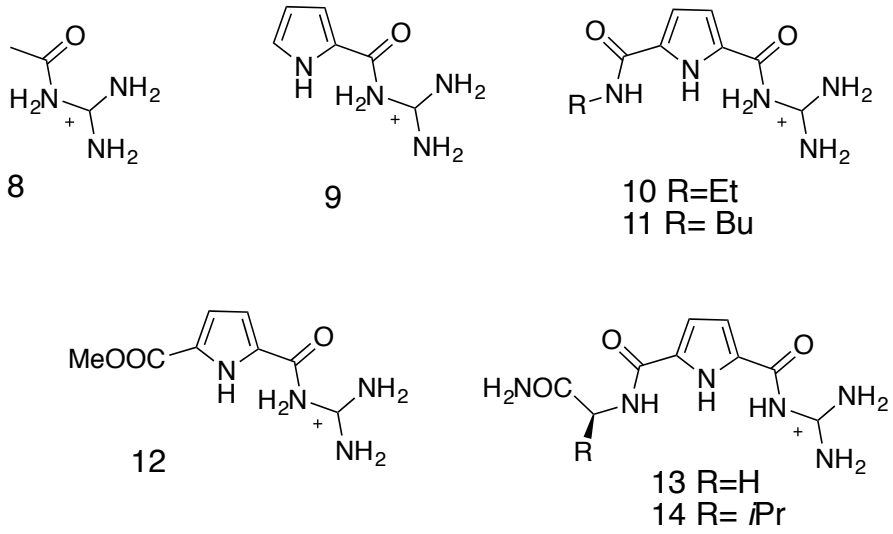

Figure 1-2. Structures of guanidinocarbonylpyrrole receptors with expanded functional groups. Figure adopted from reference [2].

Compared to a simple guanidinium salt, ($K < 10$ mol^{-1}), compound **9** exhibits a K value of 130 mol^{-1} in the presence of Ac-L-Ala-O^{-}. Removal of the pyrrole functional group affords a simple acylguanidinium cation, which displays a three-fold decreases in the K value to 50 mol^{-1}. To further support the benefit of introducing an additional hydrogen bond for carboxylate recognition, receptors **10** and **11**, which both contain an additional amide group adjacent to the pyrrole ring, bind the carboxylate substrate 5 times better than **9** at 770 and 690 mol^{-1}, respectively. Interestingly, the best binder was receptor **14** (1610 mol^{-1}), which contains a highly branched, isopropyl group that may help to induce a favorable receptor conformation. This is supported by the results from the more flexible receptor **13**, which contains a hydrogen atom in lieu of an isopropyl group and displays a weaker association value of 680 mol^{-1}. Collectively, these results demonstrate that a simple binding host guest complex, such as that between a guanidinium group and a carboxylate group, can be engineered into a more powerful

complex in water purely through the introduction of carefully placed hydrogen bond donors and acceptors.

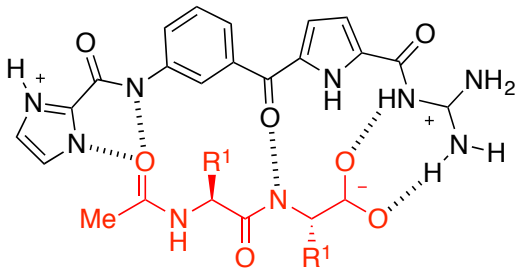

Figure 1-3. Complex between guanidinocarbonylpyrrole and dipeptide. Figure adopted from reference [3].

To further validate the utility of this scaffold, the guanidinocarbonylpyrrole receptors can be further functionalized to acquire selectivity for a specific target (**Figure 1-3**). In this case, the introduction of additional ionizable functional groups helps direct the scaffold to target dipeptides in water [3]. Taking advantage of the good association constants between the pyrrole group of these receptors and carboxylate groups of amino acids, additional hydrogen bond donors from the receptor amide and imidazole groups can further stabilize the peptide backbone, affording association constants between 15,900-54,300 mol^{-1} depending on the dipeptide sequence. The values for dipeptides were nearly 10-fold better than for simple amino acids, indicating that these receptors can be further engineered through the simple addition of hydrogen bonds to target a variety of substrates.

Moving forward with guanidinium-based receptors, Kilburn and co-workers designed an efficient, high-throughput method to identify stereoselective receptors for peptides in water based on an N,N'-dipeptide-substituted guanidinium receptor [4]. Utilizing a "tweezer" scaffold, which incorporates a guanidinium group for site-specific

detection of a peptide C-terminus and two peptidic arms, they were able to screen a library of guanidinium containing receptors on resin using dye-labeled peptide guests in aqueous media.

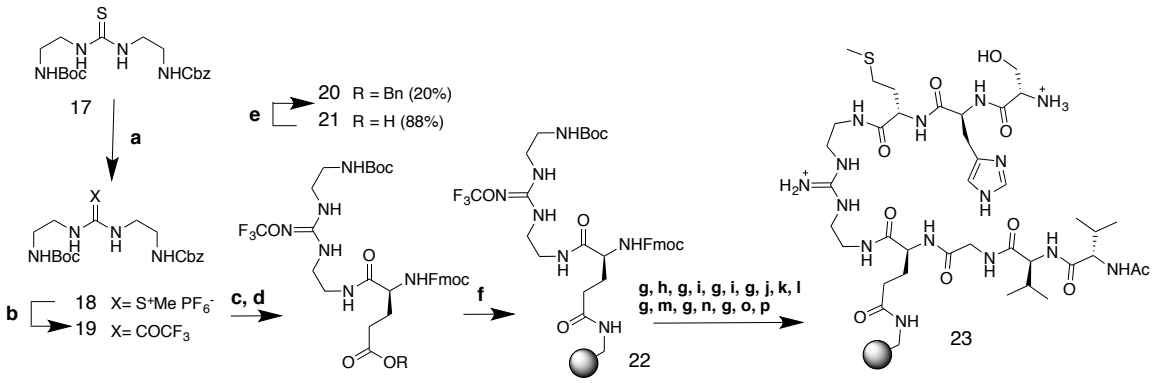

Figure 1-4. Synthesis of asymmetric tweezer library. Figure adopted from reference [5].

The limitation of this approach is in the lack of chemical diversity. Since both peptidic arms must be synthesized simultaneously, the receptors contain two identical sequences. To circumvent this issue, Kilburn and co-workers have developed an orthogonal approach to synthesize chemically diverse guanidinium-containing receptors (**Figure 1-4**) [5]. The guanidinium receptor was functionalized on a solid support, followed by Fmoc-deprotection of the first guanidyl residue, then split-and-mix synthesis to form the first peptidic arm. Removal of a Dppe-protecting group on the second arm, followed by another split-and-mix synthesis yielded chemically diverse, asymmetric receptor libraries. Using this method, they were able to identify a potent and stereoselective receptor with an estimated association constant of 1350 mol^{-1} for the substrate N-Ac-Lys-D-Ala-D-Ala, versus 250 mol^{-1} for N-Ac-Lys-L-Ala-L-Ala.

The examples listed above demonstrate how a simple receptor, such as guanidinium, can be transformed to exhibit powerful host-guest complexation properties in a highly competitive media, such as water.

1.2.2 Squaramides: A versatile and neutral warhead

Squaramides are a unique class of four-membered ring systems that can participate in up to four hydrogen bonds at a time in water. The high affinity for H-bonding is a result of the delocalization of electrons upon target binding, which in turn, enhances the aromaticity of the squaramide. In addition to these properties, the squaramide is a planar molecule, which helps to provide structural rigidity, while the precursor, squarate ester, allows the molecule to be easily functionalized via a number of synthetic methods [6]. Due to the versatility of this molecule in aqueous systems, it can act as a powerful host receptor to bind a number of diverse and biologically relevant targets.

A given aqueous solution contains many counter-ion complexes that can compete with a charged host molecule for target binding. Additionally, the non-directional nature of charged receptors makes them more promiscuous binders in water, leading to undesired off-target effects. In combination with its other properties, the neutrality of a squaramide allows it to bind guest molecules with high affinity and selectivity in water.

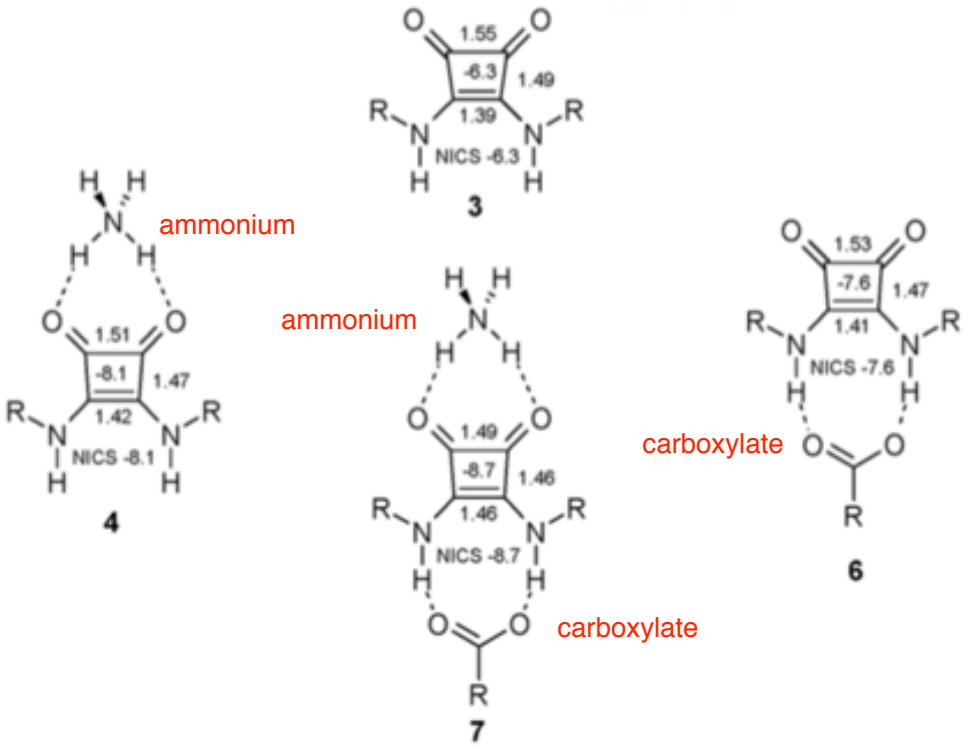

Figure 1-5. Squaramide H-bonding increases ring aromaticity. Figure adopted from reference [6].

Several studies have been conducted in which the anion binding properties of squaramides were assessed [7, 8]. Work by Quinonero and co-workers demonstrated the superiority of squaramides as H-bond donors over other neutral molecules, such as ureas [9]. Upon complexation with either a cation or an anion, the four-membered ring of the squaramide becomes more aromatic, allowing it to act as a bifunctional motif. Researchers referred to nucleus independent chemical shift (NICS) values to study the variable anion binding ability of squaramides, where a more negative NICS value denotes a more aromatic structure (**Figure 1-5**). The results demonstrate that the squaramide-anion complex (-7.6) is more aromatic than just the squaramide alone (-6.3), which explains the enhanced hydrogen bond donor character. If at the same time an ammonium

ion complexes the carbonyl oxygens of the squaramide, the entire complex (-8.7) becomes even more aromatic, denoting the potential for designing a multi-functional "warhead" that can for two simultaneous interactions with a target.

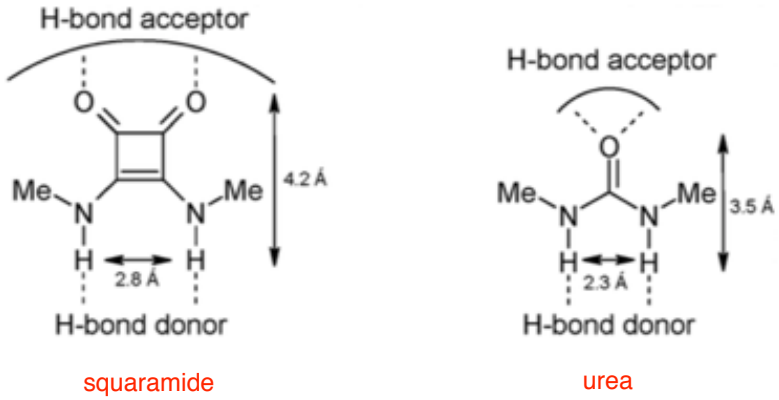

Figure 1-6. Hydrogen bonding donor-acceptor ability of squaramides versus ureas. Figure adopted from reference [6].

From a structural standpoint, the squaramide demonstrates excellent superiority towards guest molecules over other receptors, such as urea, due to the presence of two carbonyl oxygens, which helps it to form stronger acceptor interactions (**Figure 1-6**). Collectively, these favorable properties make squaramides a great candidate for developing artificial receptors of natural biomolecules and following examples will demonstrate the utility of this warhead towards target recognition.

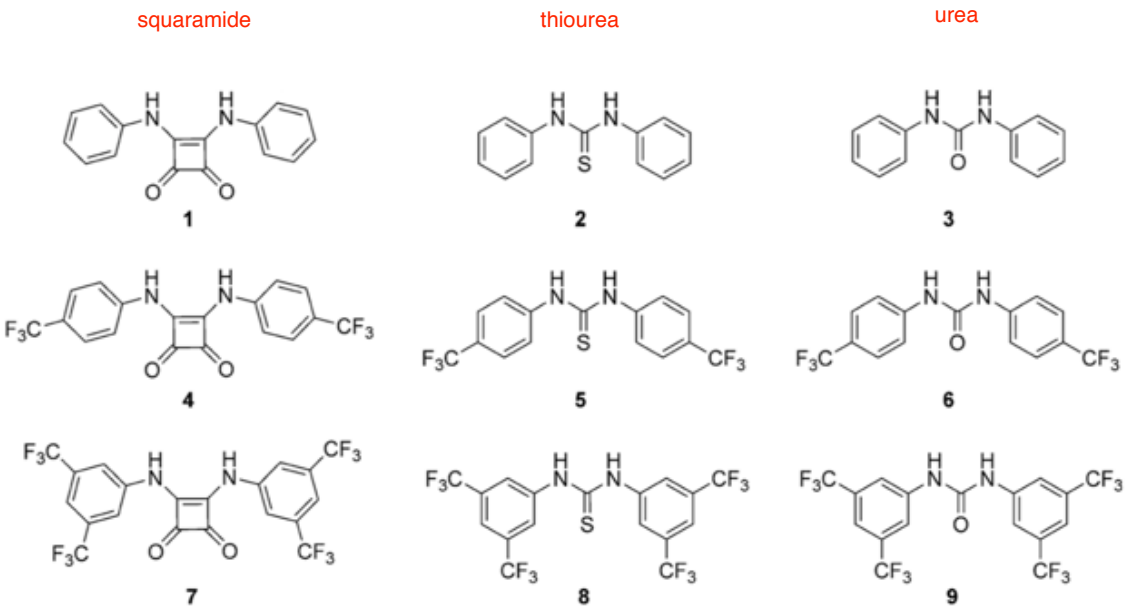

Figure 1-7. Structures of squaramide, thiourea and urea-based fluorinated molecules. Figure adopted from reference [11].

Diseases, such as cystic fibrosis, have triggered an active interest in developing drugs that can transport anions across lipid bilayers. These diseases are usually triggered by a malfunction in the ability of a transmembrane ion channel to regulate the flow of ions such as chloride and carbonate, across a membrane [10]. Therefore, the development of a receptor that can recognize and transport ions across a lipid bilayer, thus restoring their permeability, are of high interest in the biomedical field. Gale and co-workers reported the use of fluorinated squaramide-based receptors to bind and transport anions across a lipid bilayer [11].

Squaramides not only exhibit superior hydrogen bonding capabilities, but they are stable to nucleophilic attack under physiological conditions, which helps to reduce its toxicity, making it a superior drug candidate. Focusing on a carefully designed library of

molecules (**Figure 1-7**), they found that squaramide receptors 1, 4 and 7 (K_a values of 260, 458 and 643 mol^{-1}, respectively) transported chloride anions nearly 1 order of magnitude better than the urea and thiourea counterparts, with the highly fluorinated compounds exhibiting the best transport properties. Enhanced fluorination on the urea and thiourea scaffolds did not significantly enhance the transport properties, indicating that fluorination had a better electronic effect on the squaramide scaffold. Additionally, several studies have shown that squaramide-based compounds are less lipophilic than their urea and thiourea counterparts [12, 13], demonstrating that the transport properties are not simply a result of the hydrophobic nature of the receptor, but rather due to the inherent increase in aromatization upon anion binding.

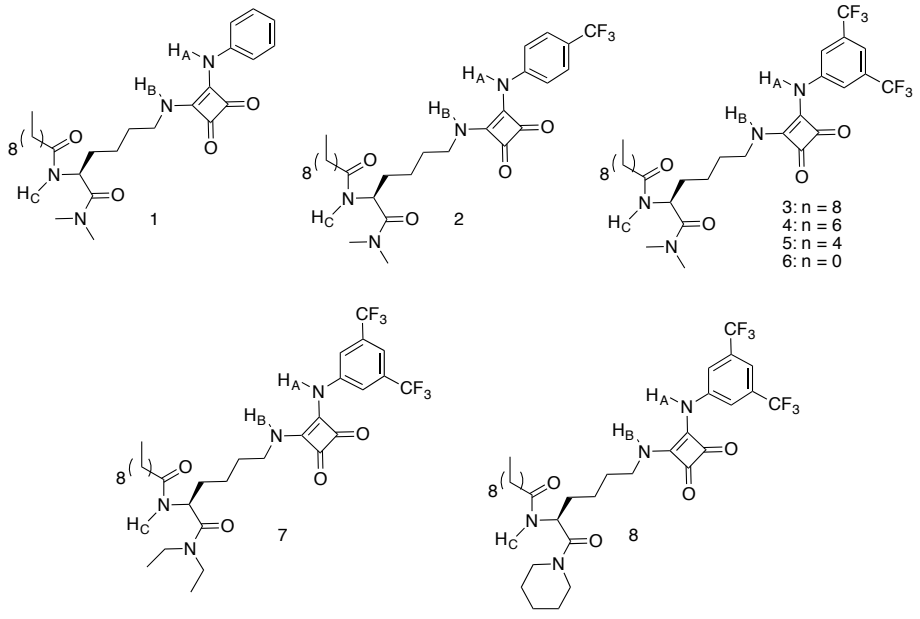

Figure 1-8. Synthesis of squaramide-based amino acids. Figure adopted from reference [14].

Joliffe and co-workers developed a library of squaramide-based amino acid receptors to study the anion complexation properties of squaramide-based amino acids (**Figure 1-8**) using ^{1}H NMR spectroscopy [14]. Any interaction between the squaramide

and anion can be characterized by signature downfield shifts, or the disappearance of amide resonances. Interestingly, a general trend was observed for receptors 1-3, where the squaramide containing the most electron withdrawing properties (3) bound Cl^- the strongest (K_a = 383 M^{-1}), followed by 2 (K_a = 209 M^{-1}) and then 1 (K_a = 180 M^{-1}). Further investigation revealed that receptor 1 selectively binds SO_4^{2-} anions, $K_a > 10^4$ M^{-1}, which may be a result of hydrogen bonding from both the squaramide and the amide NH moieties. Tuning the lipophilicity on either the N or C-terminus of the squaramide-based amino acid receptors had negligible impact on anion binding affinity, indicating that these scaffolds possess functional group tolerance and can be incorporated into larger peptide sequences without losing their intrinsic anion recognition properties.

The previous example demonstrates the ability to target a wide variety of anions in polar solvents by simply tuning the electronic properties of a synthetically designed squaramide-based receptor. The following example will demonstrate how this "warhead" molecule can be further functionalized to acquire selectivity for a specific anion through its pre-organized, multivalent display on a molecular scaffold.

Sulfate plays an important role in biology and selective targeting of this inorganic ion can yield many applications within the biomedical field. Not only does sulfate play an essential role in the formation of proteins in mucin [15] and in joints [16], low levels can be found in patients with rheumatoid arthiritis and irritable bowel disease, making it a prime target for diagnostic applications. The obvious challenge arises in targeting this ion in a highly competitive aqueous media, and oftentimes the incorporation of additional charged groups to sulfate recognition motifs is necessary to overcome the desolvation penalty. However, additional charged residues can compromise the selectivity and

enhance the toxicity, making it an undesirable approach to develop clinical candidates [17]. Nature has developed elegant receptors, such as the sulfate binding protein (SBP), to bind sulfate through a carefully placed network of hydrogen bonds [18]. Using a similar strategy to preorganize a receptor for binding, Joliffe and co-workers reporter a novel class of macrocyclic squaramide-containing receptors (MSQ's) to specifically target sulfate ions (**Figure 1-9**) [19].

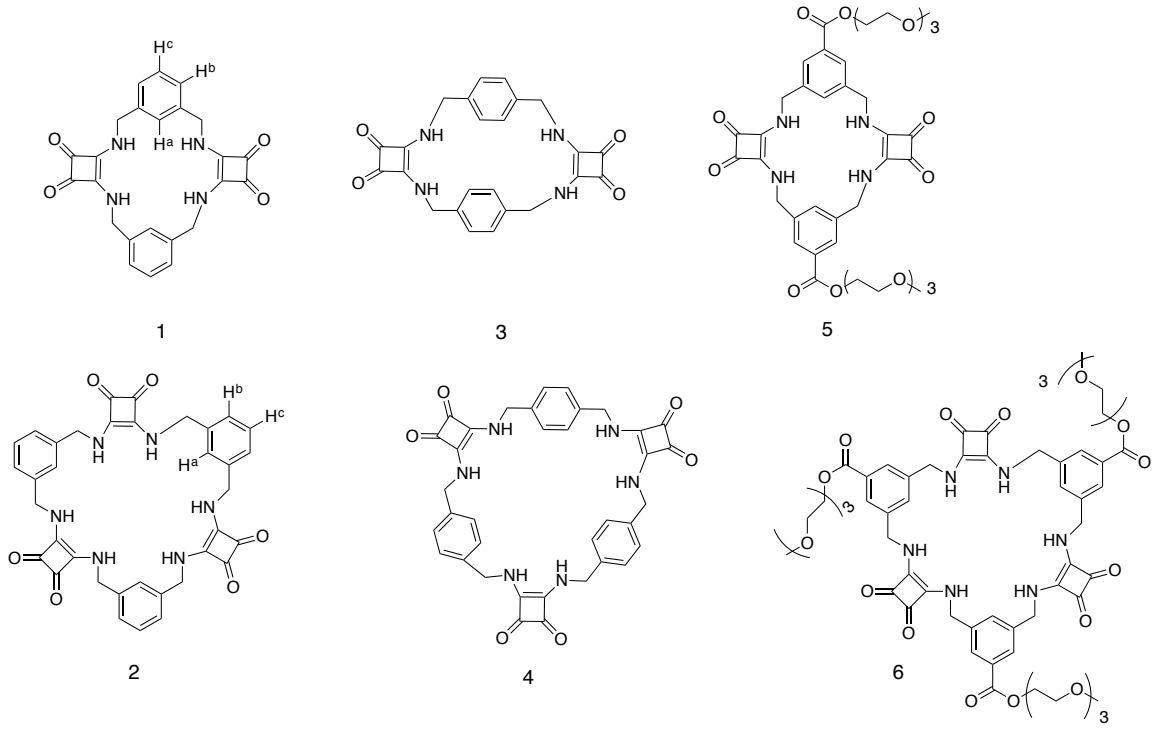

Figure 1-9. Structures of macrocyclic squaramide-containing receptors, showing various ring sizes. Figure adopted from reference [19].

The addition of SO_4^{2-} or $H_2PO_4^-$ to [2]-MSQ 1 in DMSO (0.5% H_2O) caused a distinct change in the ^1H NMR spectrum where the signals corresponding to the amide NHs, as well as the aromatic proton that sits between the two ring substituents, shifted downfield. Interestingly, upon the addition of one equivalent of SO_4^{2-}, the benzylic protons transformed from a broad peak to two very sharp peaks signals, indicating the

presence of two protons in inequivalent environments. The $H_2PO_4^-$ did not elicit a similar response, indicating that [2]-MSQ 1 can fully complex the SO_4^{2-} ion to afford a rigid, single macrocyclic conformer in solution. [3]-MSQ-2, which is a larger macrocycle, also exhibits these characteristic signatures in the ^1H NMR spectrum, but never fully collapses into a single conformer.

To investigate the activities of MSQ-1 and MSQ-2 in a more relevant, aqueous environment, water-soluble triethylene glycol derivatives of MSQ-5 and MSQ-6 were prepared and studied. Interestingly, MSQ-6 displayed remarkable selectivity for SO_4^{2-} anions in the presence of other tetrahedral anions with a K_a value of $>10^4$ mol^{-1}. Molecular modeling revealed that the high binding affinity for a sulfate ion might be a result of the optimal size of the binding cavity, which in conjunction with the additional squaramide binding site and C-H hydrogen bonding motifs, can complex the anion efficiently. Although the NMR signatures indicated a well-defined structure in the presence of the anion, the crystal structure of the MSQ-1 sulfate complex showed that the binding cavity is too small, leaving the sulfate anion sitting on top of the cavity, solvent exposed.

This piece of work demonstrates how a known small molecule anion receptor, such as a squaramide, can be further functionalized to develop larger, more refined host complexes that exhibit superb selectivity's in highly polar, aqueous media.

1.2.3 Boronic acid receptors: covalent targeting of diols

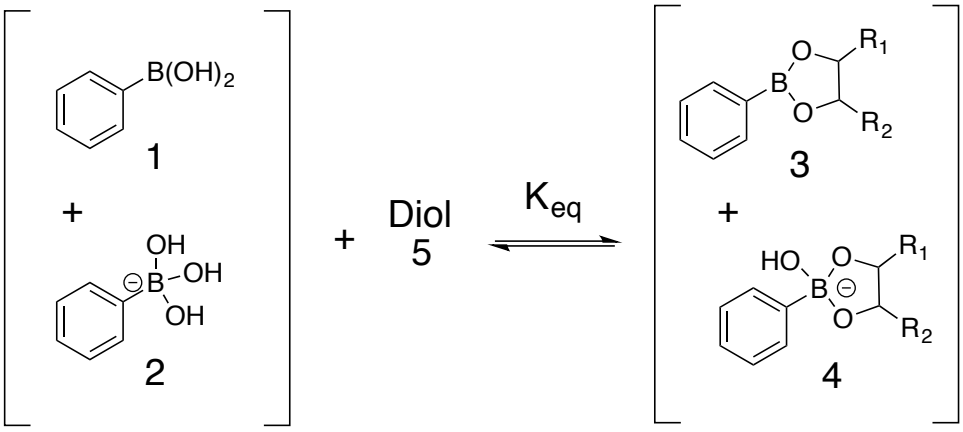

Figure 1-10. Diol-mediated boronate ester formation. Figure adopted from reference [20].

Aromatic boronic acids can reversibly interact with a variety of diols to form boronate esters under physiologically relevant conditions (**Figure 1-10**) [20]. These chemical motifs have been used to target functional groups such as 1,2- and 1,3- diols on saccharides [21, 22], as well as carbohydrates [23, 24] and glycoproteins [25]. Much like the other host receptors presented earlier in this chapter, boronic acid structures are amenable to structural modifications and their properties can be tuned to bind and recognize a specific target. Collectively, these properties make boronic acids attractive candidates in the development of recognition motifs for a wide variety of biologically relevant targets.

One of the major drawbacks in drug design is the difficulty in delivering the therapeutic agent to its target [26]. Some methods have been developed to overcome this issue, which include the use of natural ligands, such as the RGD peptide, and folic acid, to enhance the association of a chemotherapeutic agent with its cellular target [27]. Other

methods include the use of cationic peptides, such as nonarginine and HIV-TAT to accomplish the association with anionic cell surfaces [28].

Raines and co-workers have demonstrated through a series of work, how boronic acid-containing compounds can mediate the delivery of a protein into the cytosol of a mammalian cell [29]. Similar to the case of lectin conjugates [30], they sought to develop boronic acid-containing compounds that could selectively target glycocalyx, which is a cell surface polysaccharide [31], to mediate the delivery of therapeutic agents into the cell. Using bovine pancreatic ribonuclease (RNase A), which is an enzyme that promotes cell death in the cytosol [32, 33], they could assess whether the boronic acid-containing moiety and would be effective in drug delivery by monitoring the cell death.

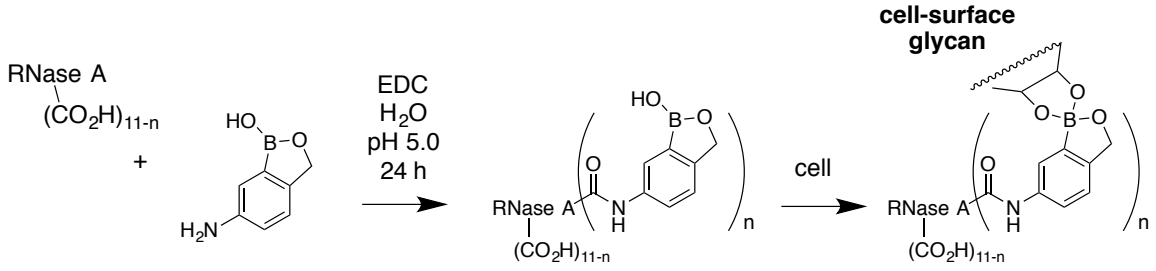

Figure 1-11. Benzoxaborole-mediated cargo delivery into cells. Figure adopted from reference [29].

Quantification of simple boronic acids with various diols revealed a particular affinity towards sialic acid, which is abundant in the glycolax of cancer cells [34], indicating that these receptors could potentially direct therapeutic agents to the site of tumors. Moving forward with 2-Hydroxymethylphenylboronic acid (benzoxaborole), which has the highest reported interaction with pyranose saccharides, also abundant in the glycolax, they conjugated this moiety on to RNase A and observed 4-5 fold enhanced uptake of this complex into the cell versus the unmodified form (**Figure 1-11**).

Specifically, boron-saccharide complexation was confirmed by the addition of fructose, which competes away this interaction. More importantly, boronated RNase A inhibited the proliferation of human erythroleukemia cells, while the chemically inactivated complex was less cytotoxic, indicating that the boronate moiety helps facilitate cellular uptake, as well as enhances the delivery of cargo into the cytosol. Although this example demonstrates the utility of a boronic acid-based receptor to target cell surface diols for potential drug delivery applications, it is still unclear as to how the selectivity will be maintained in a complex, in vivo environment.

To acquire this desired selectivity, one must take advantage of the other unique functional groups that may be present on a guest molecule. Moving beyond host-guest complex formation of boronic acids with cell surface diols, we turn to other biologically relevant guest molecules, such as neurotransmitters. Catecholamines, such as dopamine, are a major class of neurotransmitters and their malfunction in central nervous system and can have negative implications in neurological diseases [35]. There has been much interest in developing specific receptors for dopamine to study its role in disease and many recognition elements have been developed to function in an aqueous environment. Among them include the use of RNA aptamers [36], as well as membrane-association receptors [37].

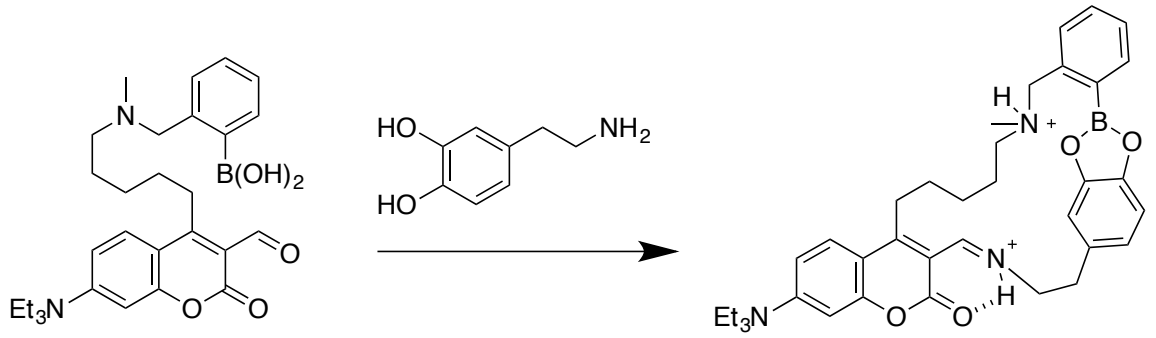

Figure 1-12. Selective recognition of catcheolamines via boronic acid-mediate imine formation. Figure adopted from reference [38].

Glass and co-workers reported in the development of a small molecule, boronic acid-based coumarin receptor to target and sense catechols under physiological conditions [38]. The aldehyde-containing scaffold exhibits an intrinsic affinity for amines; however, little selectivity is observed between various guest amines. To circumvent this problem, they installed a boronic acid to act as an additional recognition motif for the catechol group (**Figure 1-12**). Interestingly, the receptor bound dopamine, norepinephrine and epinephrine with similar association constants of 3400, 6500 and 5000 mol^{-1}, respectively. The lack of a primary amine on epinephrine indicates that the boronic acid-diol complex is a more significant driving force for complex formation than imine formation. As a colorimetric sensor, the compound demonstrated superb selectivity for dopamine and norepinephrine in the presence of other guest ligands. This example illustrates how the cooperative nature of several "warheads" can yield potent and selective receptors for biomolecules of interest.

1.3 Scaffolds

Thus far, we have discussed the properties of a variety of small molecule, synthetic receptors that can target a wide variety of guest molecules in an aqueous environment. Host-guest complexation proceeds through the intrinsic chemical functionality of the receptor, which helps to bind a target with high affinity and selectivity. Although some examples attempted to provide a structural basis for their recognition properties, the molecules were not designed to preorganize the chemical functionalities for binding.

Nature has elegantly evolved a diverse class of macromolecular receptors that adopt structurally preogranized conformations in water. The underlying cause of preorganization is the result of molecular interactions that occur either within the scaffold itself, or in the presence of a guest, such as a metal ion. The following examples provide an overview of the critical molecular recognition elements involved in the design of potent scaffolds with biological activity.

1.3.1 Vancomycin

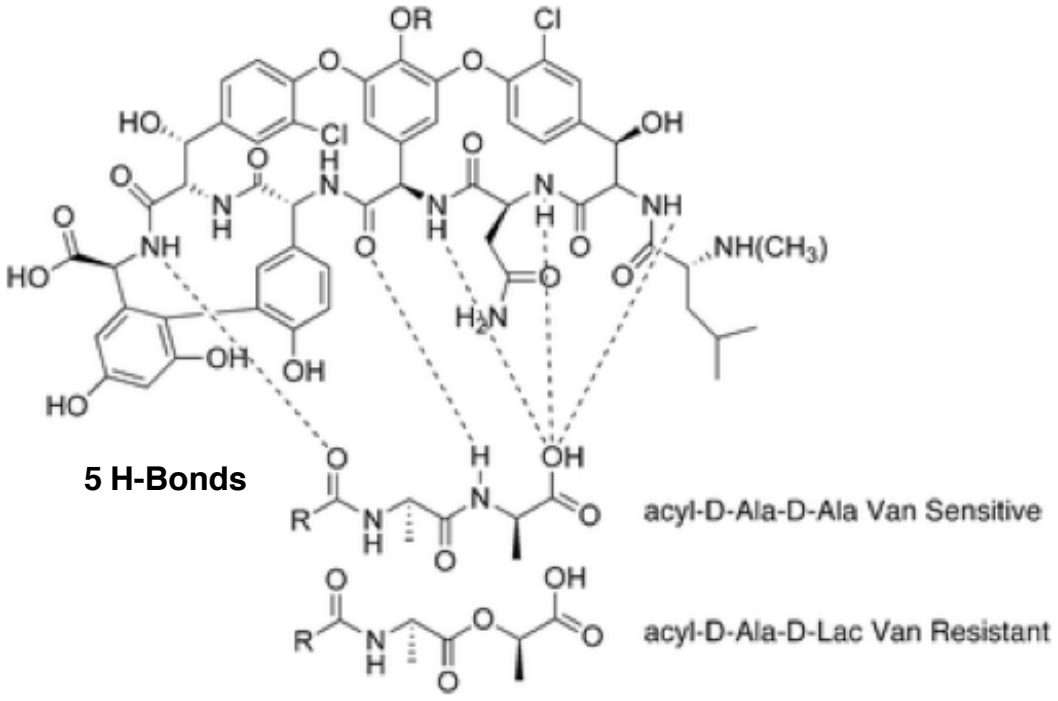

Figure 1-13. Vancomycin and D-Ala-D-Ala complex. Figure adopted from reference [39].

Vancomycin is a glycopeptide antibiotic that is generally used as a last line of defense against Gram-positive strains of bacteria, such as *Staphylococcus aureus*, which has developed highly resistant strains. It selectively recognizes the Ac-D-Ala-D-Ala terminus of the peptidoglycan component of the bacterial cell wall through a series of five, carefully preorganized, hydrogen bonds from its peptide backbone (**Figure 1-13**) [39]. Extensive structural studies were carried out to determine that vancomycin adopts a dimeric conformation in solution, providing two binding pockets into which the branched D-Ala-D-Ala side chains of the peptidoglycan wall can dock. This conformational analysis suggests that vancomycin inserts itself between different glycopeptide strands, thereby preventing their efficient crosslinking in the cell wall [40]. Although vancomycin

can selectively target these components of the cell wall, resistant strains of bacteria have emerged, in which an isosteric replacement of the D-Ala to a D-Lactate renders a hydrogen bonding interaction between the host-guest complex inert.

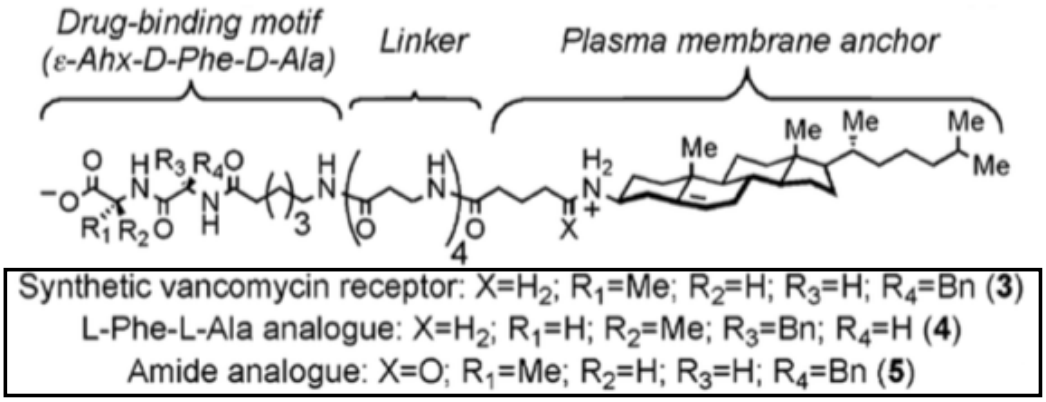

Figure 1-14. Intracellular delivery of vancomycin through native host-guest complex. Figure adopted from reference [41].

Additional drawbacks associated with highly polar glycopeptide antibiotics, such as vancomycin, include their low cell permeability, which renders them ineffective towards bacterial pathogens that are capable of replicating in mammalian host cells or in organs that are protected by a membrane barrier, such as the brain. Peterson and co-workers developed a receptor-mediated delivery strategy to circumvent this problem and to promote the efficacy of this drug in more difficult to access targets [41]. They used a synthetic derivative of the natural vancomycin ligand, called D-Phe-D-Ala, linked to a cholesterol-derived membrane anchor, in order to access the membrane trafficking pathway (**Figure 1-14**). Upon incorporation of the D-Phe-D-Ala-cholesterol complex into the mammalian cell membrane, vancomycin selectively targets this receptor, and becomes incorporated into endosomes where it is either degraded, or escapes into the cytoplasm to access the host-infected pathogens. Interestingly, the ability of D-Phe-D-Ala

to deliver vancomycin into HeLa cells infected by *L. monocytogenes* proved to be successful, while the isosteric L-Phe-L-Ala analogue was inert. Although resistant strains of bacteria have emerged against vancomycin, rendering it inert in certain cases, this work demonstrates how the molecular recognition properties of the antibiotic host-guest complex can be exploited to develop novel methods of drug delivery.

1.3.2 Lantibiotics (cinnamycin and duramycin)

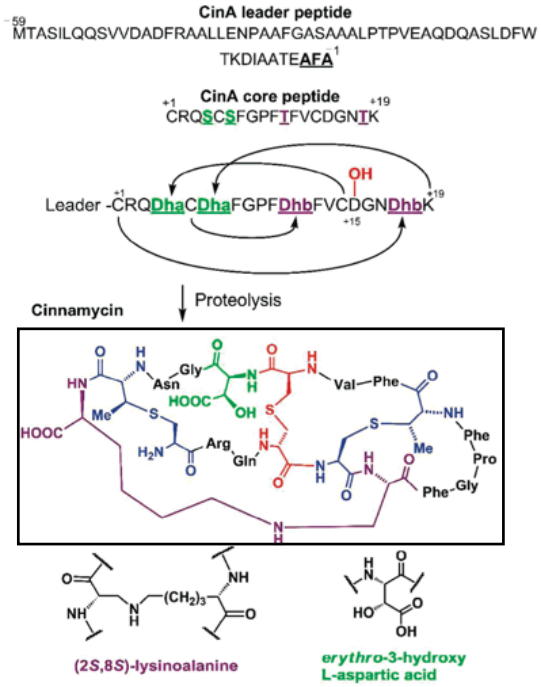

Figure 1-15. Structure and sequence of cinnamycin exhibiting high degree of crosslinking. Figure adopted from reference [42].

Cinnamycin is a highly crosslinked, tetracyclic peptide antibiotic that selectively targets phosphatidylethanolamine (PE) with nanomolar affinity on bacterial cell membranes. This 19 amino acid long sequence contains one lanthionine (Lan), two methyllanthionine (MeLan), and a lysinoalanine (Lal) crosslink, which help the peptide

adopt its rigid conformation [42]. In addition, cinnamycin contains an erythro-3-hydroxy-L-aspartic acid, which results from the hydroxylation of L-Asp at position 15. This critical residue is responsible for the peptides selective interaction with the ammonium functional group of PE (**Figure 1-15**). The well-established interaction between this peptide and PE makes is an ideal candidate for studying membrane interactions.

Its structural analogue, duramycin, differs only in that it contains a Lys instead of an Arg residue within its sequence, but both peptides exhibit considerable cytotoxicity at low micromolar concentrations in mammalian cells, which complicate the ability to study membranes. Zhao and co-workers recently reported the development of a molecular probe based on duramycin, which attaches a green fluorescent protein (GFP) to the C-terminus of duramycin using a PEG linker and found that it induced little cytotoxicity, while still retaining its PE specificity [43] . Cell imaging studies revealed that PE remains sequestered in the inner leaflet of the plasma membrane, while in apoptotic cells the asymmetric distribution is lost. Previous work using biotinylated cinnamycin and FITC-conjugated streptavidin demonstrated that the phospholipid membrane at the apical area of sperm becomes more fluid during fertilization, which results in the translocation of PE and PS occurs to the outer leaflet. GFP-duramycin also yielded consistent results, demonstrating how this novel probe can be used to study the kinetics of membrane reorganization in reproductive biology.

The ability to use lower concentrations of duramycin helps to elucidate more mechanistic insights into the peptide-membrane interaction. Using artificial membranes, they were able to show that low micromolar concentrations of duramycin can destabilize membranes and induce vesicle fusion in the presence of PE, suggesting that peptide-

membrane interaction is required to induce cytotoxic effects. Overall, this study demonstrates how a highly structured receptor, such as cinnamycin or duramycin, can be used as an efficient imaging probe to study the mechanisms of PE in the cell membrane. This powerful host-guest complex can be further implemented in more biologically relevant conditions to further understand the interaction between antibiotics and cell membranes.

1.3.3 Cucurbit[n]uril

The previous examples illustrate how nature has elegantly designed natural receptors to bind a specific target through the structural preorganization of otherwise simple amino acids. From a purely synthetic standpoint, these structures are quite difficult to access, but the following example attempts to demonstrate the potential of designing preorganized receptors for target binding.

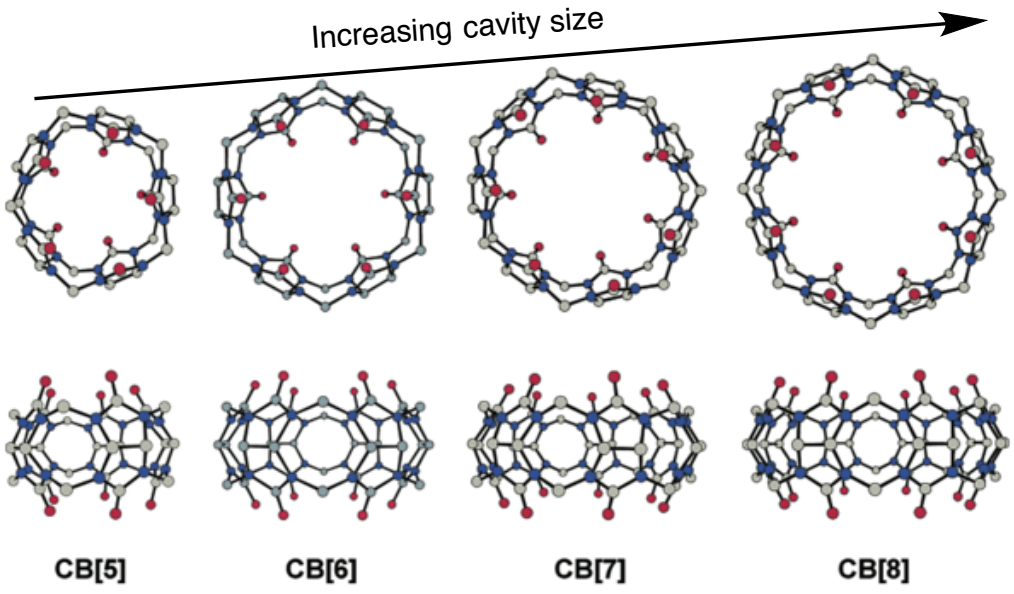

Figure 1-16. Stuctures of cucurbut[n]uril derivatives. Figure adopted from reference [47].

Cucurbit[n]urils are macrocyclic compounds made up of glycoluril monomers that are linked through methylene groups, where n denotes the number of glycoluril units (**Figure 1-16**). Although first synthesized in 1905 by Behrand [44], the structure was not elucidated until 1981 [45, 46] and since then, cucurbiturils possessing 5, 6, 7, 8, 10 and 14 repeating units have all been isolated[46, 47]. The carbonyl oxygens that line the rim of the cavity point slightly inward and promote a unique architecture for molecular recognition of cationic or neutral species. Additionally, the molecular recognition properties can be fine-tuned with the size of the cavity, allowing it to encapsulate guest molecules of various sizes [47]. For example, cucurbit[5]uril, can selectively encapsulate Pb^{2+} over other metals, such as NH_4^+ and other alkali and alkali-earth cations ($>10^{5.5}$) [48], while its slightly larger counterpart, cucurit[6]uril, can form stable complexes with more diverse guests, such as, diaminoalkanes. In the latter case, the inclusion of a non-polar methylene unit within the host cavity is the result of a hydrophobic effect, which seeks the release of "high-entropy" water to accommodate this guest molecule.

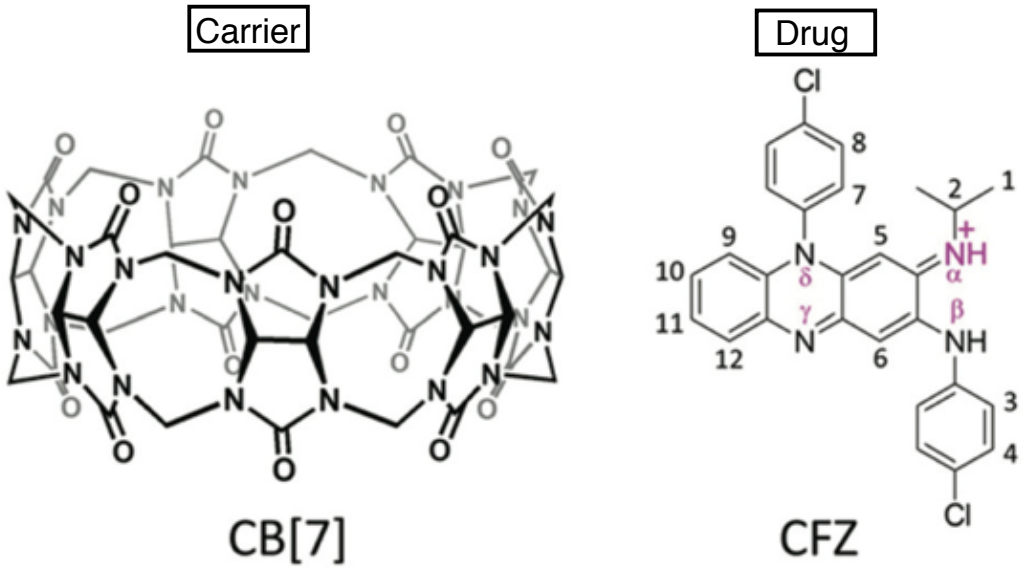

Figure 1-17. Cucurbit[7]uril and clofazimine structures. Figure adopted from reference [49].

Cucurbit[7]uril is perhaps the most applicable scaffold in drug design due its superior water solubility, as well as the unique size of its cavity, which can accommodate larger guest molecules, such as drugs. Wang and co-workers recently investigated the ability of cucurbit[7]uril (CB7) to encapsulate a model anti-tuberculosis drug, clofazimine (CFZ), which exhibits poor water solubility and high lipophilicity, lending to its poor bioavailability **(Figure 1-17)** [49]. In this study, researchers studied its influence on CFZ solubility, cardiotoxicity and antimyobacterial activity. Although CFZ exhibits poor water solubility, using ^{1}H NMR spectroscopy, they were able to observe the host-guest protons upon the gradual addition of CB7 to the solution, indicating that CFZ becomes solubilized in the presence of this scaffold. Further, a phase solubility diagram exhibited a linear increase in guest solubility upon addition of a host, indicating a 1:1 binding mode between the complex.

To analyze the efficacy of CB7 on cardio toxicity in vivo, researchers incubated a transgenic zebrafish model with toxic concentrations of CFZ and observed cardiac functions. Upon the addition of CB7, cardiac functions were significantly improved, while the CB7 alone control displayed negligible effects. Additionally, CB7 had little effect on the antimycobacterial activity of CFZ in vitro, as demonstrated by a minimal inhibitory concentration (MIC) assay, indicating that drug efficacy is well preserved in the presence of this scaffold. Overall, this study exemplifies how one can take advantage of the host properties of a well-defined scaffold to bind and solubilize a lipophilic drug, thereby enhancing its bioavailability.

1.3 Conclusion

In summary, the examples above demonstrate how the development of supramolecular chemistry relies on advances in receptor selectivity for the chemical recognition of a guest molecule, as well as the structural preorganization to display these "warheads" for target recognition. In the following chapters, I will attempt to illustrate these concepts through several projects. Chapter 2 will focus on a detailed mechanistic investigation of the cyclic peptide scaffold, cLac, towards phosphatidylserine (PS) recognition. In this work, we seek to understand the specific contribution of each receptor functional group towards target recognition and attempt to design a structural analogue that can better preorganize them for target binding. Chapter 3 moves further into the structural preorganization aspect, where we introduce a novel, prolinomycin-based scaffold that can fold in the presence of a monovalent cation to preorganize its side chains for target binding. Finally, chapter 4 focuses on the more fundamental aspects of molecular recognition, where we investigate the contribution of fluoroaromatics towards

enhancing or destabilizing a protein fold using the model protein, villin headpiece, VHP35.

Chapter 2. Understanding Phosphatidylserine Recognition Using the Model cLac Peptide

2.1 Introduction

The plasma membrane serves as a defining feature of a living cell, acting as a barrier for material exchange between a cell and its local environment. More importantly, membrane lipids are involved in mediating numerous cell-signaling events, playing active roles as receptors to recruit relevant proteins for cellular processes [50]. Mass spectrometry analysis of the lipidome suggests that there are over 1000 distinct lipid molecules on a mammalian cell membrane [51]. Combined with the important roles that they play, it is highly desirable to develop affinity ligands for the diverse range of lipids headgroups on a membrane.

2.1.1 Phosphatidylserine exposure during apoptosis

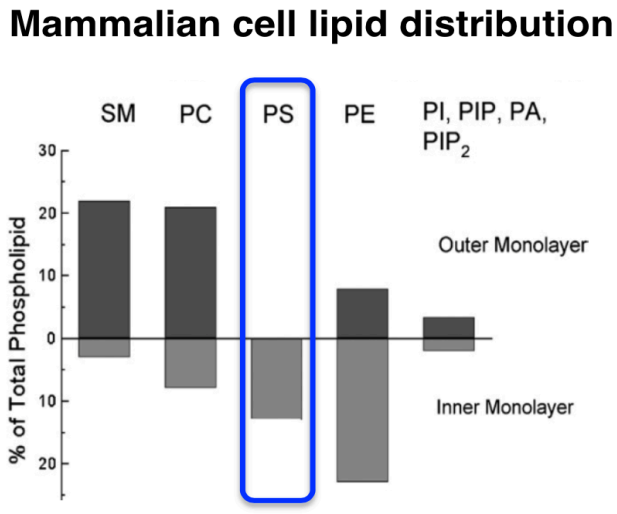

Figure 2-1. Asymmetric distribution of phospholipids on a mammalian cell membrane. Figure adopted from reference [52].

The normal distribution of phospholipids on a cell membrane is asymmetrical. The choline containing lipids, such as phosphatidylcholine (PC) and sphingomyelin (SM) make up the bulk of the matrix and are present on the outer face of the membrane, while the aminophospholipids, such as phosphatidylserine (PS) and phosphatidylethanolamine (PE) reside on the inner leaflet (**Figure 2-1**). PS is unique in that is becomes externalized to the outer leaflet of cells undergoing apoptosis, thus, this lipid has become a universal marker for apoptosis [52]. Proteins, such as aminophospholipid translocase, are responsible for transferring PS and PE to the inner leaflet of the membrane to ultimately retain the asymmetric distribution of lipids on the cell [53-55]. During apoptosis, however, the protein becomes deactivated by the presence of excess Ca^{2+} thereby disrupting this process and causing a rift in cell homeostasis [55, 56]. Scramblase, an ATP-independent protein, becomes activated by the presence of Ca^{2+} to help actively translocate PS and PE lipid molecules across the membrane, suggesting that PS exposure is not merely a passive process [57, 58]. Based on several studies, PS exposure during apoptosis can be attributed to two factors, the first being the result of impaired translocase activity, while the second is a result of scramblase activation [57].

To be able to detect and quantify the amount of apoptotic cells in patients would be extremely beneficial as a biomedical application in the clinic. For example, high levels of apoptosis have been associated with several neurological disorders, including Alzheimer's, Parkinson's and Huntington's disease [59]. Conversely, the inhibition of apoptosis can lead to excessive cellular proliferation, which is associated with tumor growth [60]. The direct recognition and subsequent imaging of PS exposure would not only be beneficial for the early detection of disease, but it would also offer a non-invasive

approach to monitor the course of treatments that act mainly through induction of apoptosis, such as chemotherapy.

2.1.2 Proteins that target phosphatidylserine

There are several natural receptor proteins that target PS, but perhaps the most commonly studied is annexin V, which is a 36 kDa peripheral membrane protein used in the clinic to target and bind apoptotic cells. Annexin family proteins generally reside in intracellular compartments, but can sometimes be found in the blood, leading to its additional properties as anticoagulant agents [61]. It's main function is to bind phospholipids and help recruit macrophages to clear apoptotic cells out of the system [62]. The fluorescent and radioactive labeled forms of annexin V have been used to image cell death both in vitro [63], as well in animal models and humans [64, 65]. Although it is the most common method for imaging apoptotic cells, there are several drawbacks, including the fact that it requires a Ca^{2+} cofactor, making it difficult to quantify apoptotic cells in the clinic. In addition, this large protein exhibits slow clearance rates, high costs of production and is difficult to synthesize and modify [66, 67]. Alternatively, lactadherin is a 47kDa protein found in milk secreted by mammary epithelial cells [68] that can also recognize surface exposed PS to help mediate phagocytosis of apoptotic cells [69]. Interestingly, this protein stereoselectively binds PS with high affinities, but unlike annexin V, does not require a metal co-factor for binding [70]. Lactadherin is emerging as a popular alternative to annexin V, with fluorescently labeled derivatives being used to detect PS on cultured cancer cells [71, 72] and on stored

platelets [73]. Several studies have been done to investigate the structure of lactadherin, including x-ray crystallography and computational analysis [74, 75].

2.1.3 Design of cLac peptide based on computational modeling of lactadherin C2 domain

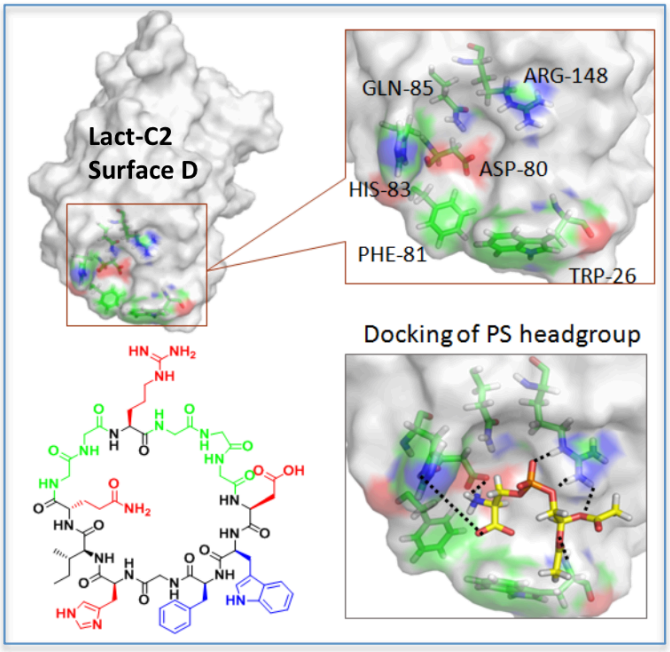

Figure 2-2. Computational docking experiments showing diacetyl PS docked to surface D of lactadherin and the initial design of cLac based on the structure, PDB: 3BN6. Figure adopted from reference [76].

The crystal structure of the lactadherin C2 (Lact-C2) domain shows a beta-barrel core with three loops that protrude from one end of the structure. Earlier work in our group demonstrated that a rationally designed cyclic peptide that mimics the PS-binding surface of lactadherin binds apoptotic cells with good selectivity and affinity [76]. The initial cyclic lactadherin scaffold, called cLac, was developed using computational docking experiments, where a short chain homologue of PC and PS was docked onto two

separate surfaces of the C2 domain, Surface C and Surface D, to determine the most favorable surface for binding (**Figure 2-2**). It was determined that loop 3 and surface D showed the most favorable binding free energy for the short-chain diacteyl PS. A closer look at surface D revealed several key residues displayed in a circular arrangement to engage the PS headgroup. The initial cLac design sought to mimic this structural feature by linking the same residues through peptide cyclization. More specifically, the hydrophobic Phe81 and Trp26 residues act as a membrane insertion motif, while the more polar residues, Asp80, His83, Gln95, and Arg148 interact in a selective manner with the PS head group.

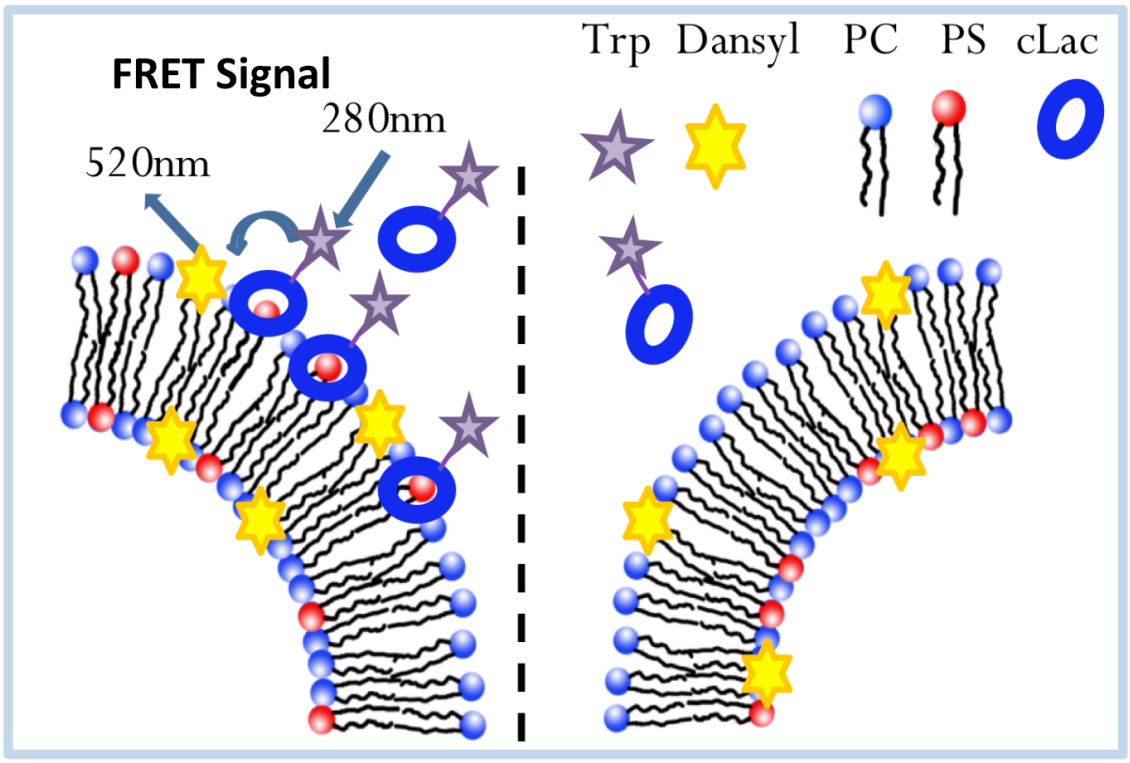

Figure 2-3. Cartoon illustrating the binding event that results in FRET between the Trp donor and dansyl acceptor FRET pairs.

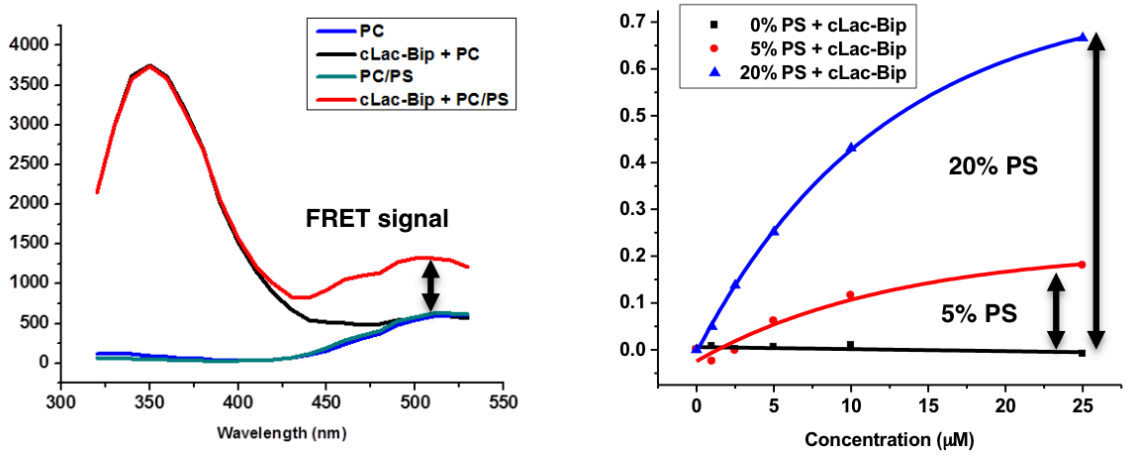

Figure 2-4. FRET assay demonstrating the dansyl emission increase of cLac-Bip in the presence of PS-containing vesicles (left) and a binding curve generated by plotting the normalized emission increase against increasing peptide concentrations (right). Figure adopted from reference [76] .

The design of this peptide scaffold began by constructing the hydrophobic membrane insertion motif with adjacent Phe and Trp residues, while the computational docking model revealed that an Arg projects away from the Lact-C2 domain, making it an important residue for docking the PS headgroup. Two glycine-containing regions, linker I to connect Gln and Arg, and linker II to connect Arg and Asp were important in the rational design of the molecule. Structure activity relationship studies using FRET analysis (**Figure 2-3**) revealed that varying the number of Gly residues on linker II had an effect on PS binding, while linker I manipulation showed little change in activity. The importance of linker II length is directly related to the critical distance between the Arg and Asp residues, which are specifically important for PS headgroup recognition. Lastly, the Ile residue projects away from the protein-PS interface, making it an ideal position for

functionalization or incorporation of a fluorophore for imaging studies. Additionally, a Phe to Biphenyl (Bip) mutation was required for cLac to partition into PS-containing vesicles, as the original sequences were relatively inert under those conditions (**Figure 2-4**). All of these components, in addition to the structure activity relationship studies, were critical in the rational design of the cLac peptide.

2.2 Design of cyclic peptides to test PS recognition

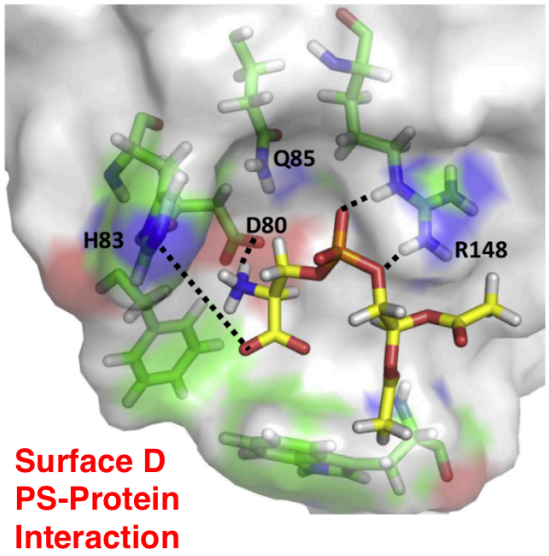

Figure 2-4. Computational docking model of Lact-C2 surface D and diacetyl PS, PDB: 3BN6. Figure adopted from reference [76].

In an effort to further understand the contribution each residue on cLac makes in targeting PS, we carried out an alanine scan where we selectively mutated specific residues to an Ala, then characterized their activities in the presence of PS-containing vesicles (**Figure 2-5**). Before proceeding with this structure activity relationship study, however, we sought to establish a robust and efficient synthetic protocol that would allow us to access a large library of cyclic peptides.

2.2.1 Development of novel intramolecular native chemical ligation reaction

Previous reports demonstrated the use of a side-chain immobilized Asp residue on resin to access the cyclic peptide [76-78]. Using this protocol, the linear sequence can be built on the Wang-Asp-OAll resin, followed by an orthogonal alloc deprotection of the main chain Asp to expose the free acid, which can then be activated by HBTU and coupled to the N-terminal residue to yield the cyclic peptide in decent yields. Due to the harsh coupling conditions, however, the reaction yields side products, including peptide dimers, as well as chain epimerization. As an alternative, we proposed the use of an intramolecular native chemical ligation protocol to accomplish the peptide cyclization [79]. In the field of cyclic peptide synthesis, Benkovic and co-workers demonstrated how cyclic peptides could be generated in bacterial cells using intein-mediated formation of thioesters [80], while Kritzer and co-workers adopted a similar strategy in yeast cells [81]

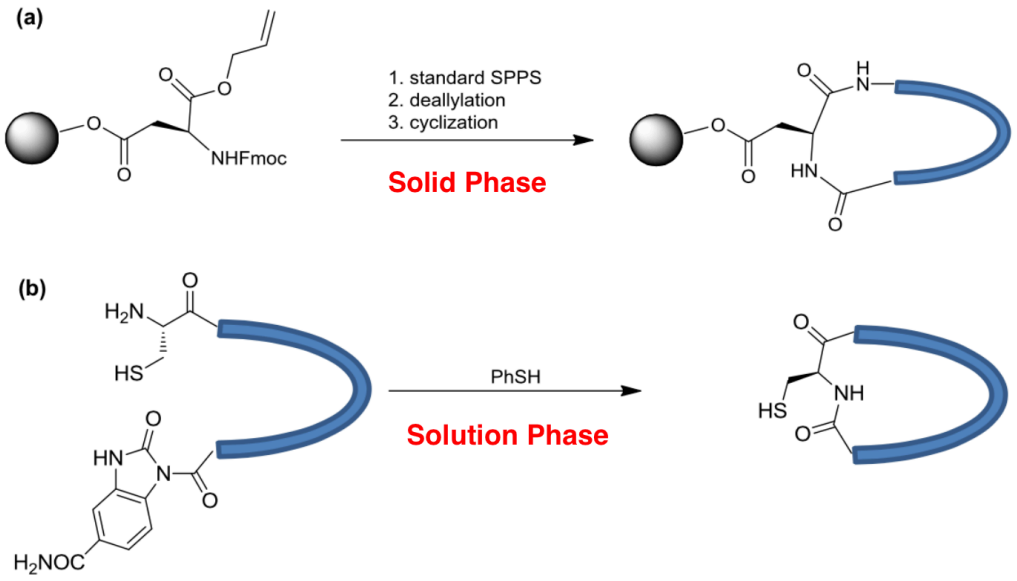

Figure 2-5. Chemical ligation strategies to access cyclic peptides. (a) Standard head-to-tail cyclization via side chain immobilized Asp residue and N-terminal amino acid using orthogonal protecting group to accomplish the cyclization. (b) Intramolecular native chemical ligation protocol accomplished using the Dawson Nbz resin via C-terminal thioester and N-terminal cysteine residue. Figure adopted from reference [79].

The adopted protocol uses the Dawson Dbz resin to build the linear peptide sequence on resin, followed by the incorporation of a main chain Boc protected cysteine residue to avoid modification at the N-terminus [82]. At the end of the linear peptide synthesis, the resin is treated with 4-nitrophenylchloroformate to convert the Dbz group into a more labile Nbz moiety for the ligation reaction. Upon global deprotection and cleavage from the resin, the peptide is subjected to a ligation buffer that contains an excess amount of the exogenous thiol catalyst, either thiophenol or 4-mercaptophenylacetic acid. During this step, the Nbz moiety is converted to a reactive thioester, which rapidly undergoes thiol exchange with the N-terminal cysteine residue, followed by an S to N acyl shift to form the amide bond of the cyclic peptide in good

yields. One benefit of this reaction is that the thiol can be used as a labeling handle for commercially available fluorophores.

Table 2-1. Mass spectrometry data of cyclic peptide library via NCL

Peptide	Calculated molecular weight	Molecular weight found in mass spectometry
cLac-wt	1448 Da	1448 Da
cLac-R/A	1363 Da	1362 Da
cLac-D/A	1404 Da	1403 Da
cLac-H/A	1383 Da	1382 Da
cLac-Q/A	1391 Da	1391 Da
cLac-H/K	1439 Da	1439 Da
cLac-Q,H/K	1439 Da	1439 Da
(L,L)-DiCys	1438 Da	1438 Da
(L,D)-DiCys	1438 Da	1438 Da

We chose to install a Cys residue for the ligation in linker I region of the original cLac peptide sequence, which was shown to better tolerate variations than linker region II. Following this modification, we synthesized a library of cLac peptides in which each of the PS-binding residues is selectively mutated to an Ala. For the convenience of discussion, the Gly to Cys variant is referred to as cLac-wt, while all other peptides are called cLac-X/A.

2.2.2 Alanine scan of cLac to test PS bnding via FRET

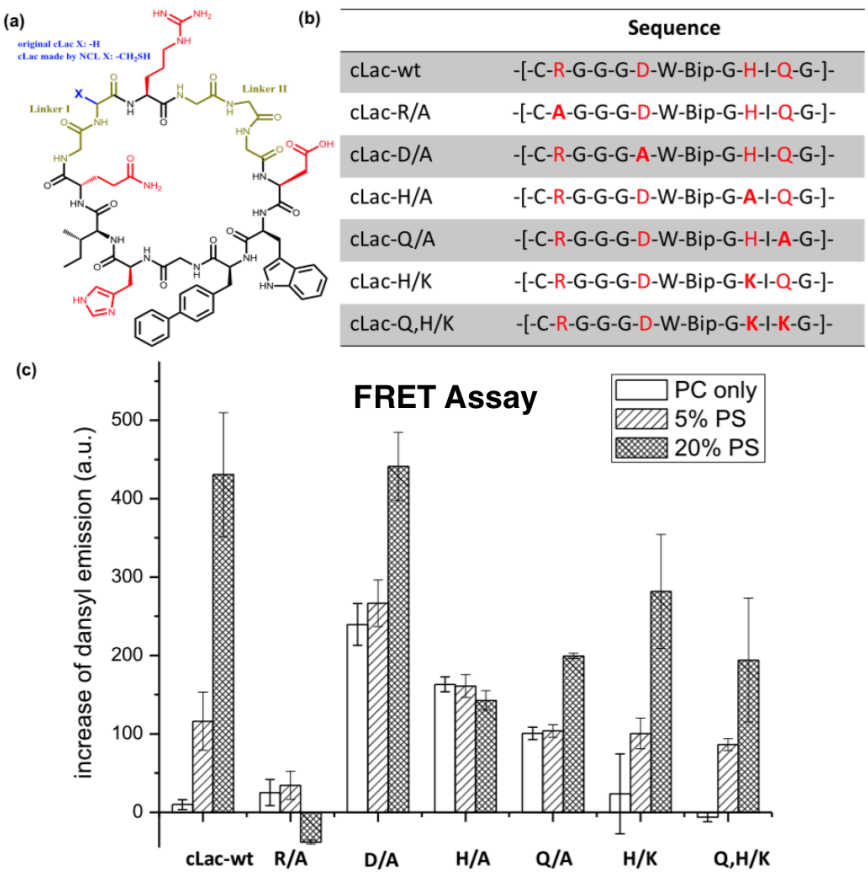

	Sequence
cLac-wt	-[-C-R-G-G-G-D-W-Bip-G-H-I-Q-G-]-
cLac-R/A	-[-C-**A**-G-G-G-D-W-Bip-G-H-I-Q-G-]-
cLac-D/A	-[-C-R-G-G-G-**A**-W-Bip-G-H-I-Q-G-]-
cLac-H/A	-[-C-R-G-G-G-D-W-Bip-G-**A**-I-Q-G-]-
cLac-Q/A	-[-C-R-G-G-G-D-W-Bip-G-H-I-**A**-G-]-
cLac-H/K	-[-C-R-G-G-G-D-W-Bip-G-**K**-I-Q-G-]-
cLac-Q,H/K	-[-C-R-G-G-G-D-W-Bip-G-**K**-I-**K**-G-]-

Figure 2-6. a) structure of cLac-wt generated by NCL strategy with polar side chains highlighted in red; b) table of cLac mutants for structure activity relationship study; c) FRET analysis of cLac-wt and its mutants against vesicles of varying lipid compositions. Figure adopted from reference [79].

To study the binding interaction between each cLac mutant and a membrane containing various compositions of PS, we opted for a FRET-based assay, in which the non-fluorophore labeled cyclic peptides were characterized against PC and PS containing liposomes. In this assay, the interaction between a peptide and vesicle is characterized by the Trp to dansyl emission profile. Each vesicle contained 5% dansyl-functionalized PE lipid to serve as a FRET-acceptor, which in the presence of Trp upon excitation, would

yield a high emission profile that could be plotted against increasing peptide concentrations to yield a binding curve.

The NCL-generated cyclic peptide, cLac-wt, displayed similar PS-binding properties to original cLac peptide made through the on resin cyclization strategy, indicating that the Cys side chain does not interfere with PS binding. Additionally, the increase in dansyl fluorescence is consistent with the percentage of PS found in each vesicle composition, meaning that cLac-wt binds 20% PS vesicles four times better than it binds 5% PS vesicles.

Interestingly, the R/A mutant failed to elicit any fluorescence increase in the presence of either PC or PS, indicating that Arg is a critical residue for binding phospholipids in general. This is not surprising due to the well-established interaction between an Arg headgroup and a phosphate group of the lipid backbone. A binding model of lactadherin-PS generated through computational docking experiments suggests that an Arg residue forms an interaction with the phosphate group of PS, acting as a membrane anchor to help the protein dock into the membrane. Elimination of this interaction would explain the dramatic loss in membrane association; further supporting claims that Arg is a critical residue in the cLac sequence.

In contrast, the D/A mutant displayed significant binding to vesicles containing any composition of lipids, either PC or PS, signifying that Asp plays a critical role in selectively targeting PS over other lipids. A closer look at the PS headgroup structure reveals the presence of a primary amino group, which can form a salt bridge with the carboxylic acid of Asp. Removing Asp, however, renders the peptide more cationic, making D/A more likely to associate with the anionic PS headgroup. This could explain

why this peptide exhibits the same affinity to PS as cLac-wt does, but it still binds PC, potentially due to the enhancing hydrophobic nature that results from introducing an Ala group. The Q/A mutation displays a similar lipid selectivity profile to D/A, but with a much less favorable membrane partition, as assessed by fluorescence intensity comparison. Based on the binding model, both Asp and Gln are buried within the protein, indicating that there is a desolvation penalty associated with binding membranes. Thus, their mutation on cLac to the more hydrophobic Ala residue renders the peptides more active towards PC-containing membranes because the peptide does not have to desolvate the residue while at the same time, has an enhanced hydrophobic driving force, most likely causing the loss in selectivity.

Perhaps even more interesting is that a His to Ala mutation completely abolished the PS selectivity, as demonstrated by both a drop in intensity towards PS-containing vesicles, as well as an increase in intensity for PC-only vesicles. Essentially, H/A binds all vesicle compositions with nearly equal affinities, which is not surprising since the carboxylate group is unique to PS, thus eliminating the His-carboxylate interaction would result in a loss in PS selectivity.

To further validate this result, we synthesized two new cLac mutants, in which we introduced either one or two additional cationic residues to the cLac scaffold. In the first mutant, H/K, the His residue was mutated to a Lys to ensure that under physiological conditions, this side chain displayed a cationic charge that could help to enhance the peptide's ability to associate with anionic membranes. Interestingly, H/K displayed a similar binding profile to that of cLac-wt, indicating that it acts through a similar

mechanism to bind PS, where the Lys side chain can form a salt bridge with the PS carboxylate group.

Going a step further, a second Lys mutation was incorporated in lieu of the Gln residue, to afford Q, H/K. Due to its higher cationic nature, this mutation was expected to further enhance the peptides' ability to partition exclusively into anionic vesicles. However, it was experimentally determined that the peptide binds with nearly equal affinity and selectivity as H/K does to PS. The comparable membrane binding observed between the two mutants can be attributed to the desolvation penalty associated with binding, making the addition of a second cationic residue more entropically costly, thereby negating any benefit that the extra charge-charge attraction would introduce. This key mutation highlights the necessity to consider desolvation penalties when designing peptides that engage in molecular interactions with a given target.

2.2.3 Fluorescent labeling of cLac mutants for fluorescence anisotropy assay

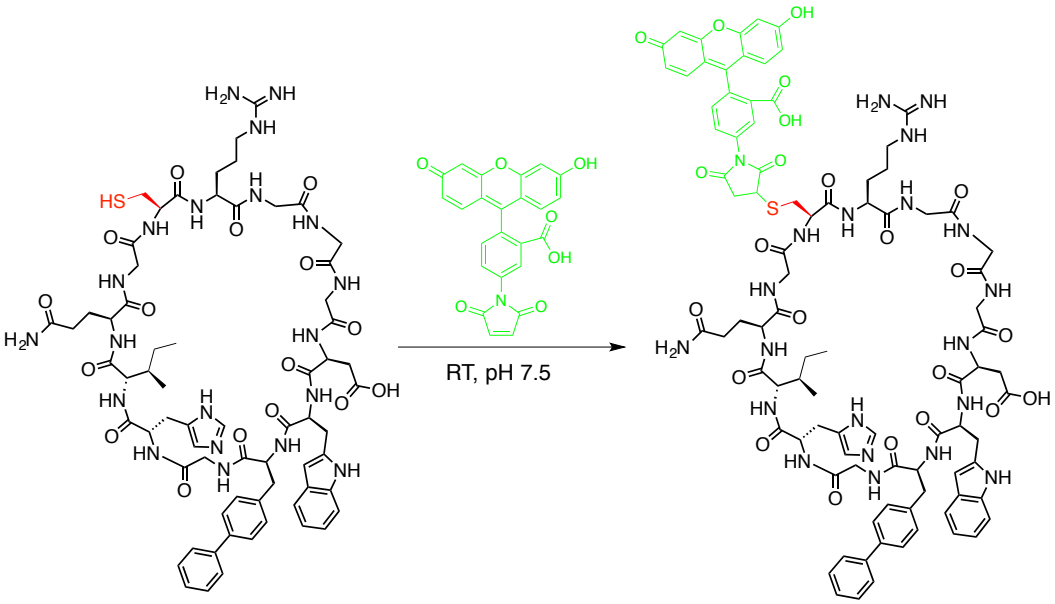

Scheme 2-1. Fluorescent labeling of cLac peptide with fluorescein 5-maleimide.

In order to further validate the FRET results, we developed a fluorescence anisotropy assay to characterize the interactions between cLac mutants and PC or PS containing vesicles. In this assay, the fluorophore-labeled peptide is fixed at a low concentration, while increasing amounts of vesicles are titrated into the solution. One drawback of the FRET assay is its sensitivity to the local environment, since the emission profile is dependent on dipole-dipole coupling interactions between the donor and acceptor pairs. Thus, we chose a fluorescence anisotropy assay instead., which circumvents this problem since the readout is based only on the excited population of fluorophores in a solution, making it a more robust and reliable binding assay than FRET. We chose to label cLac-wt and its mutants using the commercially available fluorescein 5-maleimide, which readily reacts with the free thiol presented on the peptide in an aqueous buffer at pH 7.4.

Table 2-2. Fluorescein-labeled cyclic peptide library

Peptide	Calculated molecular weight	Molecular weight found in mass spectometry
cLac-R/A FITC	1790 Da	1790 Da
cLac-D/A FITC	1831 Da	1831 Da
cLac-H/A FITC	1809 Da	1809 Da
cLac-Q/A FITC	1818 Da	1818 Da
cLac-H/K FITC	1866 Da	1866 Da
cLac-Q,H/K FITC	1866 Da	1866 Da

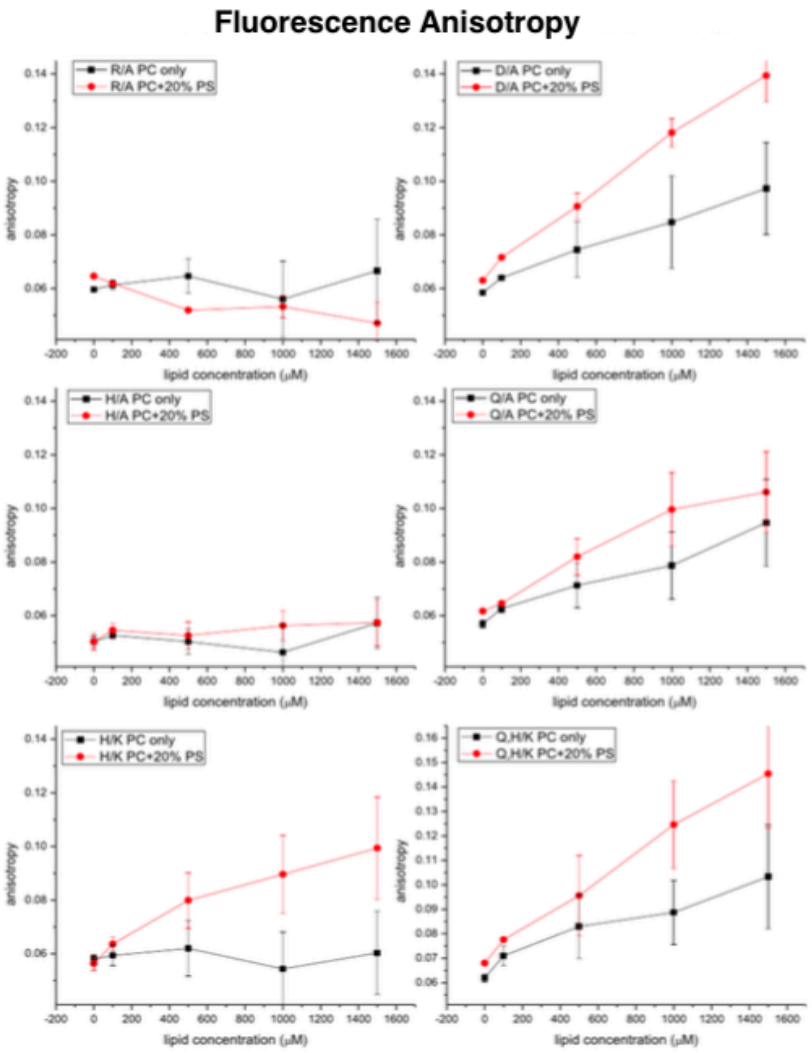

Figure 2-7. Fluorescence anisotropy results of cLac-wt and mutants using PC and PS-containing vesicles. Figure adopted from reference [79].

The anisotropy results seemed to agree well with the FRET data, further supporting our rationalization that all residues on the cLac scaffold work collectively towards exclusively binding PS. Specifically, the R/A mutant was completely inert towards any vesicles composition, validating the significance of an Arg to target membrane lipids. Both D/A and Q/A lost selectivity for PS-containing membranes by associating to PC, as well. This phenomenon can also be explained by the fact that an Ala

mutation can render the peptide more hydrophobic, which can artificially help the peptide bind other targets through hydrophobic interactions.

Surprisingly, the H/A mutant was not consistent with the FRET results, possibly due to a change in the structure upon fluorophore labeling, which may have altered the conformation of the cLac peptide in a negative way. Further experiments must be done to validate this hypothesis, but overall, the results from the Ala scan are very consistent with the FRET-based results. Additionally, the single and double Lys mutation is consistent with the FRET results, further validating the negative contribution for binding associated with a desolvation penalty.

Overall, the cLac mutants demonstrate that each residue on cLac-wt contributes to PS selectivity and affinity to different degrees. Collectively, all of these functionalities are critical in mimicking the parent protein, lactadherin, giving way to many potential opportunities to design protein mimics in the future.

2.2.4 Structural analysis of cLac mutants via CD spectroscopy

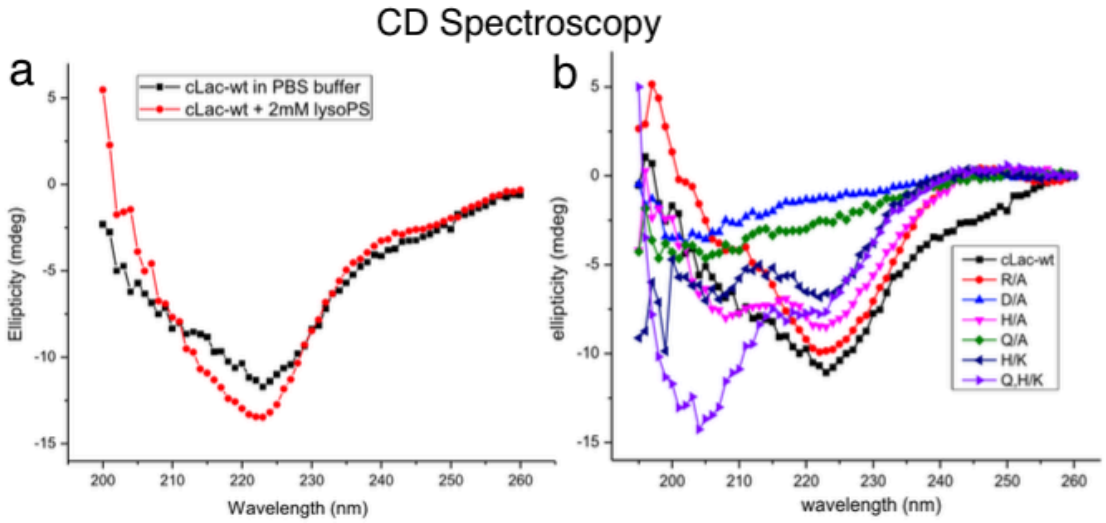

Figure 2-8. Circular dichroism anaylsis of cLac variants. (a) cLac-wt CD spectra with and without Lyso-PS micelles. (b) CD spectra of cLac-wt compared to other mutants. All experiments were done at 50 μM peptide concentration and were recorded in a cuvette with a 2 mm path length. Figure adopted from reference [79].

The cLac peptide structure activity relationship study offered a great deal of insight into the contribution of each individual residue of cLac in binding PS. Ideally, obtaining structural information of cLac in solution would help us to further understand in more detail the specific role each residue and how they are oriented in solution to bind the target. However, due to several challenges associated with characterizing a peptide in solution, such as solubility and the adaptation of multiple conformers, we opted to study the structural features of cLac and its mutants by CD spectroscopy.

We measured the CD spectra of cLac-wt in the absence and presence of PS and opted for lyso-PS micelles to avoid the light scattering effect associated with using larger vesicles. Interestingly, the CD signature of cLac-wt does not significantly change in the

presence of PS, indicating that the peptide is quite well preorganized to bind the lipid. Specifically cLac-wt displayed a global minimum at 223 nm and two minor features around 245 nm and 210 nm, respectively. In contrast, cLac mutants showed a varying degree of structure loss in aqueous solution, with all mutants losing the negatively ellipticity at 245 nm. Additionally, all mutants displayed a reduction of ellipticity at 223 nm, with D/A and Q/A completely losing this global minimum. Overall, the data presented here indicated that cLac-wt adopts a favorable conformer both in the absence and presence of PS-containing vesicles, which helps the peptide partition into these membranes without the entropic cost of preorganizing the residues for target binding.

2.2.5. Cross-linked peptide structures to improve binding

Our thorough analysis of the cLac peptide has shed some light on the key features that are required for binding PS with high selectivity and affinity. Having acquired this fundamental knowledge and understanding the chemical contributions of each functionality, we sought to further improve upon the structural features of the scaffold.

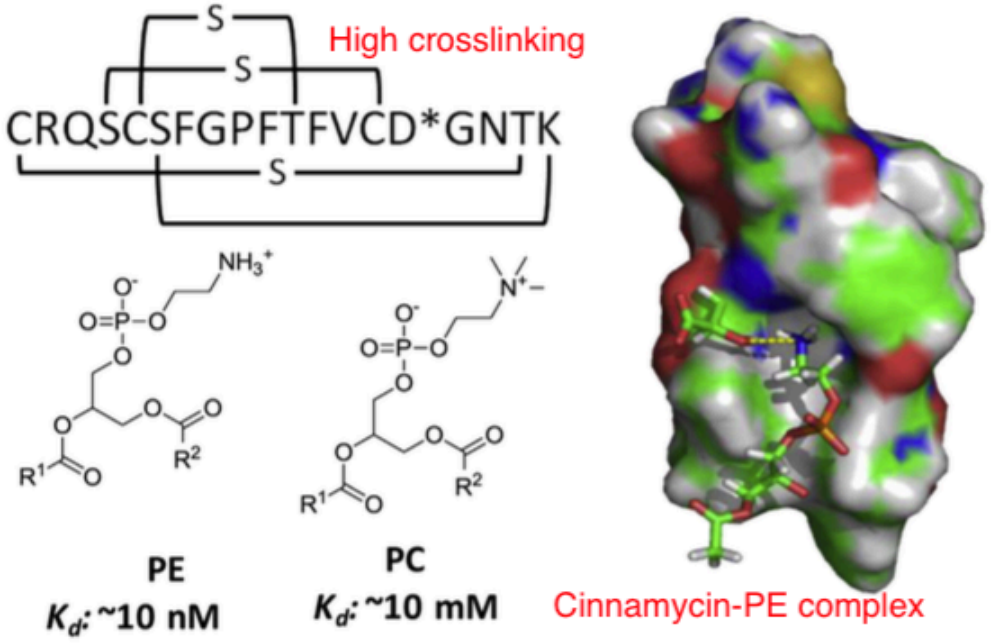

Figure 2-9. Cartoon of the peptide natural product cinnamycin, known to specifically recognize a phosphatidylethanolamine (PE) headgroup. Cinnamycin-PE complex was generated from the PDB file 2DDE with peptide showing its surface potential (blu: positive; red:negative) and lysoPE shown as sticks (C: green; O: red; N: blue; P: orange; H: white). Figure adopted from reference [79].

It is a well-established fact that structural pre-organization of a receptor can reduce the entropic cost for target binding. Countless examples in nature demonstrate how folded proteins adopt a well-defined structure for binding a target to carry out a specific function. Cinnamycin, for example, is a highly cross-linked peptide natural product that exhibits superb selectivity for PE with a K_d value of 10 nM, compared to 10 mM for PC [83]. The peptide displays four covalent thioether bonds, which help to from a binding pocket that is large enough to fit a PE headgroup. An NMR structure of a cinnamycin: lyso-PE complex (1:1) revealed that the peptide adopts an overall amphipathic structure, with the hydrophobic face containing a single Asp residue within

the binding pocket, which is responsible for a polar interaction with the lipid [84]. We sought to employ a similar strategy for cLac, where we lock the backbone of the peptide in place via bicyclization to help present the key residues for PS binding.

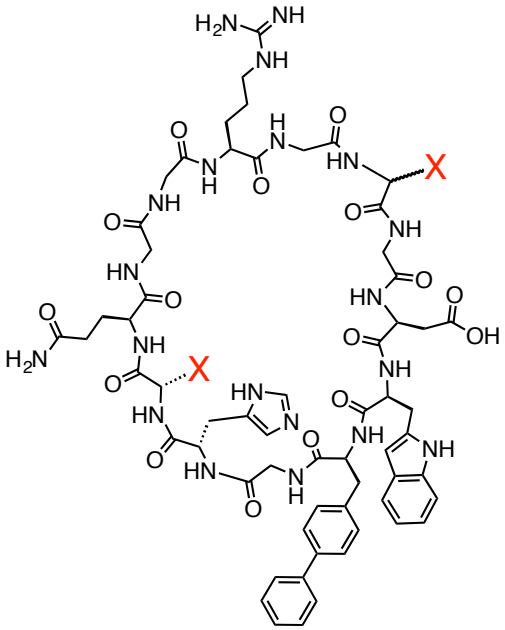

Figure 2-10. Structure of cLac peptide showing site 1 and site 2, where potential functional groups can be incorporated for subsequent stapling reaction to form bicyclic peptides.

Based on computational docking experiments, we chose to introduce the linkage between two specific sites on the scaffold where a modification would least perturb the peptide. Based on the Lact-C2 crystal structure, the Ile residue projects away from the protein-PS binding interface, making it an ideal position to incorporate site 1, while the second site would be incorporated in the middle of the glycine linker II region. The stereochemistry of site 1 would be fixed to L, while site two would be either L or D, since there is no further structural information to support its optimal orientation in solution.

2.2.6 Strategies for stapling peptides

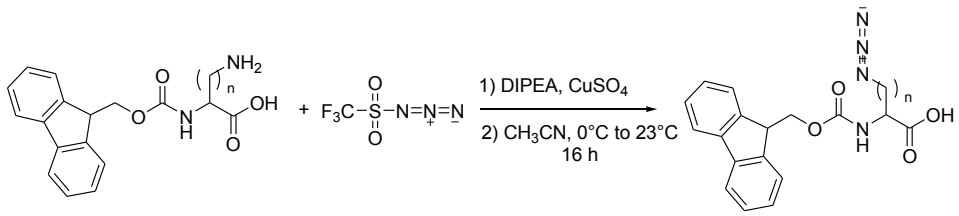

n = 1, Dap
n = 2, Dab
n = 3, Ornithine
n = 4, Lysine

Scheme 2-2. Synthetic route to access azido lysine and derivatives from commercially available amino acids. Conversion of an amino group to an azido group can be accomplished through a diazotransfer reaction.

We initially opted for an azide-alkyne click reaction to generate the peptide staple by incorporating an L-propargyl glycine at site 1 and either an L, or D-azido lysine derivative at site 2. Since both sites are spaced apart so that each is on an opposite end of the scaffold, we could control the length of the linker by incorporating azido lysine derivatives with shorter backbones. We synthesized a library of L and D-azido-lysine derivatives by subjecting Fmoc protected Dap, Dab, Orn or Lys to the diazotransfer reaction to convert the amino group to an azide.

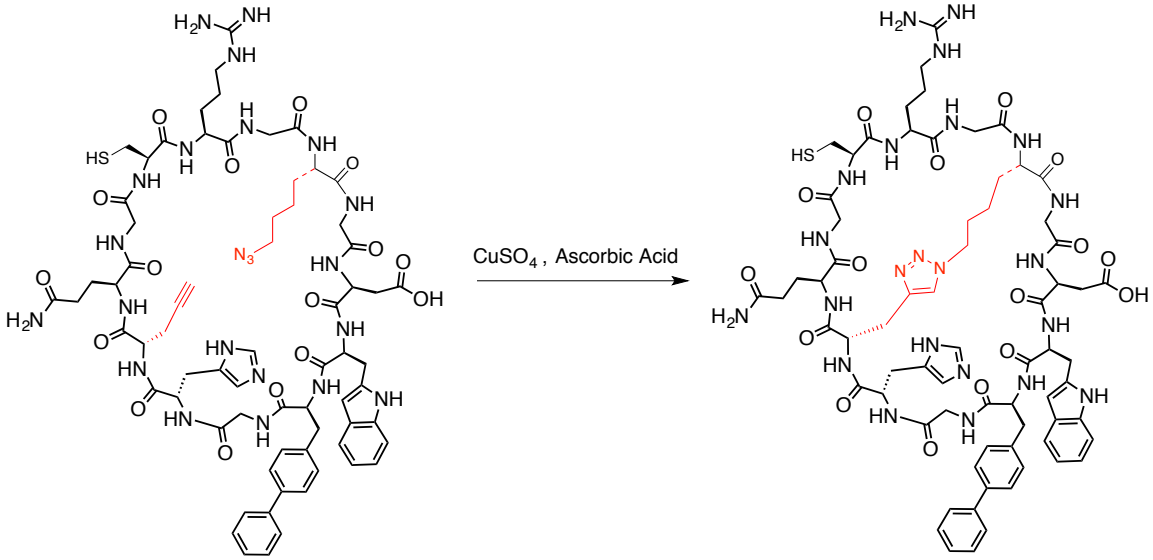

Scheme 2-3. Structure of monocyclic cLac peptide with a propargyl and an azido group incorporated at site 1 and 2, respectively to yield the bicyclic peptide product through click chemistry.

During the cyclization conditions, however, the azido group became reduced by TCEP, rendering it inert to the subsequent click reaction. Due to this synthetic challenge, we turned to an alternative strategy, in which we abandoned an intramolecular stapling reaction and turned to an intermolecular route to access the bicyclic peptides.

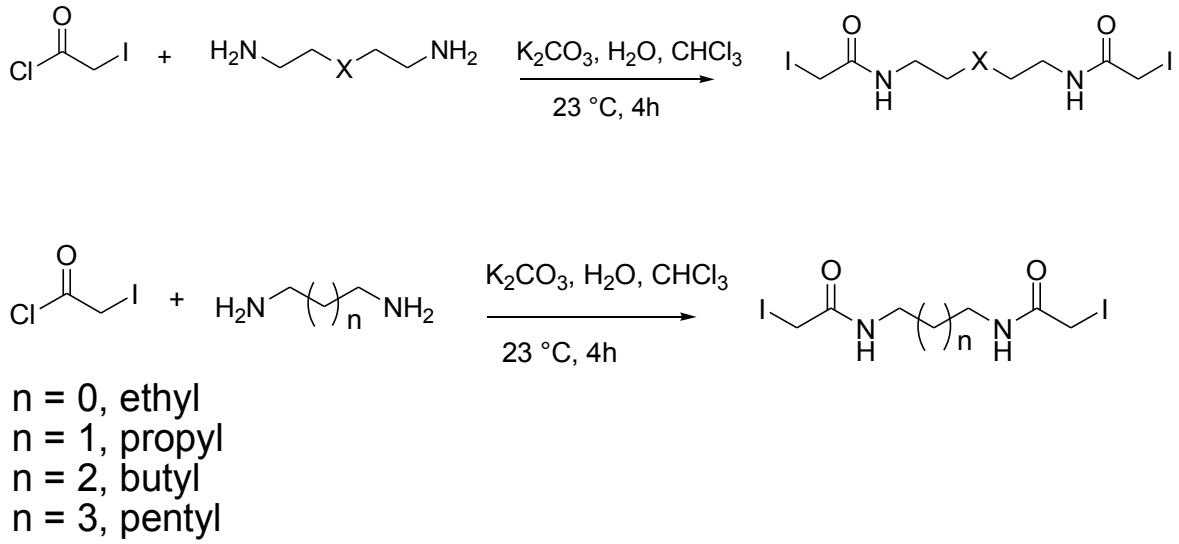

Scheme 2-4. 2-iodoacetyl chloride reaction with aliphatic diamines (left) or heterotom-incorporated diamines (left) to yield iodoacetamide linker for peptide bicyclization.

In this strategy, we introduce two cysteine residues at site 1 and 2 of cLac, followed by a reaction with an iodoacetamide linker to yield the bicyclic peptide. The benefit of using this strategy is that only two cyclic peptides are synthesized, one with (L-Cys, L-Cys) stereochemistry and the other with (L-Cys, D-Cys) stereochemistry. We can then react each monocyclic peptide with iodoacetamide linkers of various lengths, to yield the bicyclic peptides, which can then be purified and analyzed by FRET to determine their efficacies towards PS-containing membranes.

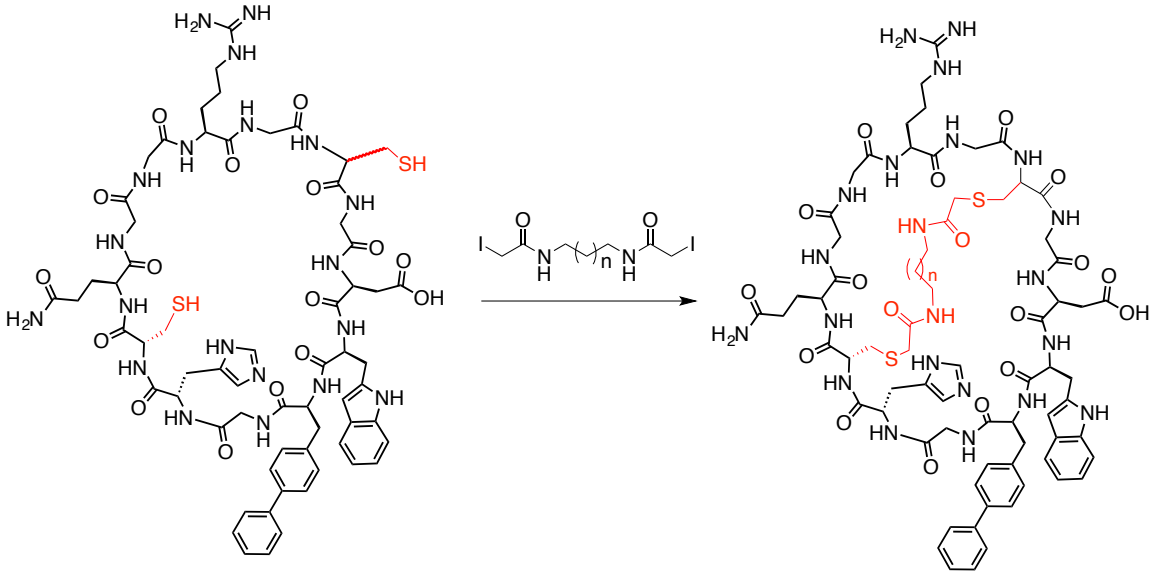

Scheme 2-5. cLac bicyclization reaction through iodoacetamide linkage between two Cys residue in the monocyclic peptide sequence.

A library of iodoacetamide linkers was designed with some containing a hydrophobic chain, while others contained a heteroatom within the chain. They were all synthesized from the commercially available diamine precursors, which were then incubated with 2-iodoacetyl chloride and potassium carbonate in a mixture of water and chloroform, overnight. A DMF stock of each linker was prepared for the subsequent bicyclization reaction with the peptides, which was accomplished by incubating each peptide in a mixture of DMF and PBS with TCEP, then adding two equivalents of the linker and heating for 1 hour or until the reaction was complete by LC-MS.

Table 2-3. Bicyclic peptide library accessed through iodoacetamide chemistry

Peptide	Calculated molecular weight	Molecular weight found in mass spectometry
(L,L)-DiCys ethyl	1578 Da	1579 Da
(L,L)-DiCys propyl	1592 Da	1593 Da
(L,L)-DiCys butyl	1606 Da	1606 Da
(L,L)-DiCys pentyl	1620 Da	1621 Da
(L,D)-DiCys ethyl	1578 Da	1579 Da
(L,D)-DiCys propyl	1592 Da	1593 Da
(L,D)-DiCys butyl	1606 Da	1607 Da
(L,D)-DiCys pentyl	1620 Da	1621 Da

2.2.7 Results of iodoacetamide crosslinked cLac peptides

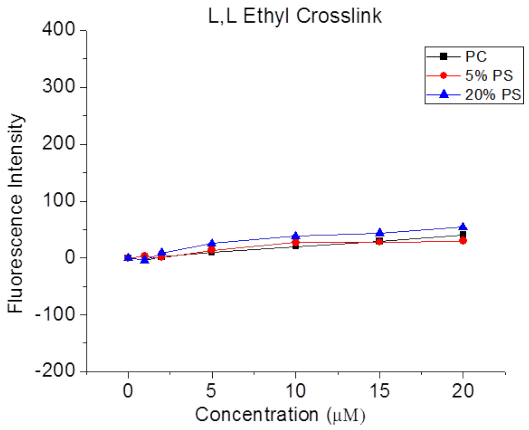

Figure 2-11. Representative FRET plot of bicyclic peptide activity towards PC and PS-containing vesicles.

A library of 8 bicyclic peptides was generated using this method, followed by their analysis by FRET. Surprisingly, none of the peptides showed promising results and were essentially inactive towards vesicles of any PC or PS composition, indicating that the staple was introducing unfavorable structural changes to the cLac scaffold.

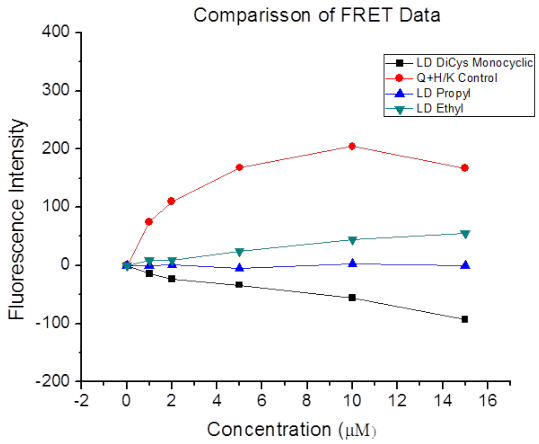

Figure 2-12. Comparison of bicyclic peptides to the monocyclic (L,D)-DiCys perecursor, as well as the positive control, peptide cLac-Q,H/K.

To investigate this hypothesis even further, we analyzed the dicysteine-containing monocyclic peptides alone and discovered that they are also inactive against PC and PS containing vesicles, signifying that incorporation of two cysteine residues at those positions leads to unfavorable activity towards vesicles. Additionally, the positive control, Q, H/K, displayed PS-binding, indicating that there was no issue with the quality of the vesicles and the negative binding of the bicyclic sequences can be interpreted as real.

2.3 Conclusion

Overall, efforts towards investigating the key properties of the rationally designed cLac peptide have been fruitful. We have come to understand, through an Ala scan, the contribution of each amino acid on the scaffold towards PS recognition and will hopefully utilize this knowledge in the future to design more efficient sequences. Additionally, we have optimized an intramolecular native chemical ligation protocol, which enables us to synthesize libraries of cyclic peptides with various modifications to the sequence. CD spectroscopy analysis was informative, as we learned that mutations at any position on cLac led to some degree of structure loss, which could have contributed to either the loss of affinity or selectivity. Furthermore, the SAR study may have foreshadowed our results with the bicyclic peptide sequences, as the introduction of an extra cysteine residue on the scaffold seemed to negate the binding altogether. Collectively, all of these results demonstrate the importance in trying to understand the components that make up a good receptor and what role each functional group plays in binding a desired target.

Experimental Procedures

I. General methods

Dawson (3-(Fmoc-amino)-4-aminobenzoyl) resin and HBTU were purchased from Novabiochem (San Diego, CA). 4-nitrophenyl chloroformate, fluorescein-5-maleimide, Tris base, and guanidine hydrochloride were purchased from Thermo Fisher Scientific (Wal- tham, MA). 4-Mercaptophenylacetic acid was purchased from Sigma Aldrich (St. Louis, MO). The phospholipids were purchased from Avanti Polar Lipids (Alabaster, AL). Fmoc-(4,4')-Biphenylalanine (Fmoc-Bip) was purchased from Chem-Impex Int'l Inc (Wood Dale, IL). All other Fmoc-protected and Boc-protected amino acids were purchased from Advanced Chemtech (Louisville, KY) or Chem-Impex Int'l Inc (Wood Dale, IL). Peptide synthesis was carried out on a Tribute peptide synthesizer (Protein Technologies, Tuscon, AZ). Peptide concentration measurements were performed on a Nanodrop 2000c Spectrophotometer (Thermo Fisher Scientific, Waltham, MA).

II. Peptide synthesis and characterization

The cLac peptides were synthesized through Fmoc/t-Bu chemistry using preloaded Dawson Dbz resin (3-(Fmoc-amino)-4- aminobenzoyl AM resin, Novabiochem), which consists of a 3,4- diaminobenzoic acid attached via the carboxyl group to the resin. The syntheses were carried out on a 0.05 mmol scale using 5 equiv of the Fmoc-protected amino acids and HBTU for the coupling reaction. Additionally, a main-chain Boc-protected cysteine residue was in- stalled at the terminal position of the peptide. A mixture of 50 mg 4- nitrophenylchloroformate in 1 mL of dichloromethane was added at the end of the synthesis and allowed to shake for 2 h to afford the C- terminal

imidazolidinone Nbz moiety, which will later facilitate the thioester formation in the subsequent native chemical ligation (NCL) reaction. The peptides were cleaved off the resin and globally deprotected using Reagent K (80% TFA, 5% H_2O, 2.5% EDT, 5% thioanisole, and 7.5% phenol). The crude products were purified by RP- HPLC (Waters Prep LC, Juniper C18 Column). All peptides were characterized with LC-MS to confirm their identities and purities.

III. Native Chemical ligation

The NCL reaction was carried by modifying a reported procedure [85]. The linear peptide was dissolved in a mixture of DMF and ligation buffer (0.2 M sodium phosphate, 3 M guanidinium chloride, 20 mM 4-mercaptophenylacetic acid, pH 8) to a concentration of 2 – 5 mM. An equal amount of TCEP was added with respect to peptide concentration. The reaction mixture was allowed to sit at room temperature with complete conversion in 4 h. The reaction mixture was acidified with buffer A (95% H_2O, 5% ACN, 0.1% TFA) and purified by RP- HPLC (Waters Prep LC, Juniper C18 column) to afford the cyclic peptide in 60-70% yield. All peptides were characterized with LC-MS analysis to confirm their identities and purities. The peptide concentrations were calibrated by measuring the UV absorption at 275 nm ($\varepsilon_{Bip,\,275}$ = 11200 $M^{-1}cm^{-1}$, $\varepsilon_{Trp,\,275}$ = 5379 11200 $M^{-1}cm^{-1}$, $\varepsilon_{peptide,\,275}$ = 11200 $M^{-1}cm^{-1}$) [86, 87] .

III. Fluorophore labeling

The labeling reaction was carried out by preparing a cyclic peptide stock in DMF, then adding 1 equivalent of fluorescein maleimide and 2% v.v. N-methylmorpholine in DMF until the peptide concentration reached 200 μM. Additionally, 1 equivalent of TCEP with respect to the peptide was added to ensure that the thiol was reduced and readily available for labeling. The reaction mixture was left to sit at room temperature in the dark and complete conversion was achieved in 1 h. The reaction mixture was purified by RP-HPLC (Waters Prep LC, Juniper C18 column) to afford the labeled product. All peptides were characterized with LC-MS analysis to confirm their identities and purities. The peptide concentrations were calibrated by measuring UV absorption at 495 nm ($\varepsilon_{fluorescein,495}$= 80,000 $M^{-1}cm^{-1}$, $\varepsilon_{peptide,495}$= 80,000 $M^{-1}cm^{-1}$).

(d) Iodoacetamide linker synthesis

Iodoacetamide linkers were synthesized according to the following protocol. Diamino (ethane, propane, butane and pentane) (1 equivalent) was dissolved in a 1:1 mixture of H_2O:$CHCl_3$ and left to stir for 5 minutes at 0 °C. K_2CO_3 (1 equivalent) was slowly added to the solution, followed by the addition of 2-iodoacetyl chloride (2 equivalents) and the reaction was left to stir overnight. The organic layer was separated and washed with H_2O (3x), dried over Na_2SO_4 and concentrated in vacuo. The crude material was purified by silica gel chromatography (1:3 EtOAc: hexanes) to yield the desired product in 40-60% yield.

(a) N,N'-(ethane-1,2-diyl)bis(2-iodoacetamide) ^{1}H NMR: CD_3OD, 500 MHz, δ=3.447 (s, 4H), 3.708 (s, 4H). HRMS calculated for $C_6H_{10}I_2N_2O_2^+$ [MH^+] 396.8909, found 396.8914.

(b) N,N'-(propane-1,3-diyl)bis(2-iodoacetamide): ^{1}H NMR: CD_3OD, 500 MHz, δ=1.719-1.678 (m, 2H), 3.307-3.198 (m, 4H), 3.681 (s, 4H). HRMS calculated for $C_6H_{10}I_2N_2O_2^+$ [MH^+] 410.9066, found 410.9070.

© N,N'-(butane-1,3-diyl)bis(2-iodoacetamide) ^{1}H NMR: CD_3OD, 500 MHz, δ=1.557-1.530 (m, 4H), 3.197-3.171 (m, 4H), 3.666 (s, 4H). HRMS calculated for $C_8H_{14}I_2N_2O_2^+$ [MH^+] 424.9222, found 424.9224.

(d) N,N'-(pentane-1,3-diyl)bis(2-iodoacetamide) ^{1}H NMR: CD_3OD, 500 MHz, δ=1.401-1.363 (m, 2H), 1.558-1.499 (m, 4H), 3.182-3.154 (m, 4H), 3.667 (s, 4H). HRMS calculated for $C_9H_{16}I_2N_2O_2^+$ [MH^+] 438.9368, found 438.9363.

VI. Peptide bicyclization

The iodoacetamide bicyclization reaction proceeded by preparing a 200 μM stock of cyclic peptide (L,L) DiCys or (L,D) DiCys in a 1:1 mixture of DMF and NaPi buffer, pH 7.4. 5 equivalents of TCEP was added and the solution was heated at 60 °C for 30 minutes, followed by the addition of the linker in a concentrated DMF stock (ethyl, propyl, butyl, pentyl). The reaction was monitored by LC-MS and upon completion, was dilution in buffer A and directly purified by RP-HPLC (Waters Prep LC, Juniper C18 column) to afford the bicyclic peptides in 40-60% yields. All peptides were characterized with LC-MS analysis to confirm their identities and purities. The peptide concentrations

were calibrated by measuring the UB absorption at 275 nm ($\varepsilon_{Bip,\ 275}$ = 11200 $M^{-1}cm^{-1}$, $\varepsilon_{Trp,\ 275}$ = 5379 11200 $M^{-1}cm^{-1}$, $\varepsilon_{peptide,\ 275}$ = 11200 $M^{-1}cm^{-1}$).

VII. Liposome preparation

Dansyl-labeled 1-palmitoyl-2-oleoyl-sn-glycero-3-phosphoethanolamine (POPE) was synthesized according to the reported protocol [88]. Liposomes were prepared by dissolving and mixing the desired phospholipids in chloroform. The solvent was removed using high vacuum for 6 h and the residue was suspended in 50 mM Tris buffer, pH 7.4. The lipid suspensions were treated through 20 cycles of a 'freeze-and-thaw' process and extruded 21 times through a membrane with a diameter of 100 nm. The concentrations of liposome stocks were characterized via the Stewart assay [89]. Liposomes for the fluorescence anisotropy assay were prepared in the same manner as stated above, with the exception of in-corporating the dansyl-labeled POPE.

VIII. FRET binding assay

The liposome binding of the cLac peptides were evaluated by monitoring the dansyl emission upon addition of peptides. The experiments were carried out on a SpectraMax M5 plate reader (Molecular Devices, Inc. Sunnyvale, CA) with a quartz cuvette of 10 mm path length. The samples were excited at 280 nm and their emission was monitored from 320 nm to 530 nm. All peptides were dissolved in DMF to give a 1 mM stock. The tests were done at a total lipid concentration of 100 μM and peptide concentration of 10 μM. The dansyl emission intensity at 520 nm was plotted against increasing peptide concentrations.

IX. Fluorescence anisotropy assay

The fluorescence anisotropy experiments were carried out on a Cary Eclipse Spectrophotometer (Agilent Technologies) with a quartz cuvette of 10 mm path length. Prior to measurements, a G factor of 1.4213 was calculated for the fluorophore on the instrument. All fluorescein-labeled peptides were dissolved in DMF to give a 100 mM stock. The experiments were performed at a peptide concentration of 100 nM prior to liposome titration. The samples were excited at 495 nm and their emission was monitored at 520 nm to afford the anisotropy values. An increasing amount of liposome was titrated into the cuvette and the anisotropy values were measured at each concentration of liposome. The anisotropy values were plotted against liposome concentration to give the binding curves.

X. Circular dichroism measurements

The CD experiments were performed on an Aviv Model 420 CD Spectrometer (Aviv Biomedical, Inc., Lakewood, NJ). All samples for the wavelength scans were prepared in buffer (PBS, pH 7.4) at a concentration of 50 μM and placed in a quartz cuvette with a 2 mm path length. The CD spectra were recorded from 190 to 260 nm at 2 °C with a 10 s averaging time for each measurement. The lysoPS experiment was performed by titrating 2 mM of the micelles from a concentrated stock of 55 mM into the peptide sample.

Chapter 3. A prolinomycin-based scaffold for developing functional peptides

3.1 Introduction

Nature has evolved proteins to bind cell-signaling molecules with exquisite affinity and specificity, making molecular recognition an essential part of biology. It has been a highly sought after goal within the chemistry field to be able to mimic the structure and function of certain proteins with smaller molecules, such as peptides [90]. Compared to proteins, which are large in size, peptides are easier to chemically modify, label and functionalize. More specifically, cyclic peptides exhibit high proteolytic stabilities and faster clearance rates compared to proteins, making them more attractive candidates for some clinical applications [91]. Although peptides are showing promise as therapeutic agents, it is challenging to rationally develop peptides that exhibit desirable functions.

3.1.1 Peptide receptor preorganization

One of the advantages that peptides have over small molecules is that they can engage a target through multiple interactions, much like a protein would. However, unlike a protein, peptides generally do not possess the ability to properly fold and display their side chains for target binding. In fact, it is energetically costly for a peptide to structure itself in solution and bind its intended partner. One way to circumvent this problem is to preorganize the side chains on a peptide scaffold, thereby locking the residues in place for a more favorable target interaction. This can be done by chemically modifying the structure to incorporate a staple, which would lock the conformation in

place, as seen in several examples with α-helices and cyclic peptides [92, 93]. However, without solid structural information, it is challenging to predict whether a staple would favor, or destabilize the structure when incorporated into the scaffold.

Herein, I will describe a novel strategy that takes advantage of the structural features of prolinomycin, a rigid peptide macrocycle, to develop protein-like receptors with high target specificity and affinity. Prolinomycin is unique in that it can undergo metal-nucleated folding in water to afford a highly structured peptide scaffold, which can be amenable to side chain mutations. I will demonstrate that in the presence of a K^+ ion, this peptide and its mutants can display protein-like folding in both vesicle and cell-based assays.

3.1.2 Metal-complexation of the natural product valinomycin and its structural analogue, prolinomycin

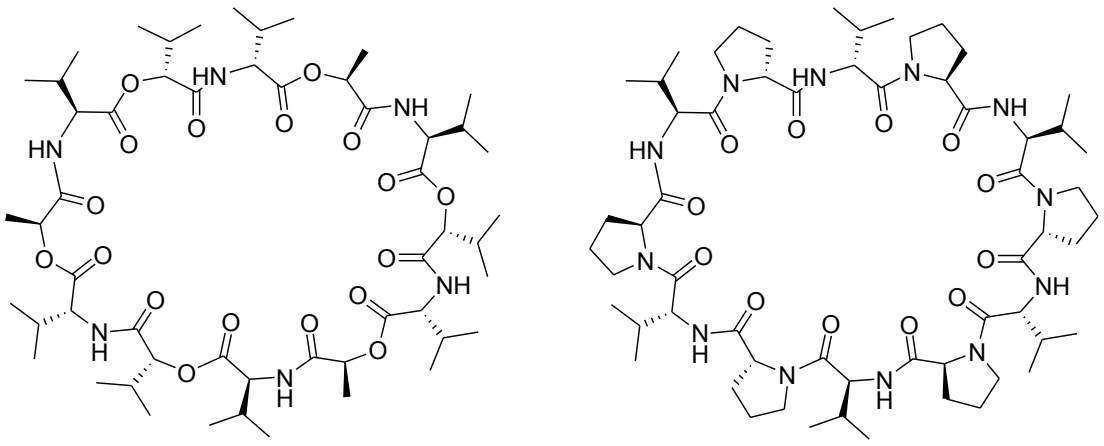

Figure 3-1. Structure of valinomycin with ester linkages (left) and prolinomycin with amide linkages (right)

Valinomycin is a depsipeptide antibiotic that has been widely investigated due to its ability to complex and transport monovalent cations (Figure 3-1) [94]. The carbonyl oxygens of valinomycin point inwards to form a polar cavity, to chelate K^+, thereby causing the hydrophobic side chains to point outwards [95, 96]. This critical change in structure facilitates the peptide to shield a K^+ ion from the bulk solvent and transport it across lipid bilayers. Acting as an ion shuttle, the peptide crosses the membrane to dissociate the K^+ ion, which disrupts the electrochemical gradient of the cell, leading to cell death.

In addition to spectroscopic methods, the metal-complexed structure of valinomycin has been characterized by x-ray crystallography to suggest that replacing its ester linkages with amide linkages should not perturb the overall geometry. Using this information, Gisin and Merrifield developed prolinomycin, a structural analogue of valinomycin, by replacing the ester linkages with proline residues possessing the same chirality [97]. Subsequent studies led them to discover that prolinomycin has a higher affinity for monovalent cations than its predecessor, valinomycin, but is a poor transporter through the lipid bilayer [98]. This can be attributed to the restricted freedom of rotation from the proline residues, which forces the uncomplexed peptide into an unfavorable, high-energy structure. In the presence of K^+ or Rb^+, the highly strained peptide has more incentive to bind the cation and adopt a lower energy conformer [99]. Conformational analysis of prolinomycin in the presence of cations was performed using spectroscopic methods to confirm peptide-metal chelation [100]. Additionally, proline residues prevent the peptide from dissociating the metal efficiently, making it a poor antibiotic candidate due to its inability to act as an ion shuttle. Although the properties of

prolinomycin differ from valinomycin, its unique structural features offer considerable potential for alternative applications.

3.2 Design of prolinomycin analogues

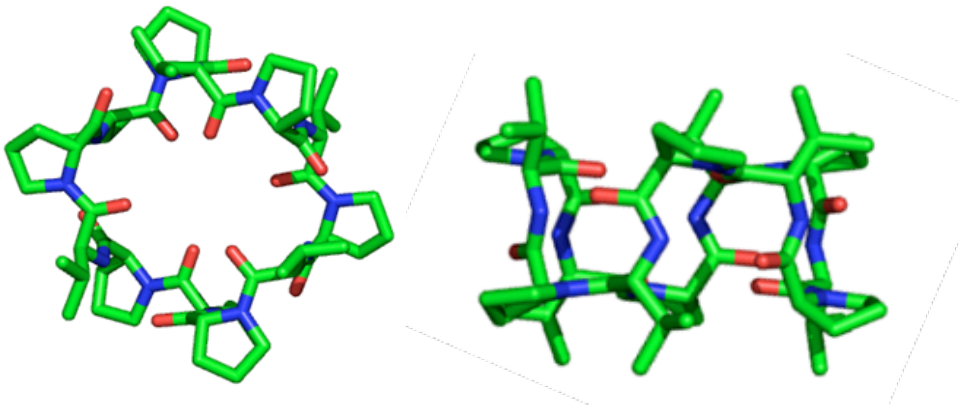

Figure 3-2. Prolinnomycin structure top view (left) and side view (right).

We sought to take advantage of the structural features of prolinomycin and design a protein-like receptor for target binding. As seen in the crystal structure of wild type prolinomycin, the metal-induced folding ability allows the peptide to adopt a "drum-like" structure with each deck displaying their side chains in opposite directions (Figure 3-2). A key feature of this scaffold is the presence of multiple proline residues, which are critical for the slow K^+ dissociation in water. We hypothesized that the non-proline side chains on the top deck of the peptide could be mutated to residues that engage in favorable interactions with a given target. In order to test whether the scaffold could tolerate any mutations to the non-proline residues, we incorporated non-beta branched amino acids in lieu of the Val residues.

One of the overarching goals of this lab has been to develop receptors with high affinities and specificities for membrane lipids. As mentioned earlier, lipids play a

significant role as signaling molecules in biology, often recruiting proteins to the membrane surface to perform critical functions. In mammalian cells, the anionic lipid PS is confined to the cytosolic leaflet and only becomes surface exposed during apoptosis. Conversely, bacterial cell membranes are abundant in anionic lipids, making cationic antibiotics a main route to target and kill these cells. To begin, we decided to employ a general approach and develop a cationic analogue of prolinomycin that could target the anionic lipids of a bacterial cell membrane. Due to the well-established interaction between arginine and phosphate groups on membrane lipids, we chose to design a poly-arginine sequence.

3.2.1 Synthesis of prolinomycin analogues via proline ligation

We sought after an efficient cyclization method that would yield high conversion and product purity. The native chemical ligation (NCL) strategy is a chemoselective method to synthesize cyclic peptides with high yields and purities [79]. Cyclization can be accomplished in solution without side chain protecting groups, making it an optimal approach to expand a library of mutants. Additionally, a free thiol displayed on the peptide after the cyclization can be used as a labeling handle for subsequent fluorescence-based experiments.

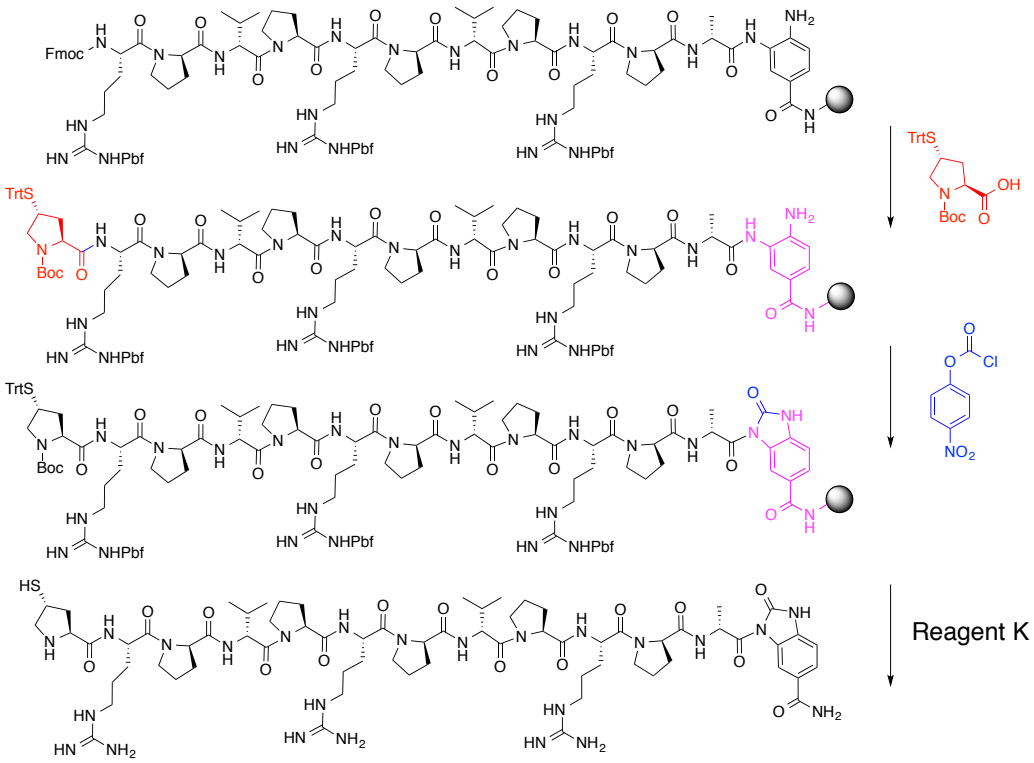

Scheme 3-1. Solid phase synthesis of the RRR linear precursor peptide.

Due to the high frequency of proline residues within the sequence, we adopted an intramolecular proline ligation protocol, which enables the chemoselective reaction between an N-terminal thioproline (tPro) and a C-terminal thioester on the peptide sequence [101, 102]. In order to secure high cyclization yields, we also chose to install an Ala residue in lieu of Val at the C-terminus, since the branched structure of Val could impede the reaction. Using this modified intramolecular proline ligation strategy, we built the linear peptide sequence on a Dawson Dbz resin using solid phase peptide synthesis (SPPS), followed by incorporation of (2S, 4R)-Boc-Mpt(Trt)-OH (tPro) at the N-terminus (Scheme 3-1). The Dbz moiety was then converted to the more reactive Nbz group by formylation with 4-nitrophenylchloroformate. Although the sequence contains a high frequency of proline residues, which are traditionally thought to be difficult couplings, LC-MS analysis revealed a relatively pure linear peptide. After global deprotection and

cleavage from the resin, the crude linear peptide was subjected to the ligation reaction conditions to yield a relatively clean conversion to the cyclic product.

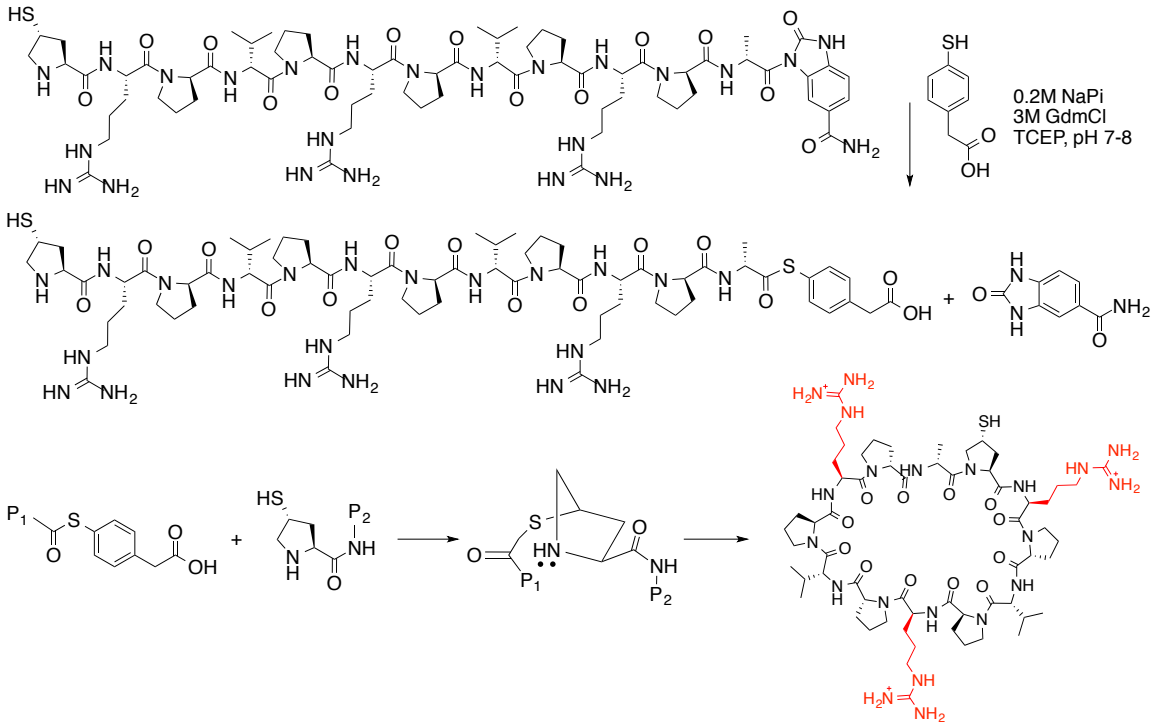

Scheme 3-2. Synthesis of RRR via intramolecular proline ligation.

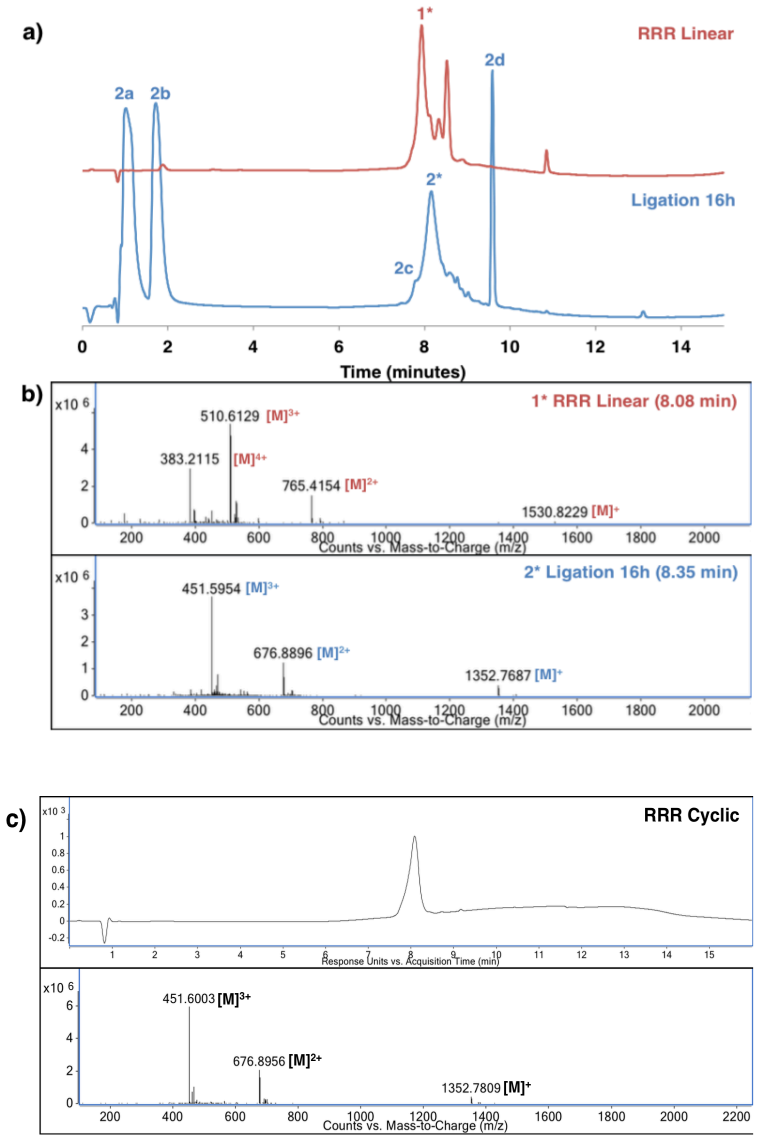

Figure 3-3. Synthesis of prolinomycin mutants. a) Exemplary HPLC traces of prolinomycin synthesis via proline ligation. Top: LC trace of the crude RRR linear precursor (1*). Bottom: LC trace of the ligation reaction at 16 h showing full conversion of linear precursor (1*) to cyclic peptide (2*). Other side products and compounds include TCEP (2a), Nbz (2b), hydrolyzed linear peptide (2c) and 4-mercaptophenylacetic acid (2d). b) ESI-MS spectra of the RRR linear precursor (top) and the ligation mixture at

16 h showing conversion of the linear peptide to the desired cyclic product. c) LC-MS of the purified RRR cyclic peptide. LC-MS analysis was carried 220 nm.

During the ligation reaction, a thiol exchange occurs between the N-terminal tPro and C-terminal thioester, forming a 5-membered ring transition state, which then undergoes an S to N acyl shift (Scheme 3-2). Therefore, it is crucial to use the trans diastereomer of tPro to allow this step to proceed easily, since the cis-diastereomer would sterically hinder the reaction to yield little or no conversion to the cyclic product (Figure 3-3). Additionally, few side products were formed during the ligation reaction, suggesting that the route can be a powerful tool to synthesize large libraries of prolinomycin mutants for screening and analysis further down the line.

In addition to RRR, we synthesized and characterized a diverse library of mutants to further investigate our hypothesis. These cyclic peptides were synthesized via the proline ligation strategy and will be discussed later on in this chapter. The sequences and masses can be found in Table 3-1.

Table 3-1. Sequences and masses of cyclic peptides

Mutant	**Sequence and Calc'd *m/z***
VVV	Cyclo-[tPro-Val-Pro-Val-Pro-Val-Pro-Val-Pro-Val-Pro-Ala-] 1181.51 $[M]^{+}$, 590.75 $[M]^{2+}$, 393.83 $[M]^{3+}$
KKK	Cyclo-[tPro-Lys-Pro-Val-Pro-Lys-Pro-Val-Pro-Lys-Pro-Ala-] 1268.63 $[M]^{+}$, 634.31 $[M]^{2+}$, 422.87 $[M]^{3+}$
RRR	Cyclo-[tPro-Arg-Pro-Val-Pro-Arg-Pro-Val-Pro-Arg-Pro-Ala-] 1352.67 $[M]^{+}$, 676.33 $[M]^{2+}$, 450.89 $[M]^{3+}$
VRR-4R	Cyclo-[tPro-Val-Pro-Arg-Pro-Arg-Pro-Val-Pro-Arg-Pro-Ala-] 1352.67 $[M]^{+}$, 676.33 $[M]^{2+}$, 450.89 $[M]^{3+}$
RRR-4W	Cyclo-[tPro-Arg-Pro-Trp-Pro-Arg-Pro-Val-Pro-Arg-Pro-Ala-] 1439.76 $[M]^{+}$, 719.88 $[M]^{2+}$, 479.92 $[M]^{3+}$
RR(ObK)	Cyclo-[tPro-Arg-Pro-Val-Pro-Arg-Pro-Val-Pro-ObK-Pro-Ala-] 1540.98 $[M]^{+}$, 770.49 $[M]^{2+}$, 513.66 $[M]^{3+}$
RR(TpK)	Cyclo-[tPro-Arg-Pro-Val-Pro-Arg-Pro-Val-Pro-TpK-Pro-Ala-] 1580.96 $[M]^{+}$, 790.48 $[M]^{2+}$, 526.98 $[M]^{3+}$

3.2.2 NMR analysis of RRR peptide

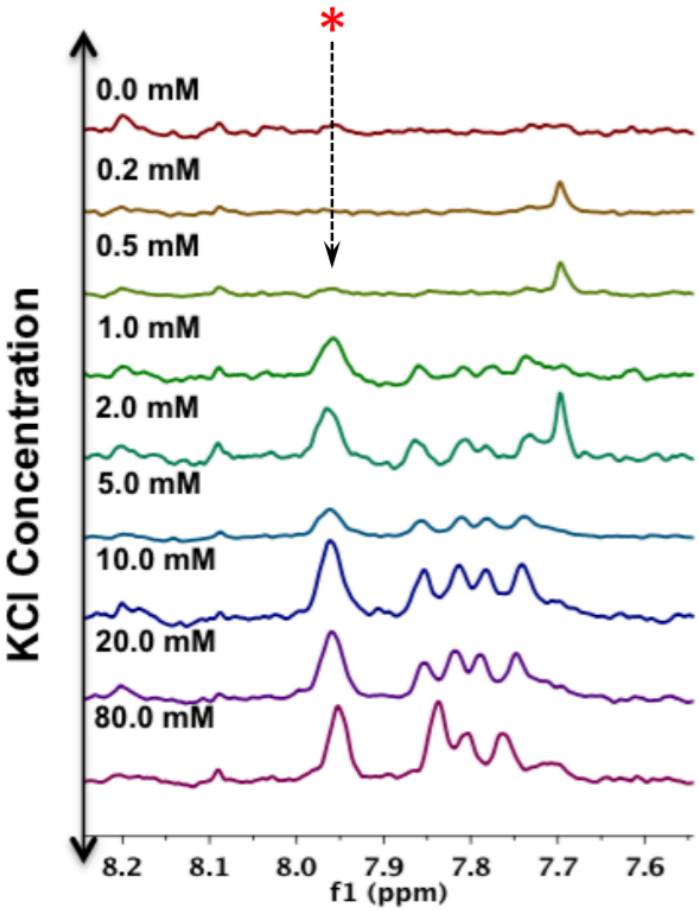

Figure 3-4. ^{1}H NMR (600 MHz) spectra of the RRR amide region with varied concentrations of K^{+}. The peak at 6.14 ppm corresponds to maleic acid used as an internal standard (0.2 mM). Sample is in 10% D_2O in 1:1 CD_3OH:NaPi buffer, pH 4.0.

We sought to investigate the metal-nucleated folding ability of prolinomycin mutants by ^{1}H NMR spectroscopy to ensure that a mutation of Val to any other amino acid would not disrupt the peptide's ability to bind potassium. Due to potential solubility and aggregation issues, we chose to analyze the peptide at 0.2 mM concentration in a buffer containing 10% D_2O and a 1:1 mixture of CD_3OH and NaPi at pH 4.0. We used methanol d-3, as well as pH 4.0, to minimize the potential deuterium exchange with the

amide protons. Interestingly, in the absence of K^+ ions, no clear peaks were observed in the amide proton region of the spectrum of the RRR peptide, indicating that several conformers could simultaneously exist in solution and would likely be exchanging. However, addition of KCl to the solution elicited the appearance of well-resolved peaks, which can be attributed to intramolecular hydrogen bonding of the amide protons to adjacent carbonyl oxygens; induced by metal-complexation of the remaining carbonyl oxygens (Figure 3-4).

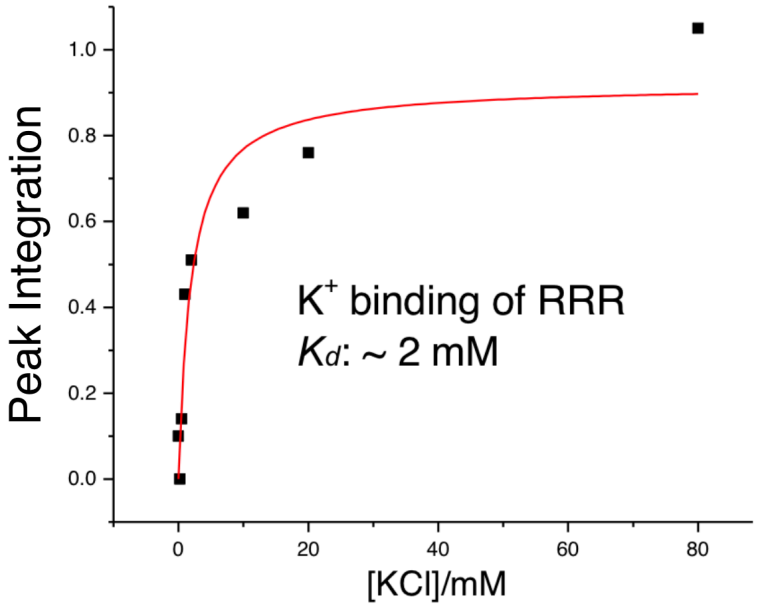

Figure 3-5. Metal-nucleated folding of prolinomycin mutants. Titration curve generated by plotting the peak integration at 7.95 ppm against KCl concentration.

The integrated area of the peak at 7.95 ppm was plotted against KCl concentration to yield a binding curve with a K_d value of approximately 2 mM for K^+ binding (Figure 3-5). Although this value is in agreement with physiologically relevant concentrations of potassium, it is still higher than wild type prolinomycin, which has a reported value of 10 μM. The underlying reasons for the difference remain to be defined.

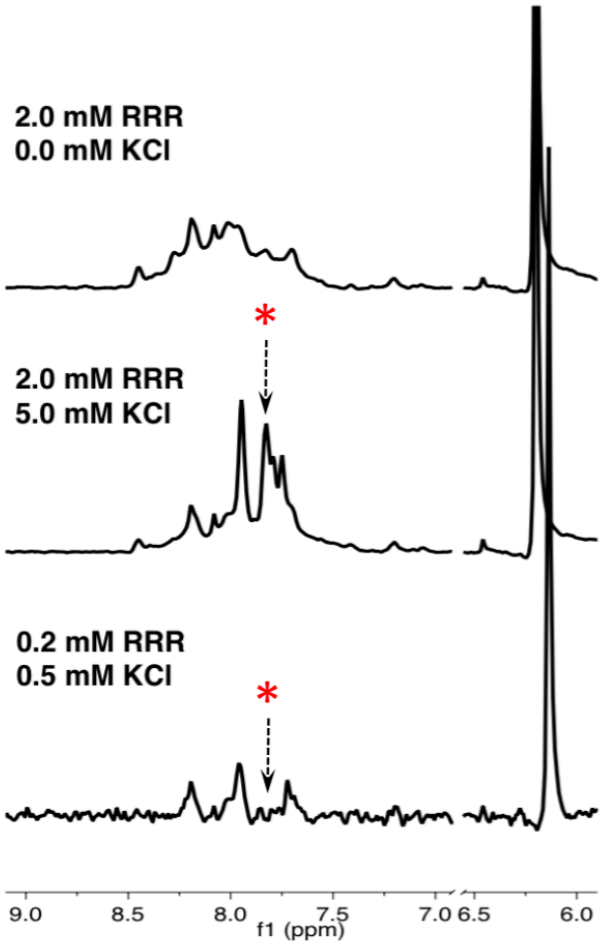

Figure 3-6. Metal-nucleated folding of prolinomycin mutants. A dilution experiment highlighting the dynamic nature of RRR for K^+ binding.

Additionally, a dilution experiment of RRR demonstrates that the K^+ chelation is reversible as select NH resonances rapidly disappear with a drop in KCl concentration (Figure 3-6). This result not only demonstrates the dynamic nature of K^+-binding, but more importantly, illustrates that the peptide can adopt a well-folded structure under physiological conditions.

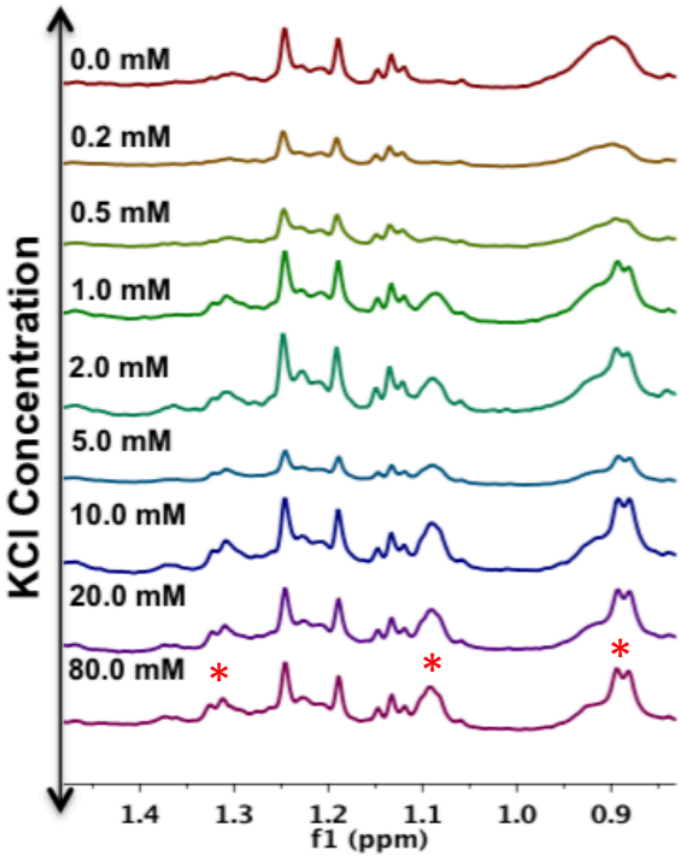

Figure 3-7. ^{1}H NMR spectra of the RRR aliphatic region with varied concentrations of K^{+}. Sample is in 10%D_2O in 1:1 CD_3OH:NaPi buffer, pH 4.0.

Focusing on the aliphatic region of the ^{1}H NMR spectrum of the RRR KCl titration experiment, we observe that K^{+} ions can also induce favorable structural changes of the peptide side chains (Figure 3-7). Specifically, we observe the emergence of a doublet at 0.88 ppm, which we attribute to a Val side chain, as well as the emergence of a doublet at 1.32 ppm, which is an Ala side chain. The increasing sharpness of these peaks with the addition of K^{+} suggests a reduction in the number of peptide conformers in solution. Although these experiments provide a great deal of information on how the peptide behaves in the presence of K^{+}, the experimental conditions do not fully represent

how the peptide would behave in a pure aqueous environment, since the solvent contains 50% CD_3OH.

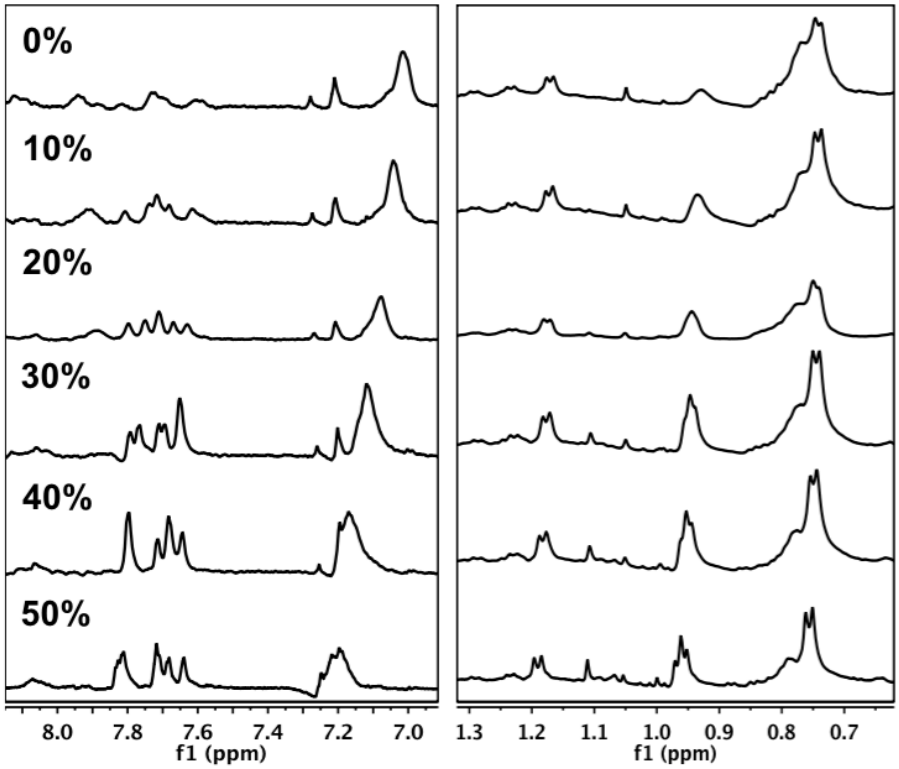

Figure 3-8. ^1H NMR spectra of the RRR amide and aliphatic regions showing a CD_3OH titration profile. The peptide concentration is initially at 1 mM in 10%D_2O: NaPi buffer, pH 4.0 with 100 mM KCl. Prior to adding CD_3OH, an equal volume of the sample was removed.

To address this issue, we performed a CD_3OH titration experiment to further examine how methanol can affect the peptide's behavior in solution. We prepared a 1 mM sample of RRR in 10%D_2O: NaPi buffer, pH 4.0 and added a fixed concentration of KCl (100mM) to ensure that the peptide is fully bound to K^+. As seen in Figure 3-8, at 0% CD_3OH, the peaks in both the amide and aliphatic regions of the spectrum are broad and not well resolved, indicating that the peptide may aggregate, or adopt several

conformers under these conditions. An identical sample of the peptide in CD_3OH with KCl was prepared and titrated into the sample at 10% by volume increments. Prior to the titration, an equal volume of the aqueous solution was removed in order to minimize any dilution. Interestingly, the addition of CD_3OH seems to help the NMR resonances become much more resolved, which could be the result of multiple factors. The high concentrations required to perform the NMR experiments may cause the peptide to aggregate in a purely aqueous environment, which could explain why we observe broad peaks, even in the presence of K^+. The addition of CD_3OH helps to break up these peptide aggregates, which in turn causes the peaks to become sharper.

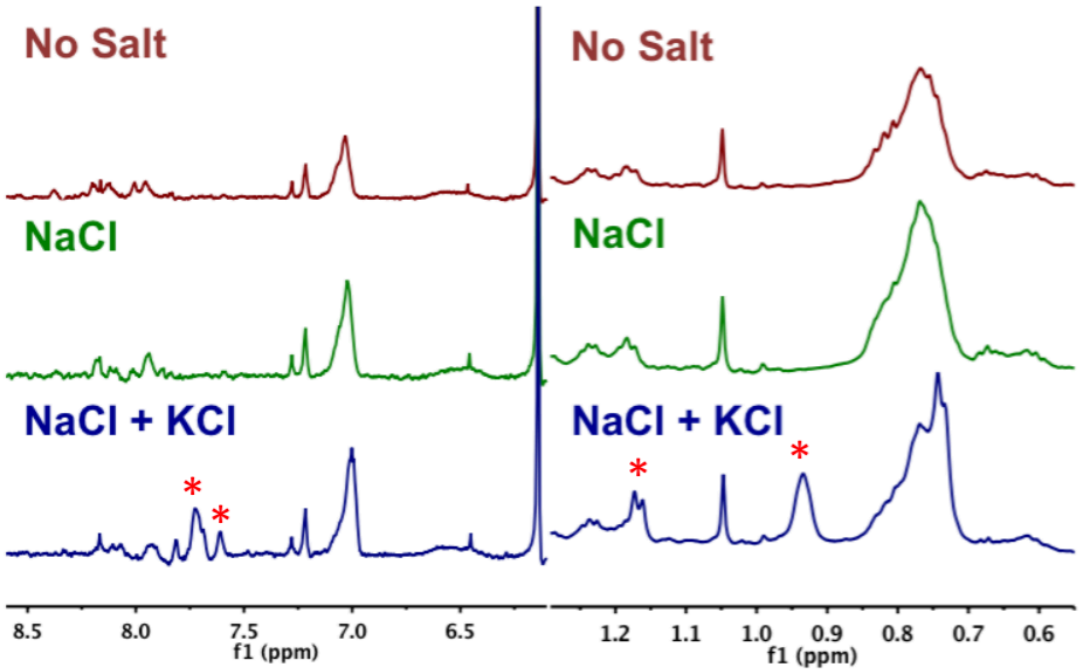

Figure 3-9. ^1H NMR data of amide and aliphatic regions demonstrating K^+ selectivity of RRR. Peptide sample is at 1 mM concentration in 10%D_2O/NaPi buffer, pH 4.0. Top trace shows peptide without added salt. Middle trace shows peptide with the addition of 100 mM NaCl. Bottom trace shows peptide with an additional 100 mM KCl.

Although the RRR peptide does not exhibit ideal behavior in a purely aqueous environment, we can still make some key observations about its structure. The KCl titration data clearly showed that RRR responds well to an influx of K^+ ions, by chelating the metal to form a reduced number of conformers in solution, as observed by the emergence of amide proton resonances. We were interested in further studying the ion selectivity of RRR in a purely aqueous environment, so we prepared a 1 mM sample of the peptide in a 10%D_2O/NaPi buffer at pH 4.0 with no additional salt (Figure 3-9). We then added 100 mM of NaCl to the sample and did not observe any change in the NMR spectrum, indicating that Na^+ ions do not induce any change to the peptides conformation. Interestingly, if we add an equal amount of KCl (100 mM) to the same sample, which already contains NaCl, we observe a clear change in both the amide and aliphatic regions of the spectrum. More specifically, the amide protons become prominent and side chain resonances in the aliphatic regions become slightly sharper, which is consistent with earlier data seen in.

Collectively, the NMR results for RRR demonstrate the dynamic nature of the cyclic peptide in both a purely aqueous environment, as well as a mixture of methanol and water. We observe the K^+-induced conformational changes of RRR by the emergence of amide proton resonances, as well as the sharpening of peaks in the aliphatic region of the spectrum. Additionally, the metal-induced folding of RRR is selective for potassium, as sodium ions do not induce any significant changes to the NMR spectrum. To investigate the generality of this phenomenon, we analyzed two additional prolinomycin mutants by NMR.

3.2.3 NMR analysis of RRR-4W peptide

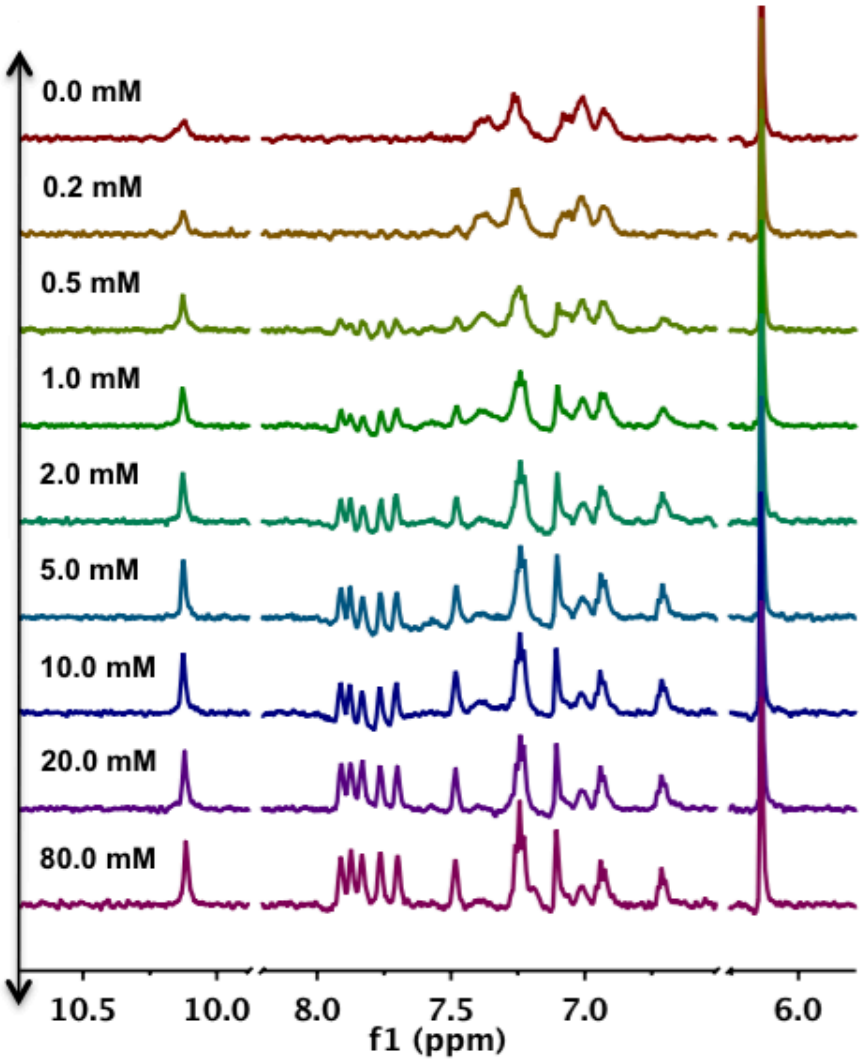

Figure 3-10. ^{1}H NMR spectra of the RRR-4W amide region with varied concentrations of K^{+}. The peak at 6.14 ppm corresponds to maleic acid used as an internal standard (0.2 mM). Sample is in 10%D_2O in 1:1 CD_3OH:NaPi buffer, pH 4.0.

The RRR-4W mutant is almost identical to RRR in sequence, except that it contains a Trp residue in lieu of a Val. Not surprisingly, the peptide also behaves similar to RRR in the KCl titration experiment (Figure 3-10). Increasing the concentration of K^{+} ions in solution helps to elicit the emergence of amide proton resonances.

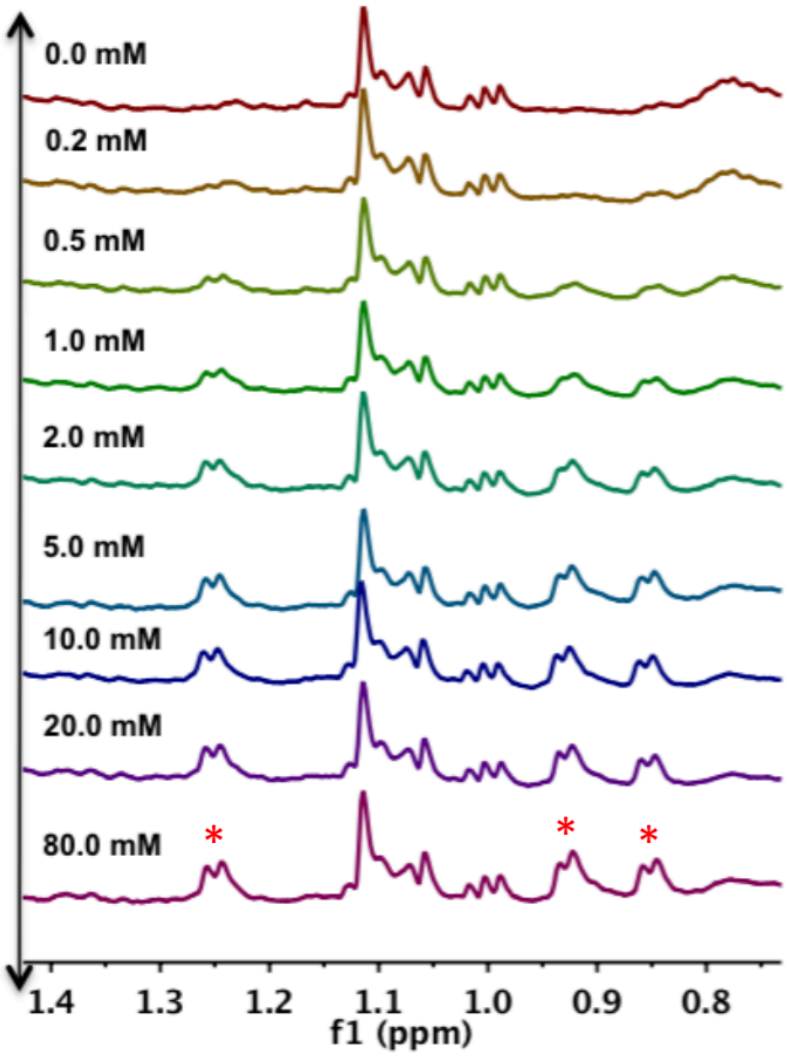

Figure 3-11. ^{1}H NMR spectra of the RRR-4W aliphatic region with varied concentrations of K^{+}. Sample is in 10%D_2O in 1:1 CD_3OH:NaPi buffer, pH 4.0.

Additionally, the aliphatic region of the NMR spectrum shows a doublet from Ala at 1.25 ppm, which becomes more resolved with increasing KCl concentration. Two doublets at 0.85 ppm and 0.92 ppm also emerge, which we assign to the methyl groups of Val. Together, the data suggest that RRR and RRR-4W behave in a relatively similar manner under the same conditions (Figure 3-11).

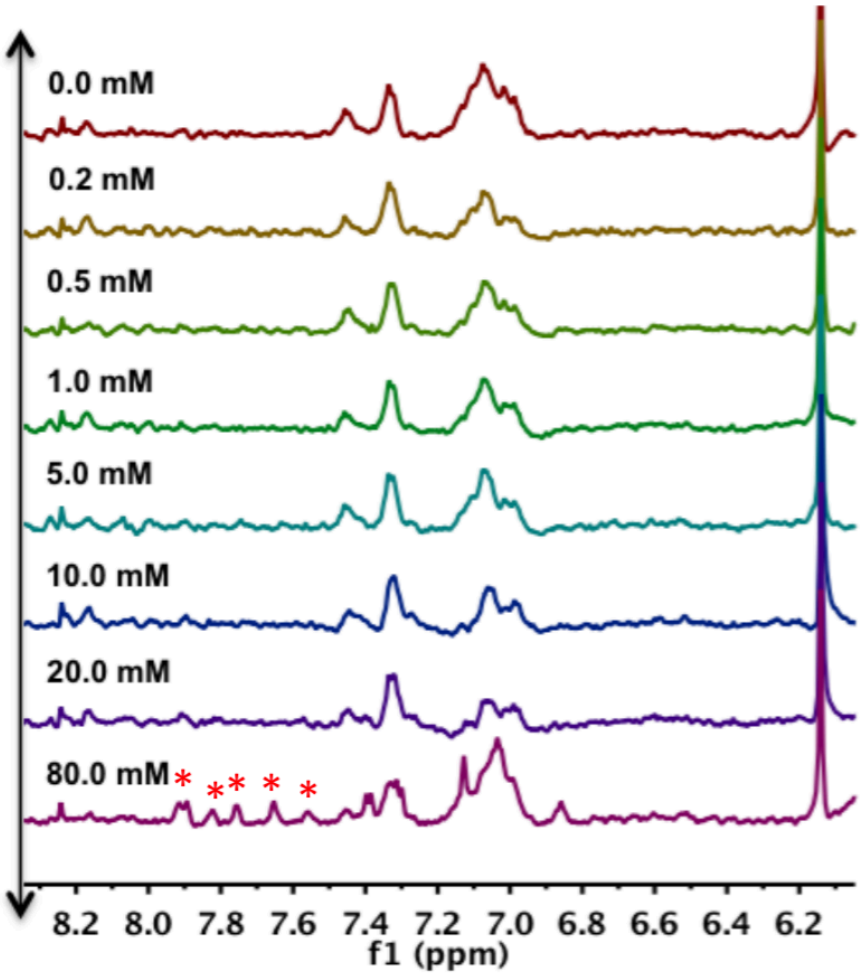

Figure 3-12. ^{1}H NMR spectra of the RRR-4W amide region with varied concentrations of K^{+}. The peak at 6.14 ppm corresponds to maleic acid used as an internal standard (0.2 mM). Sample is in 10%D_2O/NaPi buffer, pH 4.0.

We were interested in further investigating the K^{+}-induced folding of RRR-4W in a pure aqueous solution. A peptide sample was prepared at a 0.2 mM concentration in 10%D_2O in NaPi buffer at pH 4.0 and increasing concentrations of KCl were added to the solution. As seen in figure 3-12, the amide protons only emerge at high concentrations of KCl, which is likely the result of the more difficult desolvation of ions in 100% water versus a mixture of water and methanol.

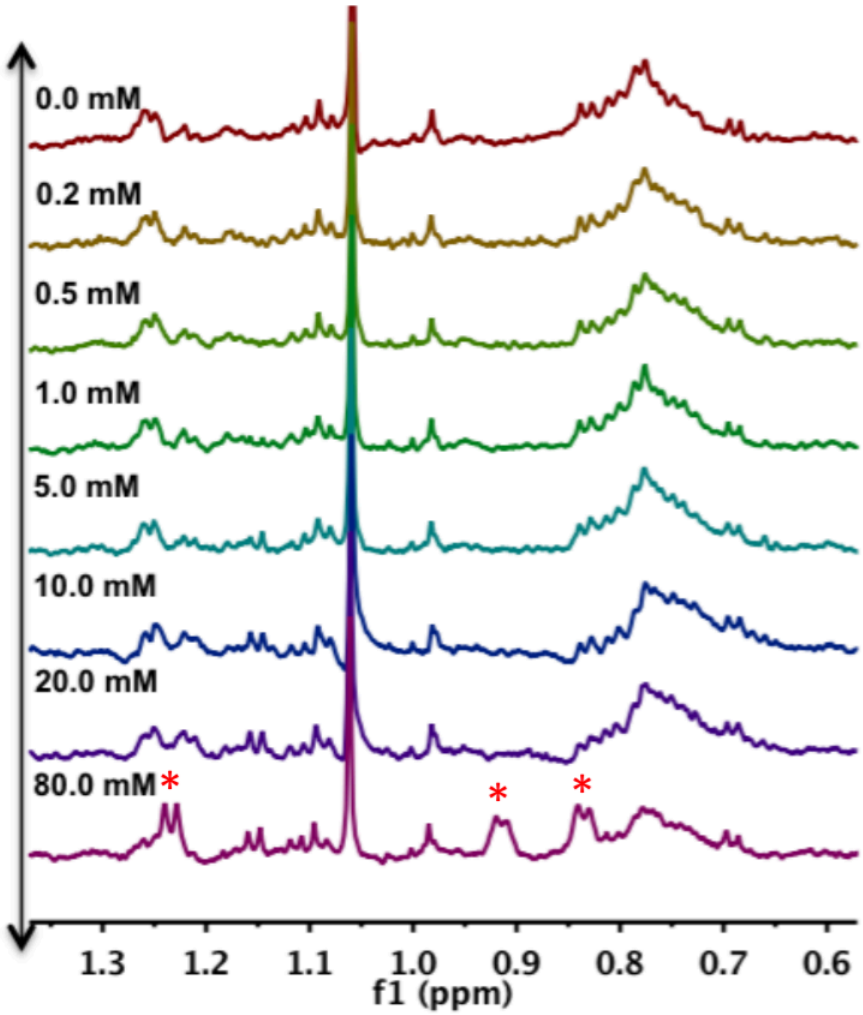

Figure 3-13. ^{1}H NMR spectra of the RRR-4W aliphatic region with varied concentrations of K^{+}. Sample is in 10%D_2O/NaPi buffer, pH 4.0.

Concomitantly, with the change observed in the amide proton region, the peaks corresponding to the Ala and Val methyl groups do not display well-resolved doublets until high concentrations of potassium. These characteristic signatures in the spectrum potentially indicate the convergence of several conformers to a single structure in solution (Figure 3-13).

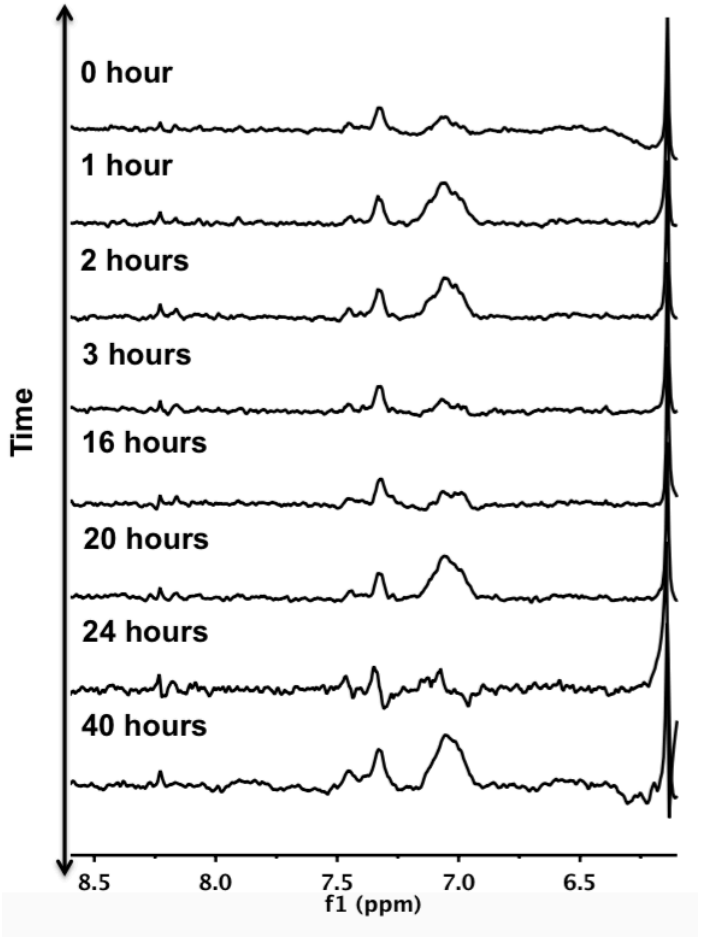

Figure 3-14. Kinetic study of RRR-4W peptide with 20 mM KCl over several hours.

RRR-4W responds to high concentrations of K^+ ions in a purely aqueous environment, whereas in a mixture of methanol and water, the K_d value is much lower. This is not surprising, due to the intrinsic difficulty in desolvating an ion in water, versus a mixture of water and organic solvent. However, to ensure that the lack of chelation at lower potassium concentrations was not due to slow kinetics, a sample of RRR-4W was prepared under the same conditions (0.2mM peptide, 10% D_2O in NaPi buffer, pH 4.0) but only 20 mM KCl was added. The sample was then monitored over a period of several hours to observe whether the amide resonances would emerge with longer incubation times. Interestingly, there was no change in the amide proton region of the NMR

spectrum, even at 40 hours, indicating that the lack of KCl binding was not due to slow kinetics, but rather the desolvation effect (Figure 3-14).

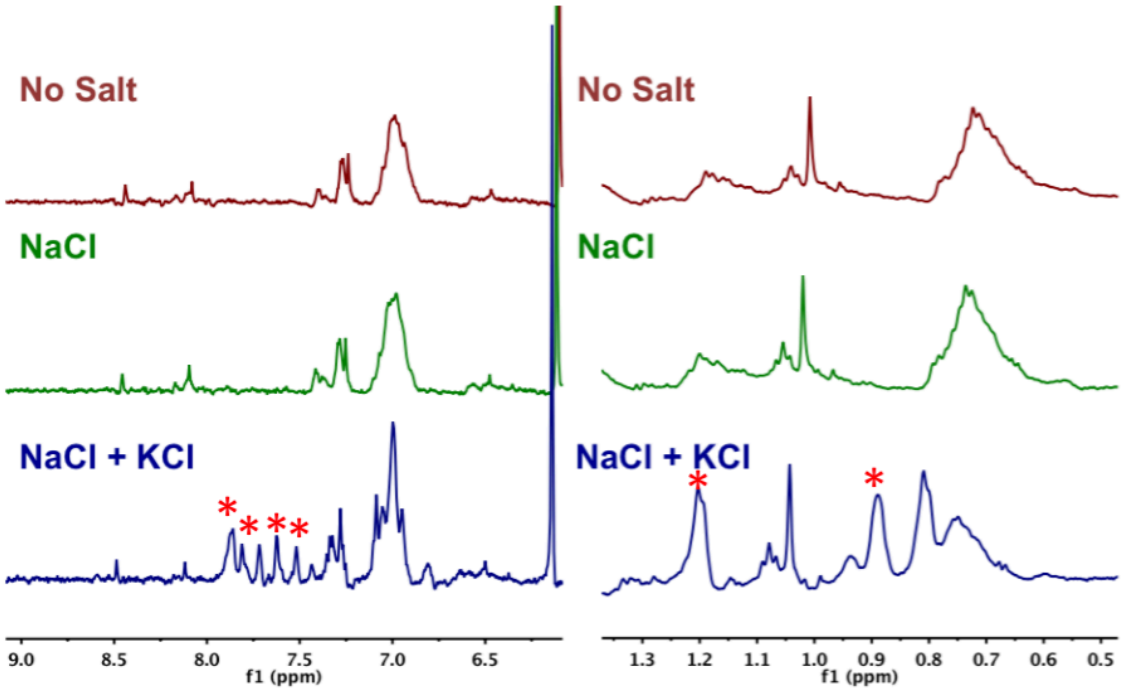

Figure 3-15. ^{1}H NMR data of amide and aliphatic regions demonstrating K^{+} selectivity of RRR-4W. Peptide sample is at 1 mM concentration in 10%D_2O/NaPi buffer, pH 4.0. Top trace shows peptide without added salt. Middle trace shows peptide with the addition of 100 mM NaCl. Bottom trace shows peptide with an additional 100 mM KCl.

Consistent with the RRR data, RRR-4W also demonstrates selectivity for K^{+} in the presence of Na^{+} ions. As seen in (Figure 3-15), a 1 mM sample of RRR-4W was prepared in 10%D_2O/NaPi buffer at pH 4.0, followed by the addition of NaCl and KCl, respectively. The amide proton resonances, as well as the Ala and Val peaks emerge only in the presence of KCl, while remaining inert towards NaCl. Previous reports on wild type prolinomycin indicate that a Na^{+} ion is too small to form a contact with all 6 carbonyl oxygen atoms, preventing the peptide from adopting a rigid, drum-like structure.

The K^+ ion, however, is large enough to form these contacts and can help induce the favorable conformation. The mutants presented above are somewhat consistent with the wild type data, since both RRR and RRR-4W exhibit selectivity for K^+ ions, as observed by the signature changes in the 1D H NMR spectra. RRR also displays dynamic behavior and can bind and dissociate a K^+ ion easily, as demonstrated by the dilution experiment in figure 3-6. Even more exciting is the fact that the metal-binding properties of prolinomycin mutants can be characterized in aqueous solution, as a result of the increased solubility of RRR and RRR-4W compared to the wild type peptide. This suggests that mutations of the non-proline side chains do not significantly alter the ability of the peptides to fold in the presence of K^+ ions. More importantly, the peptides can still adopt a rigid structure under physiologically relevant conditions, making them intriguing synthetic candidates for biological applications.

3.2.3 NMR analysis of VVV peptide

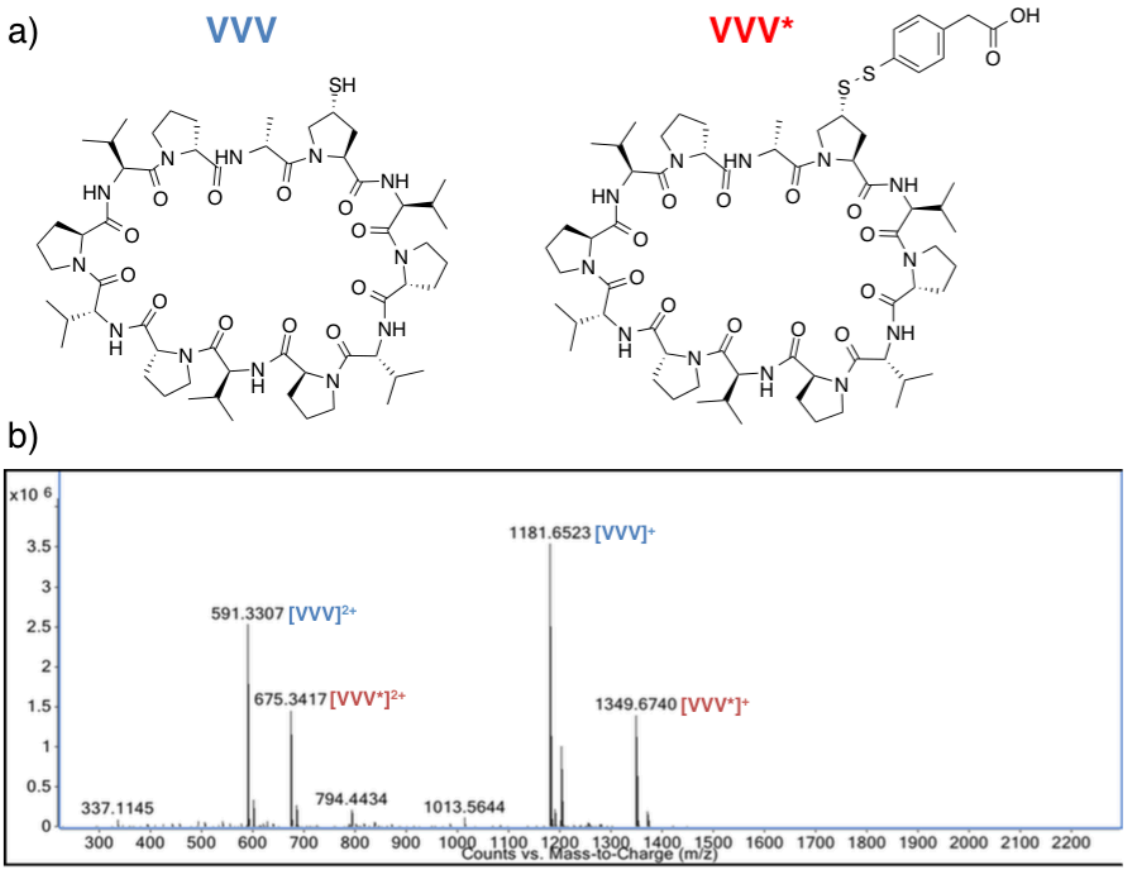

Figure 3-16. a) Structures of VVV and its adduct (VVV*) with 4-mercaptophenylacetic acid; b) ESI-MS spectrum of the purified VVV showing presence of VVV* at small quantities.

It is well established that the proline residues play a major role in the structural stability of prolinomycin, but not much can be inferred from the beta-branched, Val residues. Although they both bind K^+ under physiologically relevant conditions, RRR and RRR9W contain only two and one Val residue, respectively, which may help them to adopt more dynamic behavior in water. It was hypothesized that the multiple side chain

mutations could potentially affect the peptides behavior relative to the wild type structure; thus, a mutant called VVV was synthesized to further investigate this effect.

Due to the limitations with the proline ligation reaction, we were unable to synthesize a mutant that contains all Val residues. Instead, a single Val to Ala mutation was made at the ligation position to ensure high cyclization yields (Figure 3-16). However, during the ligation reaction, the free thiol formed a disulfide bond with 4-mercaptophenylacetic acid, which we isolated via prep hplc and further analyzed by ^{1}H NMR.

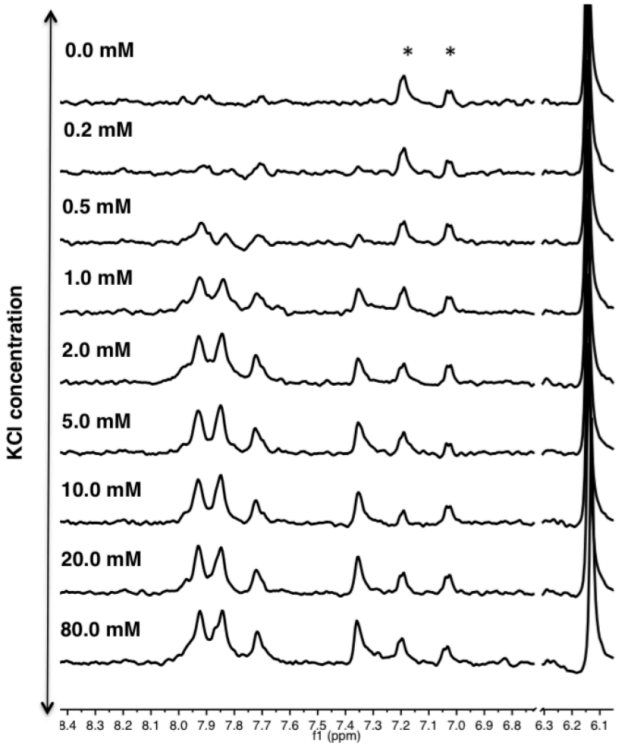

Figure 3-17. Metal-nucleated folding of prolinomycin mutants. a) ^{1}H NMR spectra of VVV with varied concentrations of K^{+}. The peak at 6.14 ppm corresponds to maleic acid used as an internal standard to (0.2 mM). The peptide sample was prepared at 0.2 mM in 10% D_2O in 1:1 CD_3OH: NaPi, pH 4.0.

The NMR data for VVV demonstrated a similar phenomenon to RRR and RRR9W, in which the amide proton resonances begin to emerge at increasing concentrations of K^+ ions (Figure 3-17).

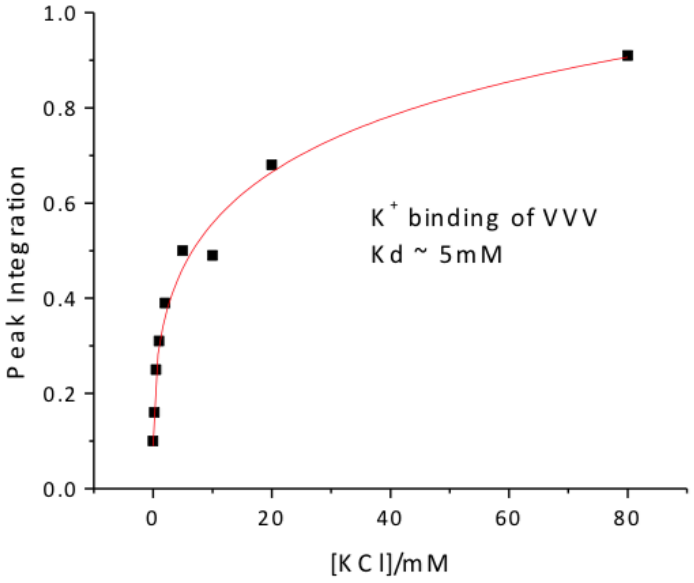

Figure 3-18. Metal-nucleated folding of prolinomycin mutants. Titration curve generated by plotting the peak integration at 7.35 ppm against KCl concentration.

Surprisingly, VVV exhibited a similar K_d value (5 mM) to the other mutants, as assessed by plotting the integration of a single peak versus the KCl concentration, which demonstrates that mutations to the Val residues do not significantly affect the peptides ability to bind potassium (Figure 3-18). As a result, it can be assumed that the beta-branched side chains do not significantly contribute to structure as much as the proline residues. Moreover, all prolinomycin analogues that were analyzed are still able to bind potassium at physiologically relevant concentrations, indicating that the scaffold is tolerant to multiple side chain mutations without compromising its metal-induced folding

effect. This opens up the potential for designing prolinomycin mutants with diverse functions for future biological applications.

3.2.4 NMR analysis of dethiolated RRR peptide

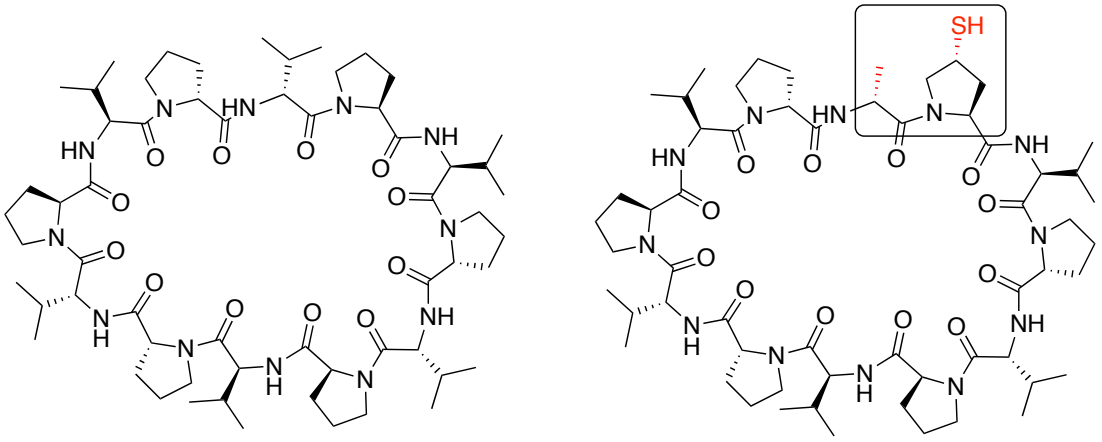

Figure 3-19. Wild type prolinomycin (left) and VVV analogue containing a Val to Ala mutation and a thiol from the ligation (right).

Although VVV, RRR and RRR-4W exhibit very similar behavior in water, there is a still a significant discrepancy between the reported K_d value of wild type prolinomycin and the experimentally determined K_d value of our mutants. The mutants presented above contain two fundamental structural differences from wild type prolinomycin (Figure 3-19). First, prolinomycin displays 6 Val residues within its sequences, whereas VVV has only five, leaving a single Ala residue. Specifically, the Val to Ala mutation could offer more flexibility to the structure, allowing the peptide to adopt lower energy conformers in its uncomplexed form. This, in turn, would lower its affinity for K^+ under physiological conditions because there would be less of a driving force to complex the metal. If this phenomenon were true, then we would expect to see worse binding for RRR and RRR-4W in comparison to VVV. Since the experimentally

determined K_d value for VVV and RRR are similar in the low mM range, it seems that mutations to non-proline residues do not seem to have a significant impact on metal binding.

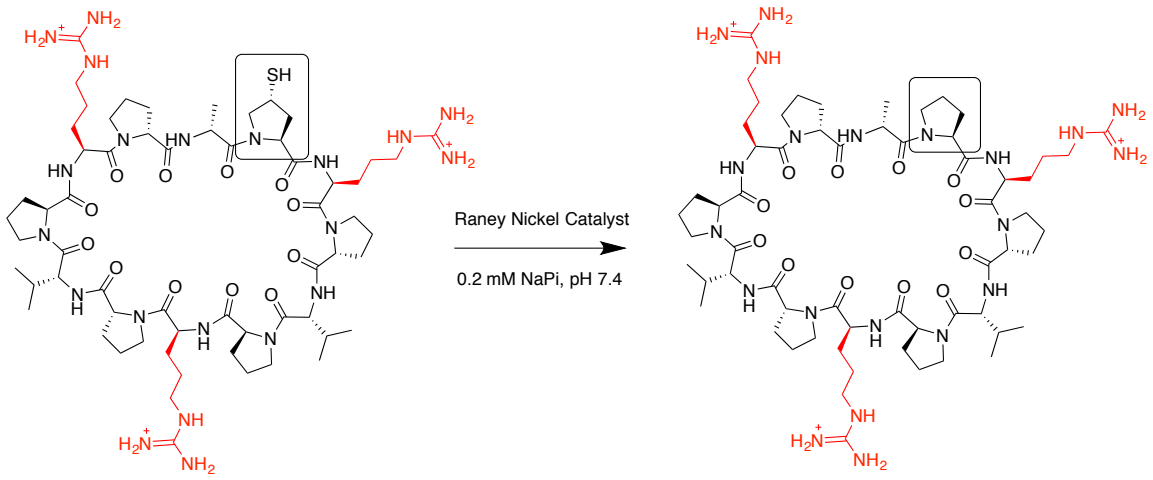

Scheme 3-3. Raney nickel reduction of RRR to remove the thiol.

The second fundamental difference between wild type prolinomycin and the structural analogues is the presence of a thiol on one proline residue, which may cause the peptide to adopt alternative conformations that would affect its ability to fold. To test this hypothesis, RRR was subjected to the raney nickel reduction conditions to yield the dethiolated cyclic peptide in decent yields (Scheme 3-3). After RP-HPLC purification, a sample of the peptide, called RRR-SH, was prepared at a 0.2 mM concentration in 10% D_2O in a 1:1 mixture of CD_3OH and NaPi buffer at pH 4.0. A KCl titration was performed by NMR spectroscopy to directly compare the K_d values of RRR versus RRR-SH.

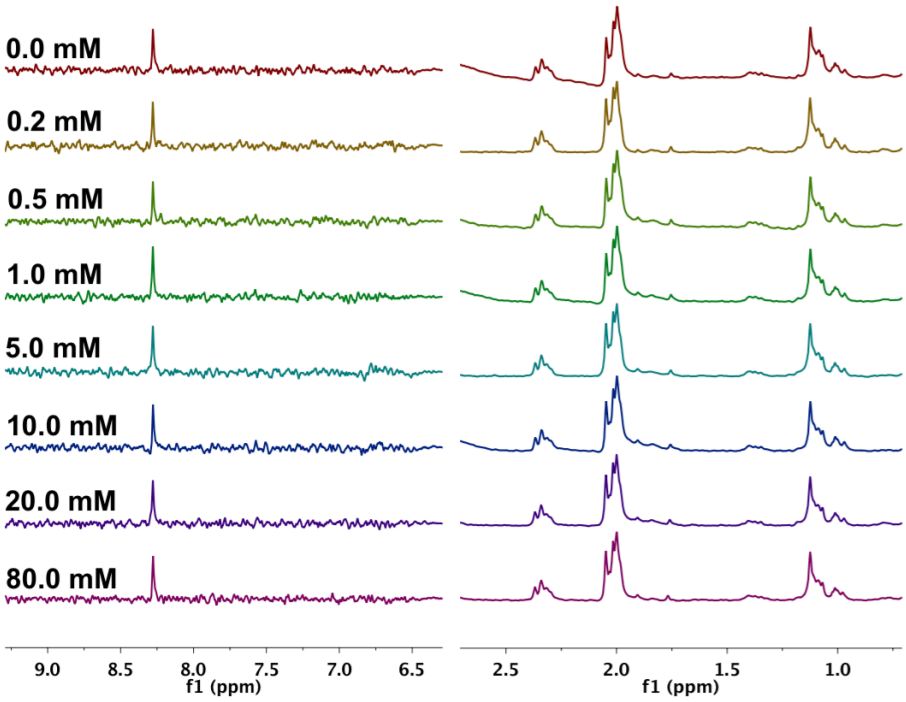

Figure 3-20. ^{1}H NMR KCl titration of RRR-SH in 10% D_2O in 1:1 CD_3OH: NaPi, pH 4.0.

Unfortunately, during the KCl titration assay, the NMR spectrum showed no distinct changes, especially in the amide proton region, indicating that K^+ does not stabilize the peptide (Figure 3-20). Our next approach was to evade the proline ligation reaction altogether and synthesize the peptide through a side-chain immobilized on-resin head to tail cyclization strategy. Unfortunately, due to the harsh coupling conditions, several isomers of the peptide were isolated, making it difficult to determine which one possessed the correct stereochemistry. Given these challenges, it was impossible to assess the effect of K^+ on the dethiolated peptides; thus, further investigations into the K_d value discrepancy between prolinomycin and its mutants will be needed in the future.

3.2.4 Vesicle-based titration assay to assess metal selectivity

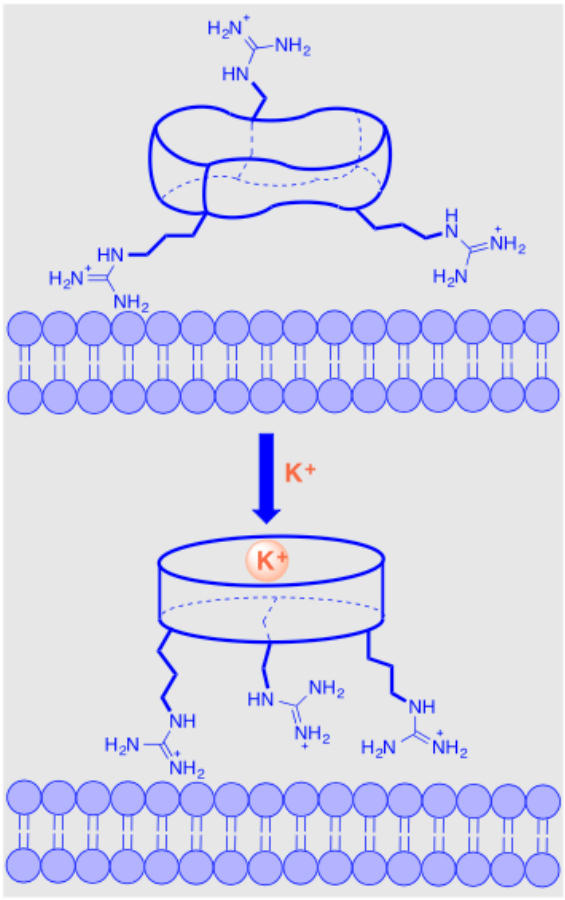

Figure 3-21. Illustration of K^+-assisted folding of RRR and binding to anionic membranes.

^{1}H NMR spectroscopy of the prolinomycin mutants revealed that K^+ ions induce a favorable conformational change to the peptides under physiologically relevant conditions. Some of the characteristic signatures include the emergence of amide proton resonances with increasing KCl concentration, as well as the sharpening of the doublets, which correspond to Val and Ala residues in the aliphatic region of the spectrum. More importantly, this phenomenon occurs exclusively in the presence of KCl, as the addition of an equal concentration of NaCl renders the peptide inert. 2D NMR experiments also revealed that in the presence of KCl, interactions between the α proton of Arg and the

side chain of Val occur, which is consistent with the β-turns observed in the crystal structure of wild type prolinomycin.

Overwhelming evidence from the NMR studies suggests that in the presence of K^+ ions, prolinomycin mutants can adopt a rigid conformation under physiological conditions in a similar manner to the wild type peptide. It was hypothesized that the mutants could also display analogous behaviors in the presence of a target, such as a membrane. For example, RRR would bind K^+, forcing the cyclic peptide to adopt a rigid conformer that helps to display the non-proline side chains in a specific direction (Figure 3-21). This metal-induced folding effect could then enhance the ability of the peptide to bind a target with high potency.

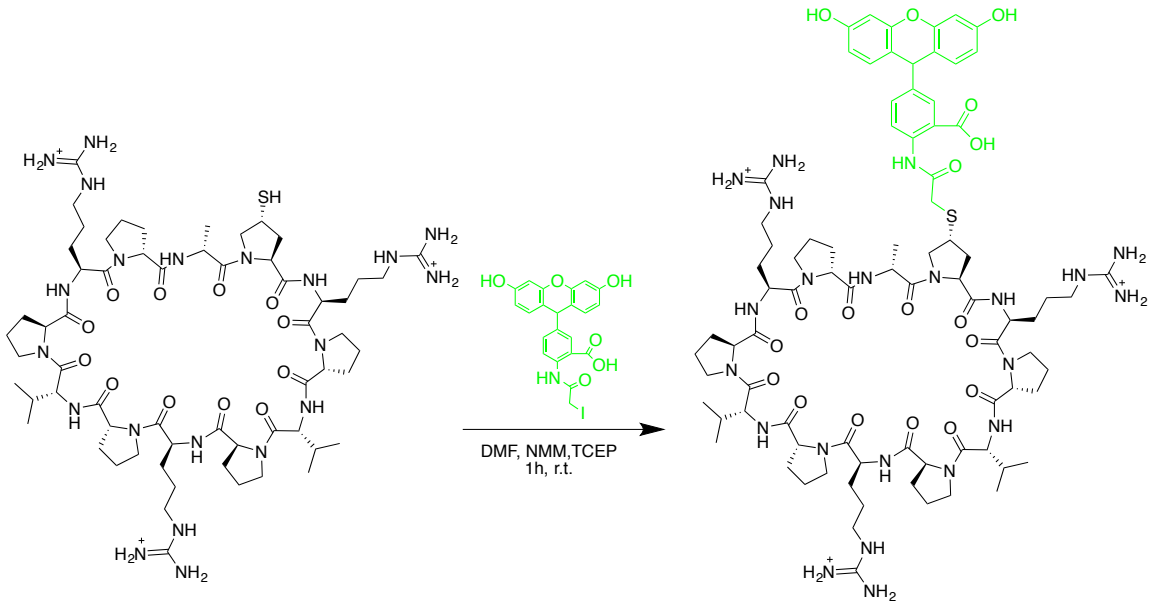

Scheme 3-4. Fluorescein labeling of cyclic peptide.

We chose to assess the activity of the prolinomycin mutants towards model membrane systems using a fluorescence anisotropy assay. The cyclic peptides easily were labeled using fluorescein-5-iodoacetamide in the presence of TCEP and a mild base, N-methyl morpholine, in DMF (Scheme 3-4). The labeling was complete in less than an

hour and the resulting peptides were purified by RP-HPLC for further analysis. Peptide masses can be found in table 3-2 below.

Table 3-2. Sequences and masses of fluorophore-labeled cyclic peptides

Mutant	Entry In Figure S7	Calculated m/z
KKK-Fluorescein	**a**	1656.84$[M]^{+}$, 828.42$[M]^{2+}$, 552.28$[M]^{3+}$, 414.21$[M]^{4+}$
RRR-Fluorescein	**b**	1740.86$[M]^{+}$, 870.43$[M]^{2+}$, 580.28$[M]^{3+}$, 435.21$[M]^{4+}$
VRR-4R-Fluorescein	**c**	1740.86$[M]^{+}$, 870.43$[M]^{2+}$, 580.28$[M]^{3+}$, 435.21$[M]^{4+}$
RRR-4W-Fluorescein	**d**	1827.87$[M]^{+}$, 913.935$[M]^{2+}$, 609.29$[M]^{3+}$, 456.96$[M]^{4+}$
RRR-Alexa	**e**	2051.89$[M]^{+}$, 1025.945$[M]^{2+}$, 683.96$[M]^{3+}$, 512.97$[M]^{4+}$
RR(ObK)-Alexa	**f**	2238.66$[M]^{+}$, 1119.335$[M]^{2+}$, 746.22$[M]^{3+}$, 559.66$[M]^{4+}$
RR(TpK)-Alexa	**g**	2278.64$[M]^{+}$, 1139.32$[M]^{2+}$, 759.54$[M]^{3+}$, 569.66$[M]^{4+}$

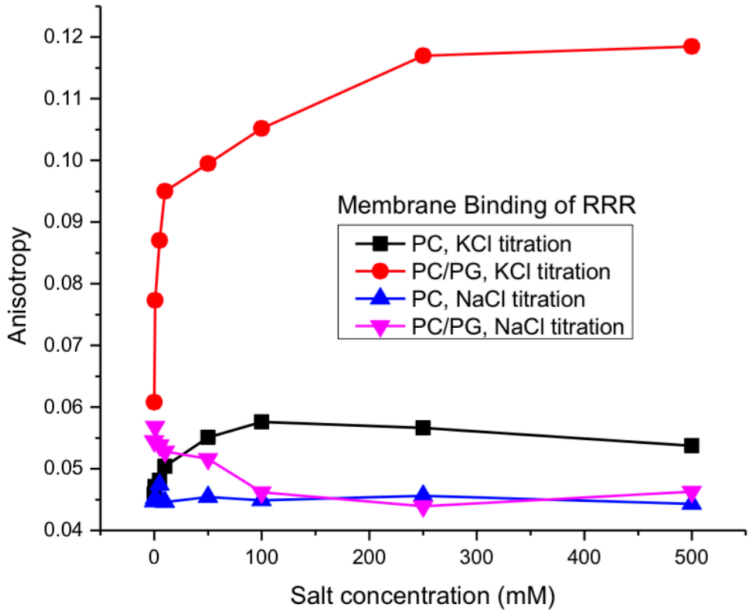

Figure 3-22. Titration experiments highlighting the differential effects between KCl and NaCl on RRR to partition into membranes. SUV's were used.

Although not an optimal model membrane, vesicles can be formulated to contain precise compositions of lipids, which can provide information on how selective each peptide is for a given membrane lipid. We hypothesized that prolinomycin mutants would fold into a "drum-like" structure in the presence of K^+, ultimately allowing the peptide to display its side chains in a preorganized manner for target binding. Consistent with the NMR data, RRR partitions towards anionic membrane surfaces in the presence of KCl, while NaCl induces no effect, as assessed by the in vitro vesicle-based assay (Figure 3-22). Although this experimental set-up does not allow the direct measurement of metal chelation to the peptide, it can be assumed that RRR adopts a structure similar to prolinomycin under these conditions, which helps it to bind the membrane target. More interestingly, the cationic nature of RRR allows it to remain selective for the anionic lipid, PG, which is a key feature of bacterial cell membranes, while little to no binding is

observed towards PC, which is found predominantly on the surface of mammalian cell membranes.

3.2.4 Vesicle-based titration assay to study side chain preorganization

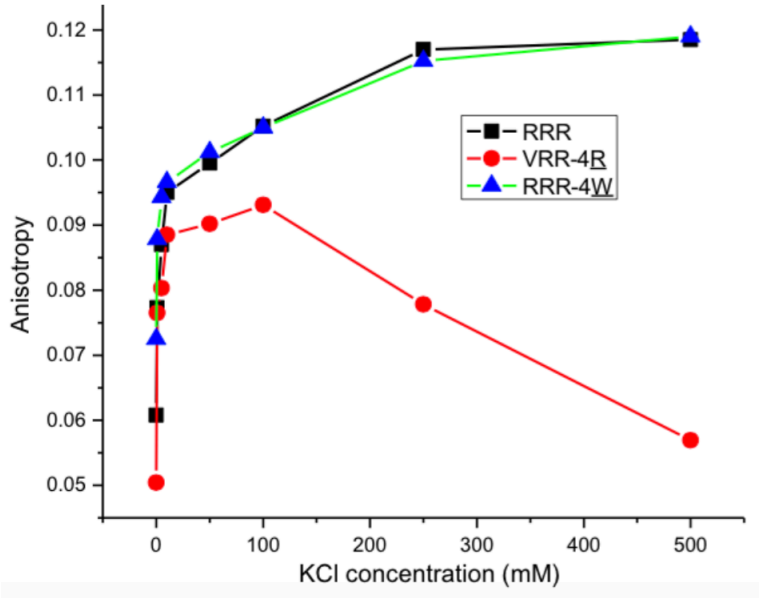

Figure 3-23. K^+-dependent membrane binding of the prolinomycin mutants. Comparison of the K^+-induced membrane binding of several prolinomycin mutants.

After establishing that RRR remains selective towards anionic membranes exclusively in the presence of K^+ ions, we sought to carry out a mechanistic investigation to study how the mutants interact with the membrane. RRR-4W contains three Arg residues on one deck of the peptide, similar to RRR but also contains a Val to Trp mutation on the opposite deck. It was initially hypothesized that the introduction of an aromatic side chain on the opposite deck could act as a membrane insertion motif, rendering the sequence more potent than RRR. On the contrary, RRR-4W exhibited nearly the exact behavior towards anionic lipids as RRR, indicating that a mutation at the position has little to no effect on the binding affinity (Figure 3-23). Perhaps more

interesting, however, is the VRR-4R mutant, which displays the exact amino acid composition of RRR, except one of the Arg residues is located on the opposite deck of the peptide. This permutated sequence displayed surprisingly lower affinity towards anionic membranes at higher concentrations of K^+. One explanation could be that a high concentration of K^+ ions screens out the interactions between VRR-4R and the membrane, again, reinforcing that the cooperative action of all side chains on the prolinomycin scaffold are required for potent target binding.

To further test the mechanism of membrane interaction, two additional mutants were synthesized containing a hydrophobic residue on the same face as the Arg. Interestingly, both RRBip and RRNp2 displayed the highest observed anisotropy values in this library of peptides, indicating that the preorganization of side chains on the same face of the scaffold is critical for potent target binding (Figure 3-24). However, the membrane-binding activity seemed to be independent of the salt in solution, indicating the hydrophobic anchors of the peptides are dominating their membrane binding behavior.

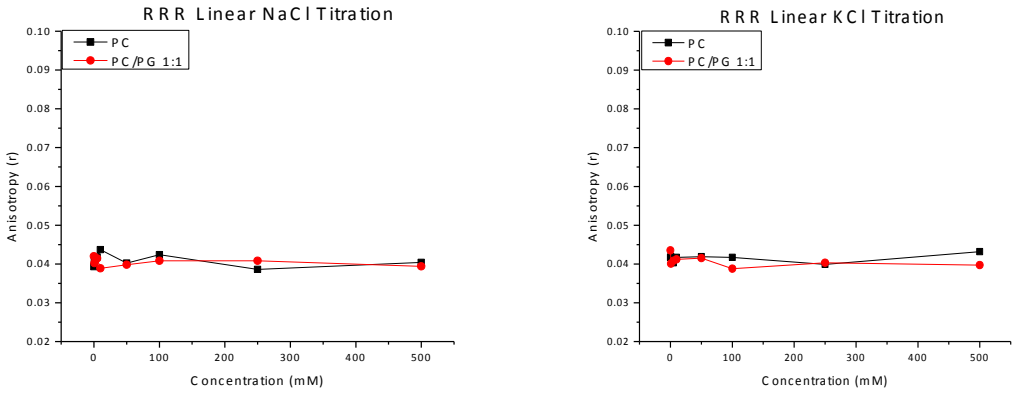

Figure 3-24. RRR linear control peptide (100 nM) binding to SUVs (250 μM) with increasing amounts of NaCl (left) and KCl (right) added.

During the proline ligation reaction, a small amount of the Nbz linear peptide hydrolyzes and can be isolated during the RP-HPLC purification step. After fluorophore labeling, the peptide was subjected to the anisotropy experiment to assess whether the sheer amino acid composition in solution displays any activity towards anionic membranes. Not surprisingly, the linear RRR was inactive against vesicles containing any lipid composition, indicating that the Arg residues are only effective binders when efficiently preorganized in a specific manner on the scaffold (Figure 3-25).

3.2.4 Bacterial cell staining of RRR mutant

The vesicle-based assay, in combination with the NMR experiments, suggests that the prolinomycin mutants behave quite well under physiological conditions. The ability of the peptide to remain selective for K^+ ions under both experimental conditions further supports the claim that introducing side chain mutations at the non-proline residues does not negatively impact the folding behavior. Moreover, this folding behavior helps the peptides to become effective and potent receptors for a membrane target in water. At this

point, we were interested in examinining whether this phenomenon remains true on cell surfaces.

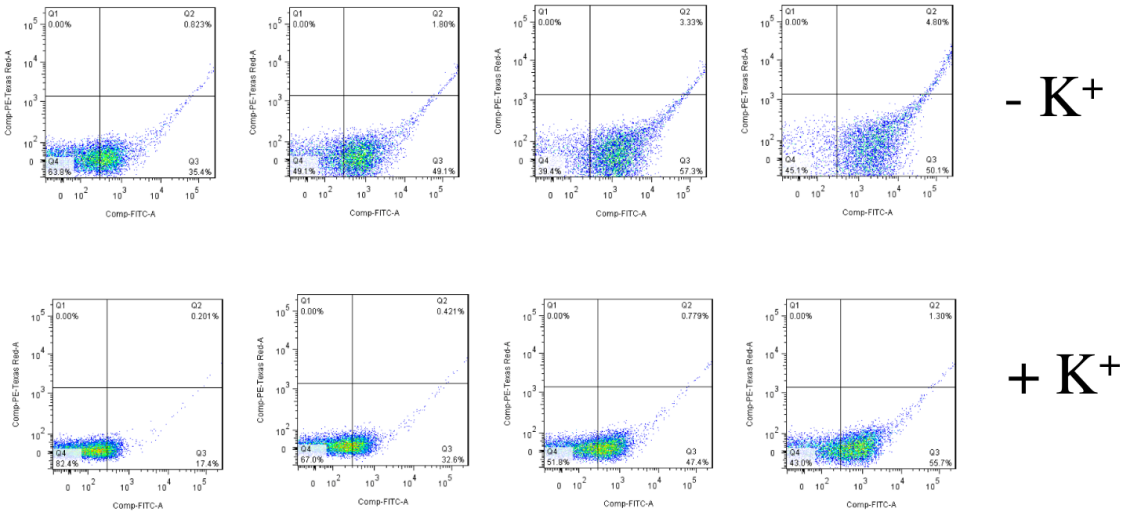

Figure 3-25. Flow cytometry results for RRR at concentrations of 100 nM, 250 nM, 500 nM and 1000 nM (left to right).

Despite the high selectivity for RRR to bind anionic model membranes in the presence of K^+ ions, the peptide was unable to partition into bacterial cell membranes. This is not surprising, given that the high membrane curvature of SUV's can generally illicit stronger receptor-ligand interactions due to the exposure of hydrophobic pockets on the membrane surface. This intrinsic property of SUV vesicles offers the extra driving force, which helps otherwise weak binders to be more active towards a target (Figure 3-26).

3.2.5 Design of hydrophobic mutants of cell staining

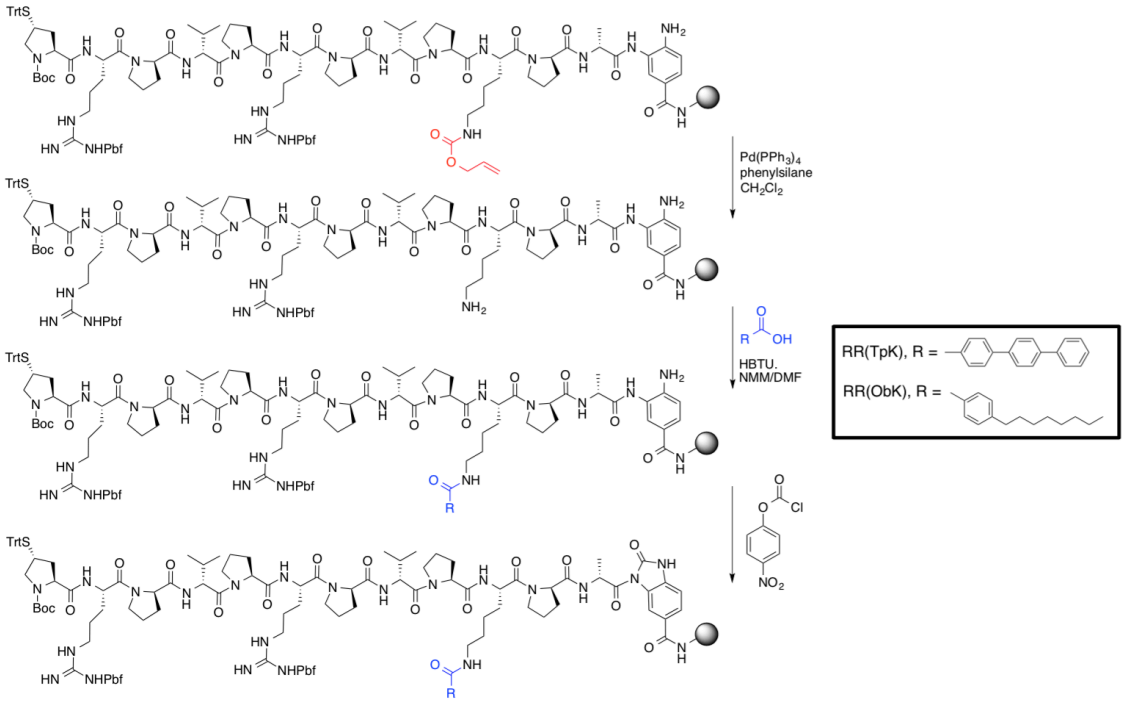

Scheme 3-5. Synthesis of hydrophobic mutants using on resin coupling strategy.

We decided to revise the sequence to include mutations with higher LogP values in order to maximize the hydrophobic driving force for binding. As demonstrated in Scheme 3-5, both an octylbenzyl and terphenyl functional group was incorporating on to RRR using an on resin coupling strategy, in which an alloc protected Lys residue was incorporated in lieu of one Arg. After synthesis of the linear sequence, the Lys can be orthogonally deprotected and coupled to either the 4-octylbenzyl or terphenyl acid deriavtives to afford the linear peptide, which would then be globally deprotected and cleaved from resin, then subjected to the proline ligation reaction to afford the cyclic peptide. We chose to install these specific hydrophobic moieties based on their relatively high LogP values compared to Bip, which exhibited low activity in the cell-based assays.

Additionally, the structural diversity between a terphenyl and an octylbenzyl residue would also provide more insight into the mechanism of binding.

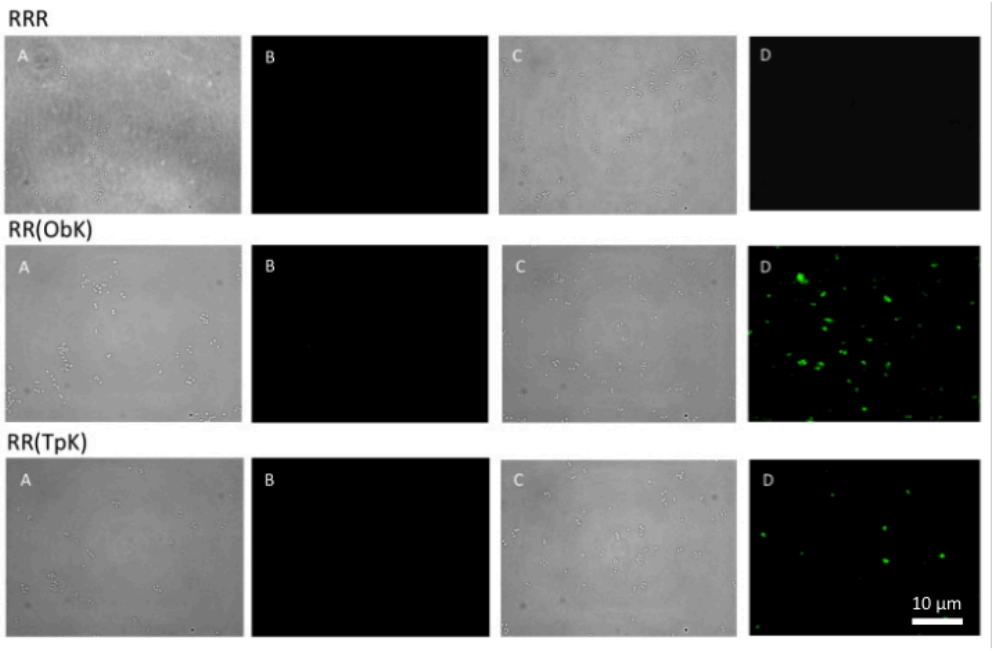

Figure 3-26. K^+-dependent staining of *S. aureus* cells by prolinomycin mutants. a) microscopy results showing cell staining only in the presence of K^+; (A) Phase contrast with no salt; (B) FITC channel with no salt; (C) Phase contrast with 30 mM KCl; (D) FITC channel with 30 mM KCl.

As assessed by fluorescence microscopy, the two mutants, called RR(ObK) and RR(TpK), were able to partition into *S. aureus* cell membranes exclusively in the presence of K^+ ions, while little to no staining was observed in the absence of the salt (Figure 3-28). Moreover, even though both mutants displayed similar LogP values, the aliphatic chain seemed to help RRR partition much better onto bacterial cells than the aromatic residue.

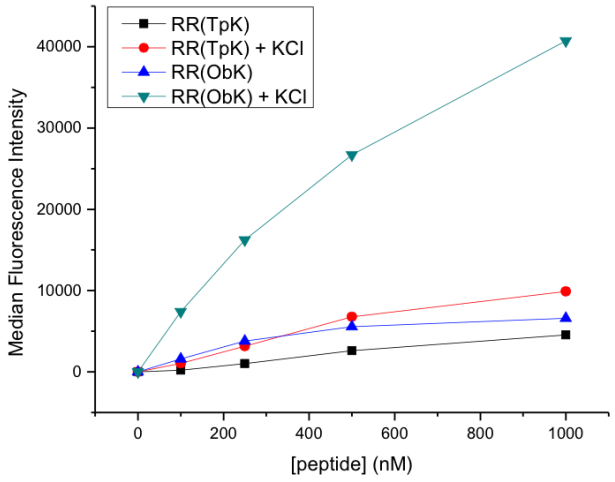

Figure 3-27. Flow cytometry results showing that the bacterial cell staining by RR(ObK) and RR(TpK) is enhanced by the addition of KCl.

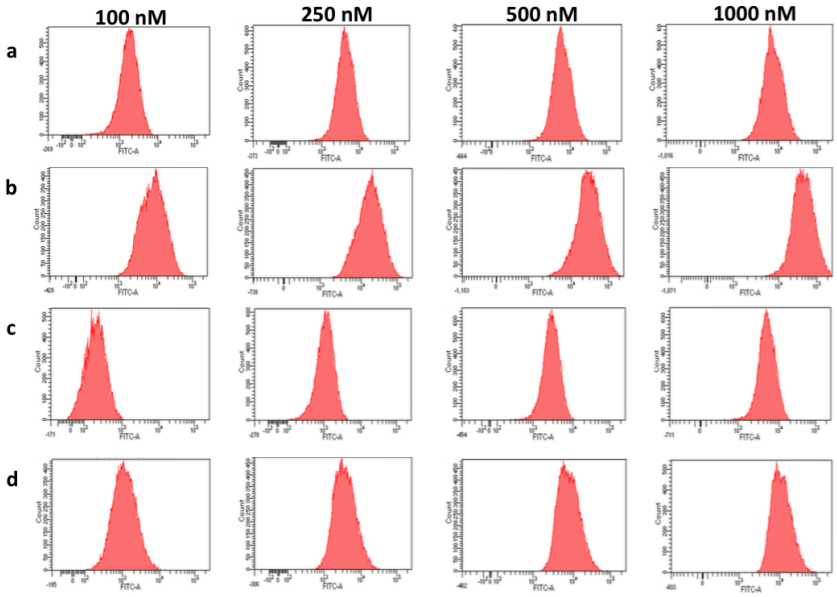

Figure 3-28. Flow cytometry histograms showing K^+-dependent staining of *S. aureus* cells by prolinomycin mutants at increasing peptide concentrations. (a) RR(ObK) no salt; (b) RR(ObK) + KCl; (c) RR(TpK) no salt; (d) RR(TpK) + KCl.

The results were further confirmed by flow cytometry analysis. Plotting the fluorescence intensities versus peptide concentrations generates a plot which suggests that RR(ObK) is the most active mutants, staining *S. aureus* cells at low nanomolar concentrations, exclusively in the presence of K^+ ions (Figure 3-29). The enhanced staining of RR(ObK) in the presence of KCl is further exemplified by the histograms (Figure 3-30).

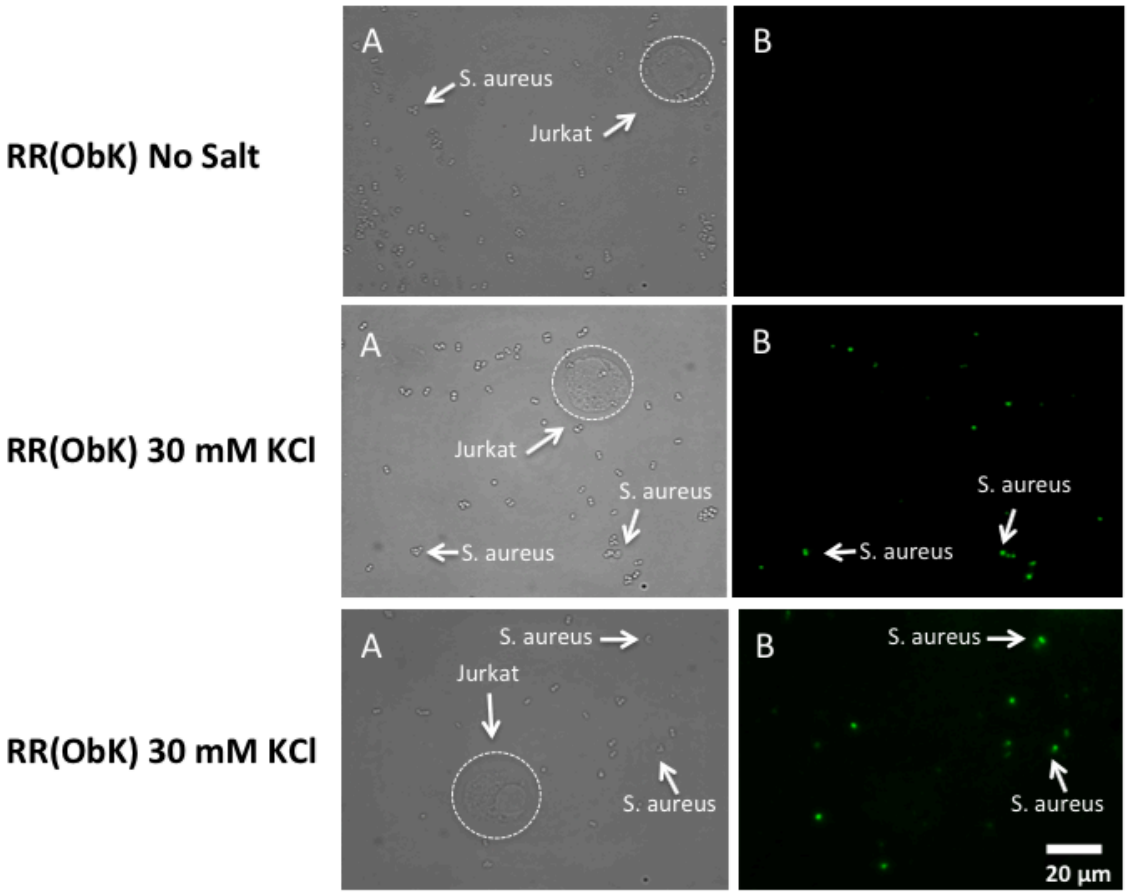

Figure 3-29. Co-culture demonstrating the K^+-dependent staining of S. aureus cells by RR(ObK) in the presence of Jurkat cells.

Additionally, the peptide RR(ObK) demonstrated superb selectivity for bacterial cells over mammalian cells, while remaining active only in the presence of KCl, as seen with the co-culture microscopy experiment (Figure 3-31). Collectively, these results demonstrate that the metal-induced folding of prolinomycin mutants help induce a favorable structure for target binding, as seen with the NMR, anisotropy and cell-based assays. Additionally, the selective behavior of the cationic sequences in the presence of KCl demonstrates that more elegant receptors can be designed for target binding in the future.

3.3 Conclusion

Overall, we've demonstrated that wild type prolinomycin is tolerant to side chain mutations of the non-proline residues and is synthetically accessible through the optimized proline ligation protocol. A thorough NMR analysis of several prolinomycin sequences suggests that this scaffold is tolerant to chemical modification of the side chain residues. Moreover, the mutants display very similar behavior in the presence of K^+ ions, suggesting that these peptides behave well under physiologically relevant conditions. This has been demonstrated by an in vitro, vesicle-based assay, which shows that the cationic RRR and its analogues remain selective for anionic membrane lipids, as well as a cell-based assay demonstrating their selectivity towards bacterial cell membranes. We hope that this scaffold will be a powerful tool to carry out a number of biologically relevant applications.

Experimental Procedures

I. General Methods

Dawson Dbz resin and HBTU were purchased from Novabiochem (San Diego, CA). Boc-cis-4-hydroxy-L-proline and all Fmoc-protected amino acids were purchased from Chem-Impex Int'l (Wood Dale, IL). Alexa Fluor 488 C5 maleimide was purchased from BD Biosciences (Chicago, IL). Fluorescein-5-iodoacetamide was purchased from Marker Gene (Eugene, OR). The phospholipids were purchased from Avanti Polar Lipids (Alabaster, AL). Methanol-d3 was purchased from Acros Organics (Geel, Belgium) and all other NMR solvents were purchased from Cambridge Isotopes (Tewksbury, MA). 4-nitrophenylchloroformate, 4-mercaptophenylacetic acid and all other chemicals were purchased from Sigma Aldrich (St. Louis, MO). Peptide synthesis was carried out on a Tribute peptide synthesizer (Protein Technologies, Tuscon, AZ). HPLC purification of peptides was carried out on a Waters 2489 Prep-LC System (Milford, MA). ^{1}H NMR data were collected on a VNMRS 500 MHz NMR spectrometer (Varian NMR Inc.) and LC-MS data were collected on an Agilent 1260/6230 LC-MS (Agilent Technologies, Santa Clara, CA). Peptide concentration measurements were performed on a Nanodrop 2000c Spectrophotometer (Thermo Fisher Scientific, Waltham, MA).

II. Peptide synthesis and characterization

N-Boc-(2S,4R)-tPro(Trt)-OH was synthesized according to a reported procedure. The prolinomycin linear precursor peptides were synthesized through Fmoc/tBu chemistry using the preloaded Dawson Dbz resin (3-(Fmoc-amino)-4-aminobenzoyl AM

resin, Novabiochem) as the solid support. The syntheses were carried out on a 0.05 mmole scale with 5 equivalents of the Fmoc-protected natural amino acids used for the coupling reaction. Incorporation of N-Boc-(2S,4R)-tPro(Trt)-OH was accomplished using 2 equivalents of the unnatural amino acid at an extended coupling time of 2 hours. RR(TpK) and RR(ObK) mutants were synthesized by incorporating Fmoc-Lys(alloc)-OH in place of Fmoc-Arg(Pbf)-OH, followed by orthogonal deprotection of the alloc group using a mixture of 60 mg tetrakis(triphenylphosphine)-palladium ($Pd(PPh_3)_4$) and 0.3 mL phenylsilane in 2 mL dichloromethane. The coupling step was accomplished using HBTU (1 equivalent) to activate either p-Terphenyl-4-carboxylic acid or 4-Octylbenzoic acid to afford the RR(TpK) and RR(ObK) linear peptides, respectively. Conversion of the Dbz resin to the Nbz moiety was accomplished by mixing the resin with 5 equivalents of 4-nitrophenylchloroformate in DCM (3mL) for 1 hour, followed by 20 min incubation with 3 mL of 0.5 M NMM in DMF. The peptides were cleaved off the resin and globally deprotected with reagent K (80% TFA, 5% H_2O, 2.5% EDT, 5% thioanisole and 7.5% phenol). The crude peptides were found to display good purity and directly subjected to the proline ligation reaction without purification.

The proline ligation reaction was accomplished by dissolving the crude, linear peptide (2-5 mM) in a mixture of DMF and ligation buffer (0.2 M sodium phosphate, 3 M guanidinium chloride, 20 mM 4-mercaptophenylacetic acid, pH 8) and allowing the reaction to proceed overnight. Upon completion of the reaction, judged by LC-MS analysis, the reaction was acidified with Buffer A (0.1% TFA in H_2O) and then purified by RP-HPLC (Waters Prep LC, Jupiter C18 Column) to afford the cyclic peptide in 40-50% yields (calculated against the crude peptide mass). According to LC-MS analysis, all

peptides except the VVV mutant displayed high purity (>95%) and clean mass-spec data that correspond to the desired product. The VVV peptide after purification showed a small amount of disulfide adduct with 4-mercaptophenylacetic acid. This material was subjected to NMR analysis without further purification as the adduct formation is not expected to interfere with the K^+ binding behavior of the peptide.

III. NMR characterization of prolinomycin mutants

All peptide samples for NMR analysis were prepared in a 1:1 mixture of CD_3OH and 50 mM sodium phosphate buffer, pH 6.0 with overall 10% D_2O by volume. Peptide concentrations were 0.2 mM and an internal standard (maleic acid) was included in each sample at a concentration of 0.2 mM. ^1H NMR spectra of the prolinomycin mutants were collected on a Varian INOVA 500 MHz NMR spectrometer. Water suppression was accomplished using a PRESAT experiment to purge and subtract the water peak.

For the salt titration experiment, NMR spectra were recorded after sequential addition of KCl into the sample. The metal-reversibility experiment was accomplished by adding 5 mM KCl to a 2 mM peptide (and 2 mM maleic acid) sample, followed by a 10 x dilution to 0.5 mM KCl and 0.2 mM peptide. NMR data were processed using MestReNova (Mestrelab Research S. L., Spain).

IV. Synthesis of fluorophore-labeled peptides

The fluorescein conjugates of the prolinomycin mutants were synthesized using fluorescein-5-iodoacetamide (Marker Gene, Eugene, OR) as the labeling reagent. The peptide (1 mg) was dissolved in 300 μL of DMF and TCEP (7.5 μL of a 100 mM stock in H_2O) was added to reduce any disulfide bonds. N-methylmorpholine (20 μL) and fluorescein-5-iodoacetamide (150 μL of a 5 mM stock in DMF) were added and the reaction was left to sit in the dark for 1 hour. The reaction was diluted with Buffer A (0.1% TFA in H_2O) and purified by RP-HPLC (Waters Prep LC, Jupiter C18 Column). Alexa Fluor 488 (AF488) labeling of the peptides was accomplished by following a similar protocol with AF488 C5 maleimide (100 μL of a 1 mM stock in DMF) as the labeling reagent. The fluorescein and AF488 labeled peptides were confirmed by LC-MS.

The linear control peptide, RRR-OH was synthesized through hydrolysis of the Nbz RRR linear precursor. The crude peptide was dissolved in 2 M NaOH and allowed to sit overnight. The sample was lyophilized and directly labeled with fluorescein-5-iodoacetamide, following the protocol stated above. The peptide was purified by RP-HPLC (Waters Prep LC, Jupiter C18 Column) and the purity and mass confirmed by LC-MS.

V. Vesicle binding assay using fluorescence anisotropy

Small unilamellar vesicles (SUVs) were prepared by dissolving the desired phospholipids in chloroform, then mixing the stocks to get the desired ratios. Chloroform was evaporated and the lipid mixtures were re-suspended in 50 mM Tris buffer, pH 7.4 and left to sit for 1 hour. The lipid suspensions were ultra-sonicated using a 20 second pulse for 20 minutes, then filtered. The Steward assay was used to determine the concentrations of the resulting liposome stocks. This is a colorimetric method that is based on the complex formation between phospholipids and ammonium ferrothiocyanate. Briefly, 2 mL of 0.1 M $NH_4Fe(SCN)_4$ in aqueous solution was added to 2 mL of chloroform containing a small volume of the phospholipid stock. The resulting mixture was vortexed for 1 min and then centrifuged at 5,000 rpm for 5 min. The UV absorption of the chloroform layer containing the phospholipids was measured at 465 nm and the concentrations of the vesicles were calculated using the reported extinction coefficient of PC (7960 $M^{-1}cm^{-1}$).

VI. Vesicle binding assay using fluorescence anisotropy

Stock concentrations of fluorescein-labeled peptides were measured by recording the UV-Vis absorbance at 495 nm (ε = 80,000 $M^{-1}\cdot cm^{-1}$). Fluorescence anisotropy experiments were carried out on a Cary Eclipse Spectrophotometer (Agilent Technologies) with a 10 mm path length quartz cuvette. A G factor of 1.4213 was calculated for fluorescein prior to the titration experiments. The fluorescein-labeled cyclic peptides were dissolved in DMF to give a 1 mM stock, which was diluted (with 50 mM Tris buffer, pH 7.4) to 100 nM peptide concentration for the vesicle binding

measurement. The samples were excited at 493 nm and their emissions were monitored at 520 nm to generate the anisotropy values. Metal dependence was measured by titrating increasing amounts of NaCl or KCl to a peptide sample containing 250 μM SUV's, while membrane binding was assessed by adding increasing amounts of SUV's into a peptide sample containing 20 mM salt. Anisotropy values were plotted against liposome or salt concentrations to generate the binding curves.

VII. Cell culture experiments

Stock concentrations of the AF488-labeled peptides were measured by recording the UV-Vis absorbance at 495 nm (ε = 80,000 $M^{-1}cm^{-1}$).

Staphylococcus aureus Cells

Staining of *Staphylococcus aureus* bacteria by AF488-labeled cyclic peptides was assessed using flow cytometry and fluorescence microscopy. Bacteria from a single colony were grown overnight in LB broth at 37 °C with agitation. An aliquot was taken and diluted 100 times in fresh broth and sub-cultured for 3 hours until the cells reached OD_{600} of 1.0. The bacterial cells (200 μL) were centrifuged, re-suspended in 4 mL of Tris buffer (50 mM Tris base, pH 7.4), then an aliquot (100 μL) was mixed in with peptide samples at 100, 250, 500 and 1000 nM concentrations. 30 mM KCl was added to each peptide sample in a separate batch to assess binding in the presence of salt. The flow cytometry experiments were carried out on a BD FACS Aria cell sorter (BD Biosciences, San Jose, CA) and the data analysis was performed with FlowJo (Tree Star, Inc., Ashland, OR) and Origin (OriginLab Corp., Northampton, MA).

Microscopy samples were prepared using a similar protocol as stated above, except after sub-culturing, aliquots (100 μL) of the cells were centrifuged and directly re-suspended in 50 μL of the peptide solution (1000 nM in Tris buffer, pH 7.4). A separate batch of peptide samples was prepared containing 30 mM KCl each to assess bacteria staining in the presence of the salt. 3 μL of cells were transferred to a slide (Fisherfinest premium, 3"x1"x1 mm) and fixed with a cover glass (Fisherbrand, 22x22–1.5) Fluorescence images were taken on a Zeiss Axioplan 2 microscope equipped with filters that allow the detection of FITC (488 nm excitation, 515-520 nm emission) using a 100 x objective. All images were captured using an exposure time of 300 ms and processed in ImageJ following the same protocol.

Jurkat Cells

The co-culture experiments were performed using the same protocol stated above for bacterial cell preparation. Jurkat cells were grown in RPMI 1640 media with 10% FBS and 1% Pen/Strep at 37 °C and 5% CO_2 and passed for less than 20 generations. An aliquot (2 mL) of cells was centrifuged and directly re-suspended in 200 μL of buffer (50 mM Tris, pH 7.4). Cell stocks were combined and the peptide was added to a concentration of 1 μM from a concentrated stock. A separate batch of samples was prepared containing 30 mM KCl in the same buffer to assess the staining in the presence of salt. The staining and microscopy imaging were carried out using the same protocol as the *S. aureus* cells.

Chapter 4. Dissecting the energetic consequences of fluorinating a protein core

4.1 Introduction

Proteins have emerged as a powerful class of therapeutic agents due to their superior properties over small molecules in the clinic [103]. Some of the key advantages include their large surface areas and highly defined structures, which allow them to perform very specific functions that are generally not reproducible with traditional small molecule scaffolds. Due to this high specificity, proteins do not generally induce adverse side effects in patients and they are less likely to interfere with otherwise normal biological processes. Additionally, since many of the proteins used in the clinic are already native to the body, they are better tolerated as drugs and are less likely to elicit an immunological response [104].

The ability of a protein to properly fold is an essential part of life. These macromolecules rely on the precise, non-covalent molecular interactions between their specific side chain residues to achieve a desired 3-dimensional structure. Remarkably, nature can accomplish this using only the 20 natural amino acids with commonly observed interactions including hydrogen bonding, salt bridges and hydrophobic interactions. Although these elements work cohesively to help the protein adopt a well-defined structure, it is thought that the latter interaction plays a rather significant role in protein stabilization. A survey of the protein data bank reveals that aromatic clusters are prevalent in protein structures with around 60% of aromatic side chains forming a close contact with another aromatic residue [105]. These interactions are often found buried within a hydrophobic core and until now have been difficult to study since side chain

mutations at these sites will inevitably perturb several factors at a time. While it is thought that these interactions play a key role in helping a protein to fold, it is difficult to introduce a mutation at this site without perturbing the overall structure.

4.1.1 Contribution of fluorine in protein design

Fluorination is an increasingly sought after strategy in protein engineering due to its small size, high electronegativity and of course, its absence from biological systems [106, 107]. It is the most electronegative atom, displaying highly unique electrostatic properties, while its small size renders it analogous to a hydrogen atom (1.35 Å for F and 1.2 Å for H). The result is that a fluorine atom will introduce minimal steric perturbation, an important quality to consider when attempting to not only maintain a protein structure, but also to further enhance it. Additionally, fluorocarbons display superior hydrophobic properties while also exhibiting selective self-association behaviors with other fluorinated molecules [108]. Its absence from biological systems also offers a great opportunity to selectivity trace a fluorine atom in both cells and in living organisms with little to no background [109]. Some of the few methods used to accomplish this include ^{19}F NMR spectroscopy, which can be a powerful tool to analyze a protein structure, as well as its interaction with a target [110]. Other methods include positron emission tomography (PET), which utilizes ^{18}F as a tracer to analyze 3-dimensional images while other techniques, such as MRI and CT and x-ray can only provide structural information [111].

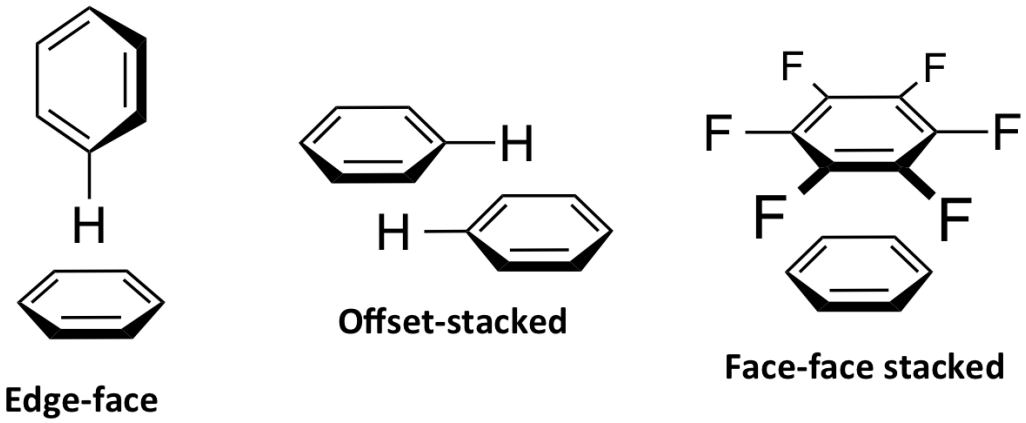

Figure 4-1. Geometries of π-π interactions. Left: edge-face; middle: offset-stacked; right: face-face stacked.

Taking the simplest aromatic molecule, benzene, we can begin to understand how they interact with one another in solution. A benzene dimer, for example, preferentially interacts in the edge-face manner, where the electropositive hydrogen atom of one benzene ring forms a contact with the electronegative π cloud of the other [112]. This specific orientation ensures that the two molecules adopt the most energetically favorable conformation. Conversely, perfluorination of a benzene molecule reverses its electrostatic properties, allowing it to interact in the face-face stacking geometry with a benzene ring.

4.1.2 Fluorinated aromatic residues and protein stability

To further demonstrate this fundamental principle in the context of a protein, Waters and co-workers incorporated steric mimics of native aromatic residues and analyzed their energetic properties [87]. They incorporated perfluorophenylalanine (f_5F), which displays an electron deficient center as a result of perfluorination, into Ala-Lys to study the difference between F-F and F- f_5F pairs and their effects on aromatic stabilization in α-helices. Incorporating an F-F pair at the C-terminus peptide resulted in

an energetic gain of -0.80 kcal/mol versus an internal position (-0.26 kca/mol), potentially due to the flexibility at that position, allowing side chains to reorient themselves and adopt a more favorable conformation. Incorporating the F- f_5F pair at the same position resulted in a smaller energetic gain (-0.55 kcal/mol), indicating that this is not purely a result of hydrophobic interactions, but instead, a result of the partially electrostatic nature of F-F.

The electronic and hydrophobic contributions towards aromatic packing were further studied with a model β-hairpin structure [113]. Examining a generic sequence, Ac-Arg-X_1-Val-Orn-Val-Asn-Gly-Lys-Glu-Ile-X_2-Gln-NH_2, in which residues X_1 and X_2 interact pack against one another. They incorporated either a Phe or a cyclohexylalanine (Cha) mutation. Although sterically similar to Phe, Cha exhibits dramatically different behavior in that it is electronically deficient and unable to engage in a π-π interaction. Interestingly, they observed that peptides containing either Phe-Phe or Cha-Cha pairs were comparable in stability, whereas the mixed pairs were less favorable. NMR analysis further supported this result by revealing a tight, edge-face geometry between the Phe-Phe pair, reinforcing the importance of self-association when it comes to aromatic residues.

Conversely, reports by Nowick and co-workers described a similar study in which they incorporated Phe and Cha residues into a model β-sheet template, which undergoes dimerization to form contacts between the R1 position from one monomer and the R5 position from the other [114]. Interestingly, they observed that all four possible dimers were found to exist at equal percentages in solution. Although conflicting with earlier results, this is perhaps not too surprising given that a high frequency of Phe-Phe

interactions are generally observed in hydrogen-bonded cross strand pairs of antiparallel β-sheets, while this study examined a nonhydrogen-bonded cross-strand pair [115, 116].

4.1.3 Studying edge-face interactions in a model protein

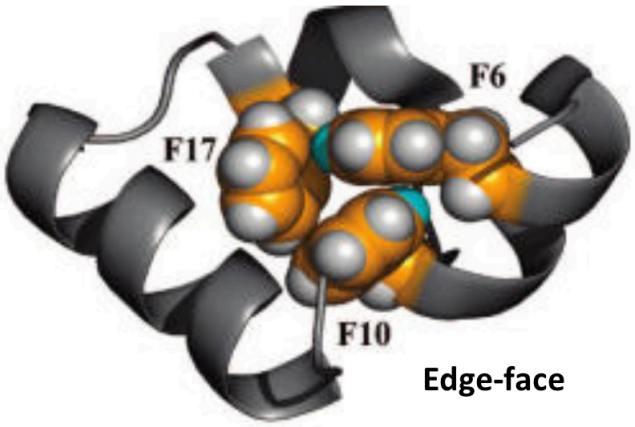

Figure 4-2. Structure of VHP35 hydrophobic core illustrated aromatic stacking. Figure adopted from reference [117].

These fundamental studies, although significant, have only described the contributions of aromatic interactions at solvent exposed positions. Since most aromatic interactions occur within hydrophobic pockets of protein structures, it is imperative to understand how these molecules behave in the context of a more relevant environment. The villin headpiece subdomain (VHP35) is a widely studied α-helical model peptide. The core consists of three interacting phenylalanine residues with the H-4 of F6 packing against the phenyl ring of F17, while the H-6 atom of F10 packs against the π cloud of F6. Earlier work described by Gellman and co-workers nicely demonstrated that perfluorination of side chain F10 acts to stabilize the overall protein structure, but at positions F6 and F17, destabilizes it [118].

Intrigued by these results, Gao and co-workers set out to further examine this event by implementing various fluorine mutations to the aromatic residues within VHP35's hydrophobic core [117]. Fluorination of these side chains would render them more hydrophobic, but would also eliminate the critical CH- π interactions between the aromatic hydrogens of F6 and F10 and the π clouds of F17 and F6, respectively. It was proposed that highly, but not fully fluorinated analogues of these aromatic side chains would allow this key interaction to occur, while simultaneously introducing a hydrophobic driving force. Two phenylalanine analogues, called 2,3,4,5-tetrafluoro-L-phenylalanine (Z_o) and 2,3,5,6-tetrafluoro-L-phenylalanine (Z_p) were synthesized and incorporated into VHP35 and their resulting thermal and chemical stabilities were compared to a perfluorinated analogue, called pentafluoro-L-phenylalanine (Z).

Interestingly, the F10Z_o mutant, which presents a fully fluorinated aromatic side chain with the exception of one aromatic hydrogen at the ortho position, displayed higher stability (-4.7 kcal/mol) in comparison to the perfluorinated mutant, F10Z (-3.6 kcal/mol). The difference here can be rationalized by the presence of a single hydrogen atom at the ortho position of F10Z_o, which allows it to engage in a critical CH- π interaction with F6. This is further supported by the F10Z_p result, which also exposes a single hydrogen atom, but exhibits lower stabilities (-3.2 kcal/mol), even worse than the WT (-3.3 kcal/mol). Collectively, the results suggest that in order to be effective, a fluorine mutation must be incorporated with careful consideration of the surrounding environment.

It is thought that the superior behavior of F10Z_o could be attributed to a combination of factors. In the case of VHP35, the CH- π interaction between F10 and F6

aromatic residues contributes a great deal of stability to the protein fold. However, other factors, such as the hydrophobic effect, as well as the electrostatic interactions between atoms have not been thoroughly investigated. In an effort to further understand the specific contributions of a fluorine atom in the context of the VHP35 protein core, I have embarked on a research program to investigate how each of these factors plays a role in the proteins ability to fold.

4.2 Studying edge-face interactions with fluorinated F10 Phe residues

It is well established that maintaining the CH- π interaction between F10 and F6 side chains of VHP35 results in a well-folded protein. Therefore, we focused on this specific aromatic pair and designed a series of amino acids containing various degrees of fluorination to be incorporated at the F10 position. In contrast to earlier studies where the aromatic side chain displayed only one hydrogen atom, we sought to carry out a more detailed investigation by introducing a fluorine atom at carefully selected positions and observing the resulting effect on the proteins structure. More specifically, we were interested in determining whether the free energy gain associated with a fluorine mutation at F10 is context dependent, or whether this phenomenon is independent of the amount of fluorine atoms present.

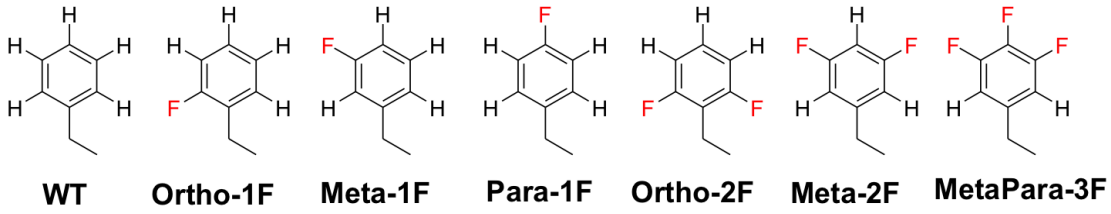

Figure 4-3. Series of fluorinated amino acids used to study an edge-face interaction in VHP35 model peptide.

4.2.1 Synthesis and design of fluorinated aromatic amino acids and VHP35 peptides

We designed a series of amino acids that would help us to answer these questions. Included within this library is a set of mono-fluorinated Phe residues with a fluorine atom incorporated at either the ortho, meta or para position of the ring. These amino acids will help us to explore the chemical space within the VHP35 hydrophobic core by determining whether a fluorine atom is better tolerated at one position over another, or whether it causes steric perturbation. The di-fluorinated amino acids, ortho-2F, meta-2F and metapara-2F have been specifically designed to complement the mono-fluorinated variants, since they also occupy the ortho, meta and para positions. However, this set of molecules is unique in that we expect to see both an enhanced hydrophobic driving force with the addition of an extra fluorine atom, as well as an increased chance of steric perturbation. Ultimately, if the di-fluorinated analogues display no enhanced free energy gain, then we can contribute this loss to the unfavorable steric bulk that an extra fluorine atom introduces at that specific position. This does not apply, however, to ortho-2F mutant, since it is missing the critical aromatic hydrogen atoms to engage in a CH- π interaction with F6. Finally, metapara-3F, which contains the highest degree of

fluorination in this series, would offer insight on the potential additive effect of fluorination.

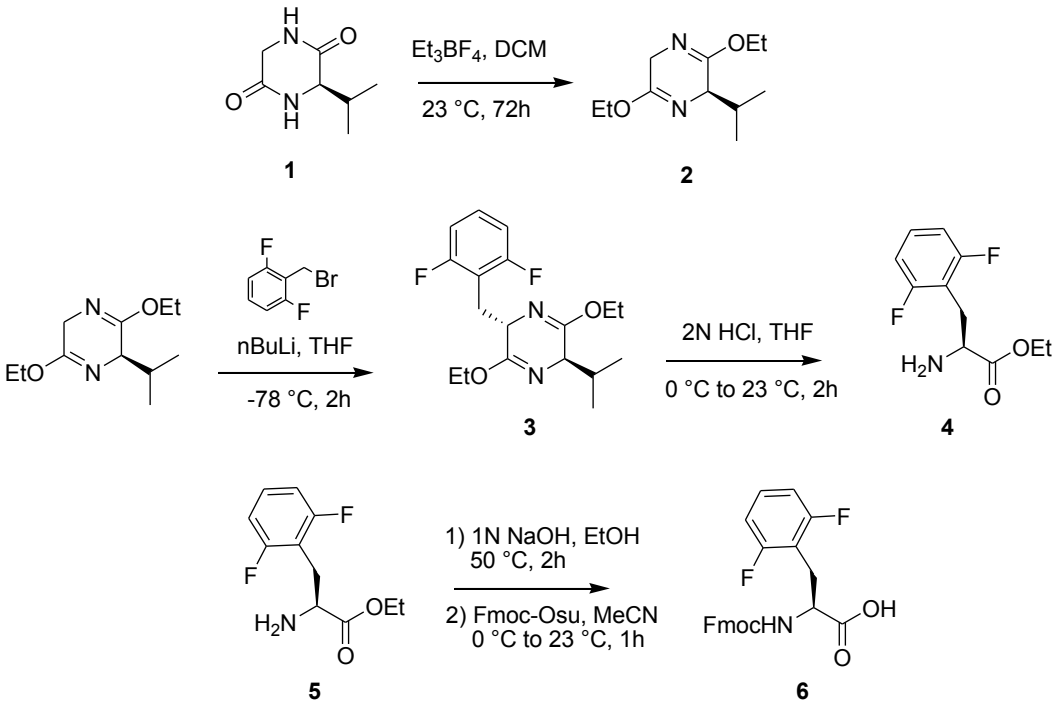

Scheme 4-1. Preparation of Fmoc-2,6-difluorophenylalanine from 2,6-difluoro benzyl bromide. The Schöllkopf's Chiral Auxiliary 2 was prepared according to the reported protocol.

The fluorinated Phe amino acids can be accessed using a well-established synthetic route. Although most of the amino acids used in this study were commercially available, we had to synthesize the Fmoc-2,6-difluoro-L-phenylalanine in house. The 2,6-difluorobenzyl moiety was installed onto Schollkopf's chiral auxiliary using standard alkylation reaction conditions. The steric nature of the chiral auxiliary helps to direct the stereochemistry of the resulting product. Specifically, the beta-branched functional group introduces the necessary steric bulk that helps nBuLi deprotonate the least hindered

hydrogen atom, which is the one trans to the isopropyl group. The absolute stereochemistry has been confirmed by 2D-NMR experiments [119]. Following alkylation, the diastereomer was subjected to acid hydrolysis to break apart the ring and yield two amino acid derivatives, 2,6-difluoro-L-Phe and D-Val, which can be separated via column chromatography. Upon isolation of the desired product, intermediate 5 is subjected to base hydrolysis to convert the ester into the free carboxylic acid, Fmoc protection of the free amino acid yields Fmoc-2,6-difluoro-L-Phe in good yields, which was then incorporated into the VHP35 sequence via solid phase peptide synthesis.

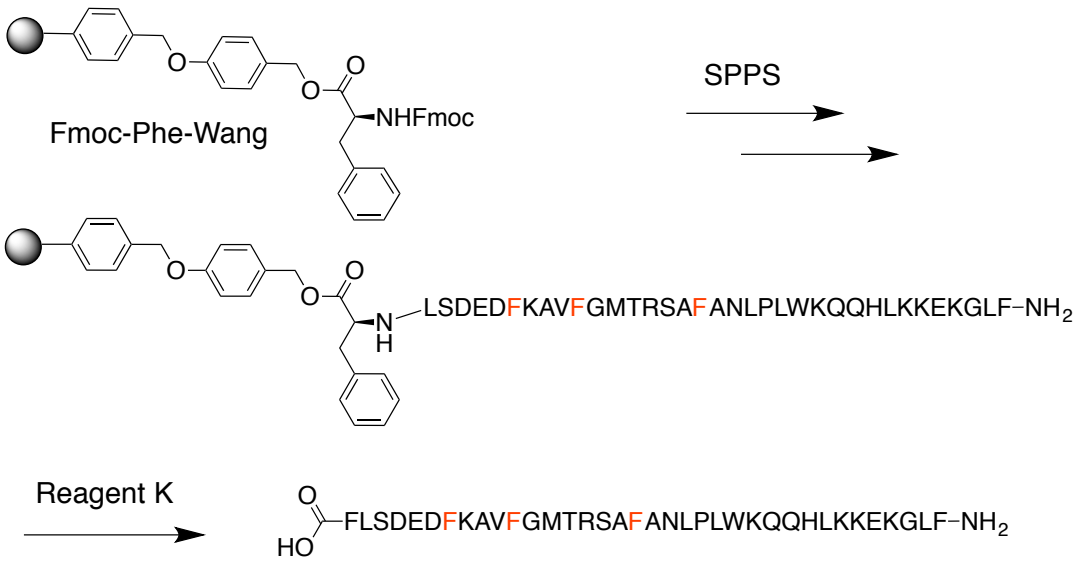

Scheme 4-2. Synthetic route of to access VHP35 peptide and its fluorinated mutants using Fmoc-Phe-Wang resin.

Peptide synthesis was accomplished using Fmoc-Phe-Wang resin using standard Fmoc/tBu chemistry. Linear sequences were built until the F10 residue, at which point, the unnatural amino acid was incorporated and checked by LC-MS to ensure efficient coupling. Following completion of the synthesis, the peptides were cleaved off the resin

and purified using RP-HPLC. Due to the length of the sequence, some optimization was required to ensure that the crude peptides contained little to no truncation products, which would in turn facilitate the purification step. For example, there are certain residues, such as Arg, Val and Pro, which are more difficult to couple due to their steric bulk. To circumvent this problem, we opted to use HATU as a coupling reagent, which reacts faster and with less epimerization than HBTU does. Additionally, we increased the coupling time of all residues from 30 minutes to 1 hour, which greatly reduced the number of truncation products. Collectively, all of these factors afforded the VHP35 peptide and its mutants in high purities and yields.

Table 4-1. Mass spectrometry data for VHP35 peptide mutants

Peptide	**$MW_{calculated}$ (Da)**	**MW_{found} (Da)**
WT	4082	4081
Ortho-1F	4100	4099
Meta-1F	4100	4100
Para-1F	4100	4099
Ortho-2F	4118	4117
Meta-2F	4118	4119
MetaPara-3F	4136	4135

4.2.2 Structural characterization of VHP35 mutants

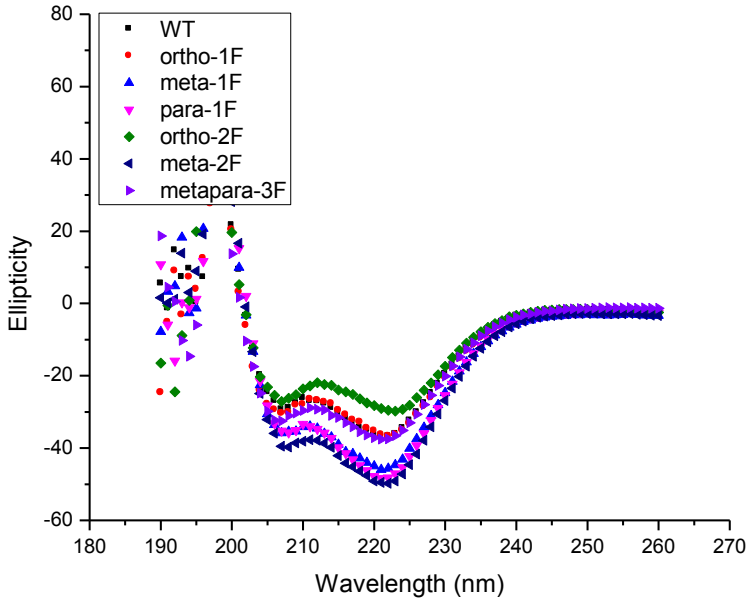

Figure 4-4. Wavelength scan of VHP35 mutants by CD spectroscopy

The peptides were subjected to spectroscopic analysis using circular dichroism to confirm that all mutants maintained a structure similar to the WT. Wavelength scans were performed in the far-UV region of the spectrum and the experiments were carried out at 2 °C to ensure that the peptides were folded. Indeed, a wavelength scan reveals an ellipticity minimum at 208 and 222 nm, which is indicative of α-helicity. Compared to WT, however, ortho-2F exhibited a very weak CD signature, suggesting that it is not well folded under the experimental conditions. This is not surprising due its lack of aromatic hydrogens at the ortho positions, which prevents it from engaging in the critical CH- π interaction necessary for folding.

4.2.3 Thermodynamic characterization and analysis of VHP35 mutants

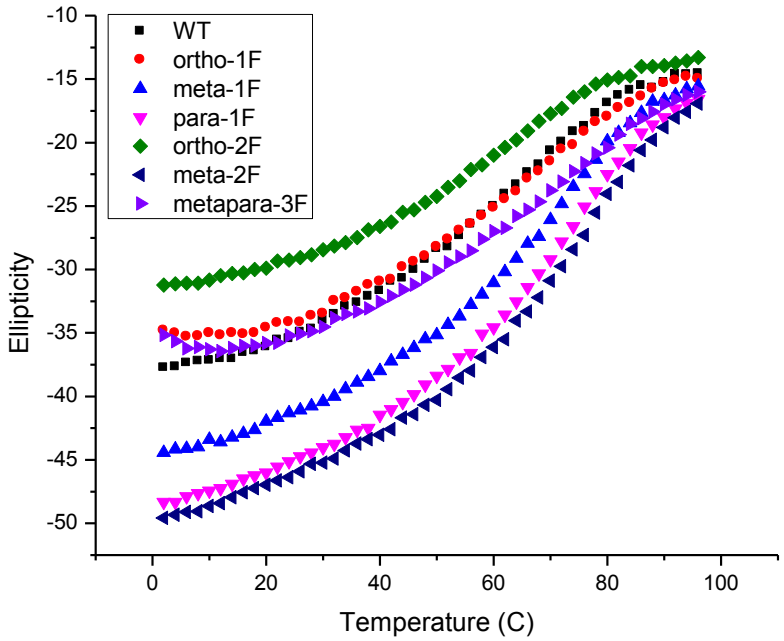

Figure 4-5. Thermal denaturation curves of VHP35 mutants generated by CD spectroscopy

We investigated the thermal stabilities of VHP35 WT and its mutants by performing thermal denaturation experiments and monitoring the results at a wavelength of 222 nm via CD spectroscopy. The peptide samples were prepared in native buffer A and heated up at 2 °C increments until the temperature reached 98 °C. After each 2 °C temperature increase, the sample was equilibrated for 90 seconds before recording the ellipticity value. The signals were averaged for 30 seconds to ensure no variation in the data. Not surprisingly, all of the thermal denaturation curves displayed a sigmoidal transition, which was then tabulated to yield the melting temperature (T_m) values. It must be noted that for VHP35 and its mutants, the folding and unfolding was completely reversible.

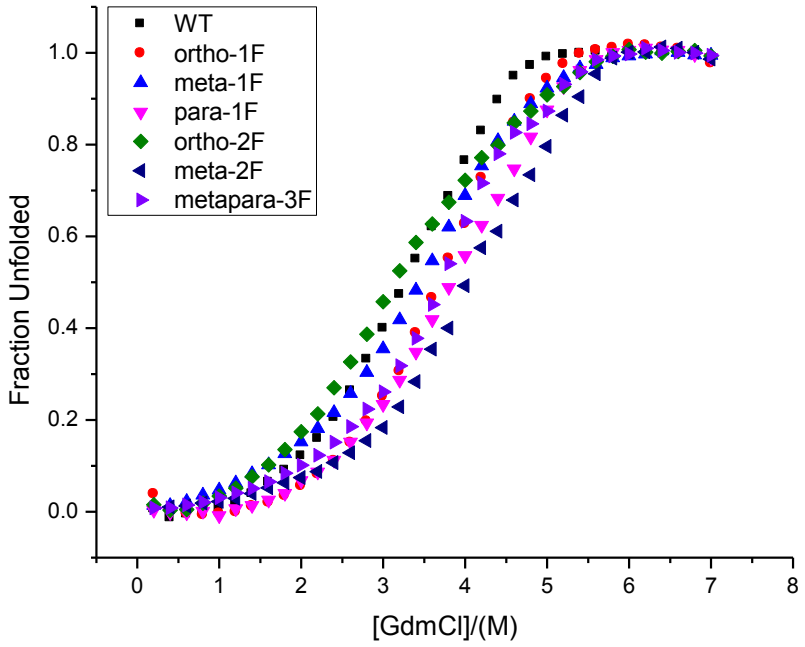

Figure 4-6. Chemical denaturation curves of VHP35 mutants generated by GdmCl titration via CD spectroscopy.

Chemical denaturation experiments were also performed to generate ΔG_f values for all mutants. In this experiment, CD spectroscopy was used to determine the peptides conformation by plotting the ellipticity values at 225 nm as a function of GdmCl concentration. Titrations were performed at increments of 0.2 M GdmCl and the sample was stirred for 30 seconds after each addition and equilibrated for 2 minutes before recording the ellipticity values. Thermodynamic fitting of the resulting curves using a standard baseline extrapolation method yielded the thermodynamic parameters listed in Table 4-2.

Table 4-2. Tabulated thermodynamic data for VHP35 mutants

Protein	T_m (°C)	C_m (M)	m value (kcal/(mol·M))	ΔG_f (kcal/mol)	$\Delta\Delta G_f$ (kcal/mol)
WT	**64**	**3.2**	**0.81**	**-2.6 ± 0.1**	**0**
Ortho-1F	**70**	**3.7**	**0.84**	**-3.1 ± 0.1**	**-0.5 ± 0.1**
Meta-1F	**70**	**3.3**	**0.82**	**-2.7 ± 0.1**	**-0.1 ± 0.1**
Para-1F	**74**	**3.9**	**0.76**	**-3.2 ± 0.1**	**-0.6 ± 0.1**
Ortho-2F	**62**	**2.9**	**0.76**	**-2.2 ± 0.1**	**+0.4 ± 0.1**
Meta-2F	**74**	**4.1**	**0.93**	**-3.8 ± 0.1**	**-1.2 ± 0.1**
Parameta-3F	**70**	**3.4**	**0.88**	**-3.0 ± 0.1**	**-0.4 ± 0.1**

4.2.5 Synthesis of fluorinated amino acids for LogP studies

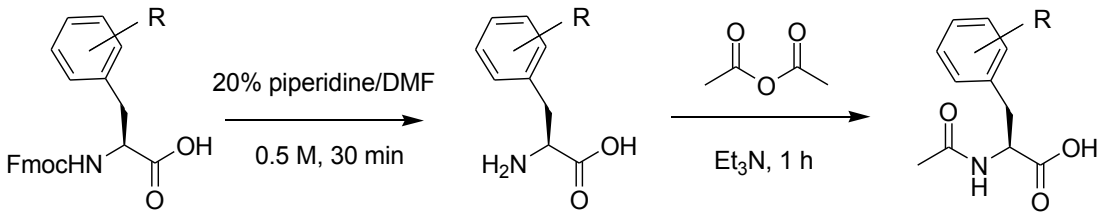

Scheme 4-3. Synthesis of acetyl capped amino acids for LogP studies

To further understand the hydrophobic contribution of a fluorine atom, we embarked on a study to experimentally determine the LogP value of each fluorinated Phe mutant. We began by Fmoc deprotection of the amino acids, followed by acetylation using acetic anhydride. After prep-HPLC purification, the molecules were dissolved in an acidic Gly buffer (pH 2) to ensure that they would remain neutral for the subsequent LogP determination.

Table 4-3. Mass spectrometry data for acetylated amino acids

Molecule	MW $_{calculated}$ (Da)	MW $_{found}$ (Da)
Ac-Ortho-1F-OH	224.08	224.0785
Ac-Meta-1F-OH	224.08	224.0757
Ac-Para-1F-OH	224.08	224.0754
Ac-Ortho-2F-OH	242.06	242.0672
Ac-Meta-2F-OH	242.06	242.0761
Ac-MetaPara-3F-OH	260.06	260.0606

To calculate the octanol to water partition coefficients, the samples containing each molecule in a Gly buffer were added to an equal volume of octanol and mixed and allowed to sit for 15 mins at room temp. Following complete separation, an aliquot of each layer was extracted and injected into the LC-MS to determine the resulting concentrations and the values were used to calculate the LogP values (**Table 4-4**).

Table 4-4. Calculated LogP results of VHP35 mutants

Mutant	Trial	Trial 2
Phenyl	4.27	4.44
Ortho-1F	4.88	4.72
Meta-1F	3.78	3.84
Para-1F	3.58	3.78
Ortho-2F	4.01	4.67
Meta-2F	10.22	11.91
Metapara-3F	20.62	23.03

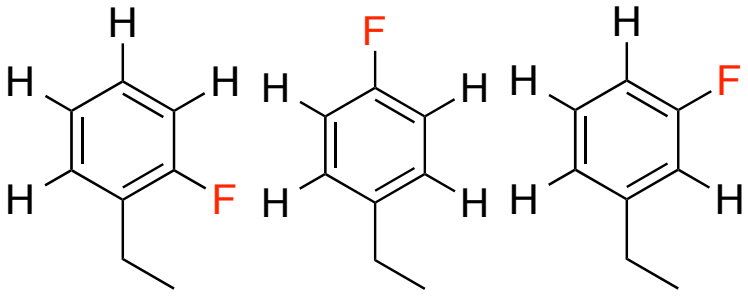

Figure 4-7. Comparison of monofluorinated F10 mutants.

We began our analysis by focusing on the monofluorinated mutants, ortho-1F, meta-1F and para-1F. By introducing a single point mutation at each position of the aromatic ring, we expect to determine the steric contribution of a fluorine atom within the hydrophobic core of VHP35. Not surprisingly, all three mutants exhibit similar logP values, indicating that if the hydrophobic driving force is a significant event in helping the protein to fold, then all three mutants contribute equally. Compared to WT, which displays a ΔG value of -2.6 kcal/mol, both ortho-1F and para-1F introduce an additional 0.5 kcal/mol and 0.6 kcal/mol, in binding free energy, respectively. If we further dissect the structural differences between ortho-1F and para-1F, we remember that the presence of an ortho hydrogen atom is crucial for maintaining the CH-π interaction with the F6 side chain. Although both peptides are capable of engaging in this interaction, ortho-1F contains a fluorine atom at one of those positions, which we expect will force the aromatic ring to discriminate between one orientation over another. Para-1F, however, is expected to be more dynamic and perhaps require more energy to fold. The thermodynamic data suggests that both peptides contribute equally in folding free energies, thus, blocking a site of interaction does not bias the structure in a favorable way. On the other hand, Meta-1F displays a nearly identical free energy value to WT, at -2.7 kcal/mol. Although it displays a similar LogP value to the other monofluorinated mutants, we hypothesized that the fluorine atom may present itself on the F10 ring in an unfavorable orientation where it is involved in a steric or electronic repulsion with another atom in the core. Another possibility could be that a fluorine atom at the meta position is inert, while at the ortho and para positions is favorable.

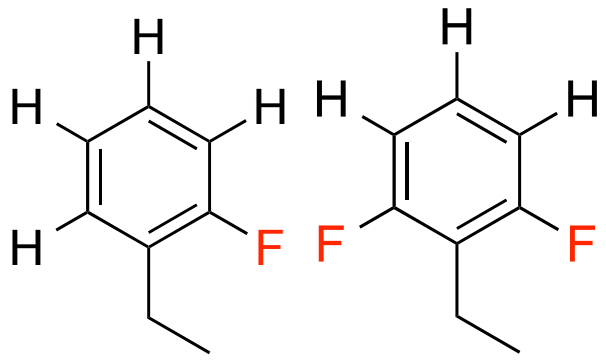

Figure 4-8. Comparison of mono and difluorinated mutants at the ortho position of F10.

Perhaps even more obvious is the difference between mutant's, ortho-1F and ortho-2F. We expect to see no benefit of an extra fluorine atom at the ortho position of F10, since we would essentially be eliminating any possibility of a CH-π interaction. The thermodynamic results agree, as ortho-2F exhibited the poorest free energy value in this series, nearly 0.5 kcal/mol worse than the WT. If we recall the previous studies done in our group comparing F10Z and F10Z_o, we remember that the former is also not capable of engaging in a CH-π interaction, since every hydrogen atom on F10 has been replaced with fluorine. However, compared to the WT, F10Z exhibited a slightly favorable binding free energy value ($\Delta\Delta G$ = -0.3 kcal/mol), indicating that perfluorination may offset the negative impact of removing the CH-π interaction. Ortho-2F displays only two fluorine atoms, which may not be enough to compensate this effect.

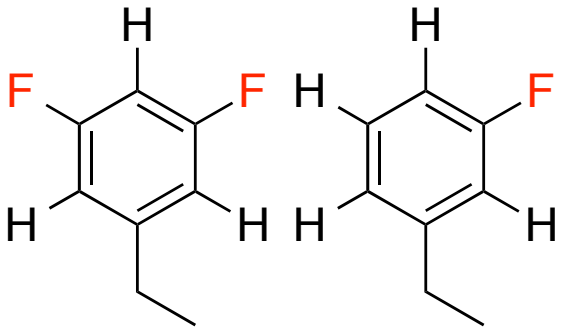

Figure 4-9. Comparison of ortho and di fluoro mutants at the meta position.

The previous example is not appropriate for evaluating the additive effect of fluorination because one of the mutants completely abolishes the critical CH-π interaction that is a huge driving force for VHP35 folding. To circumvent this problem, we chose to analyze two mutants, meta-1F and meta-2F, which both expose these critical ortho hydrogen atoms. Meta-2F (-3.8 kcal/mol) displays far superior free energy values compared to meta-1F (-2.7 kcal/mol), which we attribute to the huge discrepancy in LogP values (10.22 vs. 3.78). In this case, we can argue that the hydrophobic effect is a huge contributing factor, which may have offset the potentially negative steric and electronic repulsion effects that meta-1F displayed in comparison to the other monofluorinated mutants. This could be a lesson to demonstrate how a mediocre mutant, such as meta-1F can transform into one of the best and most stable proteins candidates by the addition of a single fluorine atom at a carefully place position. In terms of protein engineering, this result validates the potential of using a fluorine atom as a directing group.

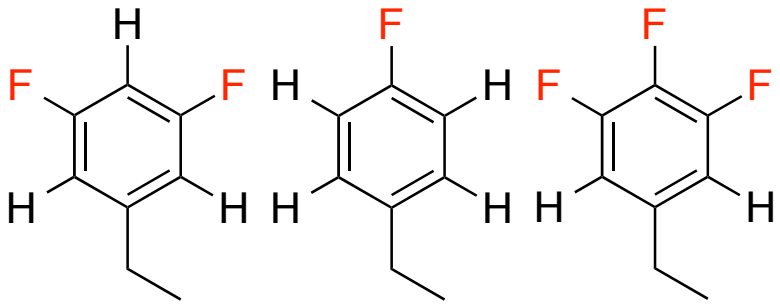

Figure 4-10. Comparing the additive effect of fluorination in VHP35

We attempted to take it a step further and examine whether the best mutant, meta-2F could be engineered even further to display an even more favorable folding free energy value. Based on previous results, we've shown that blocking a single ortho position with a fluorine atom does not favor one conformer over another, so we focused on introducing the additional fluorine mutation at the para position, yielding metapara-3F. Interetsingly, metapara-3F displayed the highest LogP value in the entire library, but its folding free energy was mediocre (-3.0 kcal/mol). In fact, meta-2F, which has nearly half the LogP value of metapara-3F, is nearly 1.0 kcal/mol more stable. This result demonstrates how there may be a very intricate mechanism within the VHP35 hydrophobic core where simply enhancing the hydrophobicity of F10 is not enough to enhance the folding properties.

4.2.6 ^{19}F NMR analysis of ortho-2F and meta-2F peptides

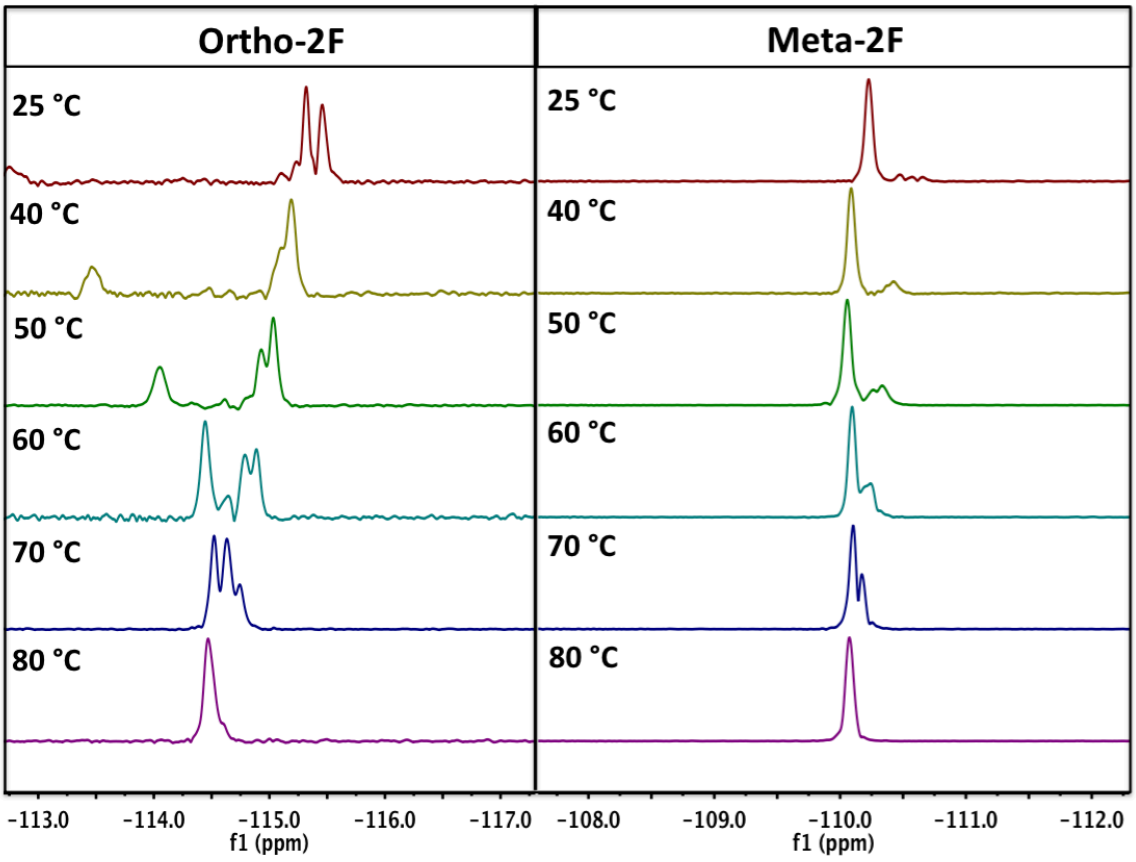

Figure 4-11. ^{19}F NMR data of ortho-2F and meta-2F demonstrating temperature induced denaturation.

Thermodynamic characterization of the peptide library allowed us to compare the subtle difference between each mutant upon fluorination of the F10 residue. We can rationalize the differences based on a number of factors including, but not limited to, hydrophobicity, steric bulk and of course, the presence of a CH-π interaction. We were interested in going a step further and analyzing the best and worse mutants at the atomic level via ^{19}F NMR spectroscopy. We subjected ortho-2F and meta-2F to a temperature gradient experiment and compared the resulting spectra to one another. Consistent with both thermal and chemical denaturation data, ortho-2F seems to display multiple

conformers at room temperature, suggesting that the fluorine atoms are not well tolerated at the ortho positions of F10. However, with an increase in temperature, we expect the peptide to denature, until it reaches a fully unfolded state. It's not until we reach the maximum temperature at 80 °C, that we observe the presence of a single conformer, which we assume to be in the fully unfolded state.

On the other hand, meta-2F, which is the most stable mutant in the library, seems to adopt one major conformer at room temperature, which we presume is the fully folded one, while the smaller peaks can be attributed to the presence of a small percentage of conformers. As the temperature increases, we observe that the smaller conformers begin to coalesce into the larger peak until it reaches its fully denatured state at 80 °C. One critical difference between these two mutants is that meta-2F displays one major conformer at every temperature, indicating that the peptide is indeed well folded, while ortho-2F seems to adopt multiple conformers, never displaying a major conformer until the peptide is fully denatured.

4.3 Conclusions

To conclude on this model, we have demonstrated that fluorine atoms are well tolerated, and in some cases, even favorable at certain position of F10. The exception is a mutation at both ortho positions (ortho-2F), where the edge-face interaction is not existent. In terms of steric tolerance, it seems that the contribution of a fluorine atom at a single meta position, meta-1F, does not introduce any benefit, while at the ortho and para positions, contributes nearly 0.5 kcal/mol in enhanced free energy values. The most interesting result, however, suggests that a poorly folded peptide, such as meta-1F, can be

transformed into an extremely stable mutant with the addition of a single fluorine atom at a carefully placed position, as demonstrated with meta-2F. Although originally rationalized to be a result of the added hydrophobic driving force, we have proven that adding even more hydrophobicity to the best mutant, which yield metapara-3F, does not further enhance the folding free energy values. In fact, it destabilizes the structure by nearly one full kcal/mol.

Finally, ^{19}F NMR spectroscopic analysis reveals that peptide conformers can be studied in solution at various temperatures to determine their stabilities. We've compared the best (meta-2F) and worst (ortho-2F) mutants and shown that the former maintains a well-defined structure at various temperatures, whereas the latter displays a bunch of conformers, only collapsing into the fully denatured, major one at high temperatures.

Experimental Procedures

I. General Methods

Fmoc-Osu and HBTU were purchased from Novabiochem (San Diego, CA). All Fmoc-protected of acetyl-protected amino acids were purchased from Advanced Chemtech (Louisville, KY) or Chem-Impex (Wood Dale, IL). All other chemicals were obtained from Fisher Scientific or Sigma Aldrich unless otherwise indicated. Peptide synthesis was carried out on a Tribute peptide synthesizer (Protein Technologies, Tucson, AZ). ^{1}H and ^{13}C NMR measurements for the amino acids were performed on a Varian INOVA 500 MHz spectrometer. ^{19}F NMR measurements of the peptides were taken on a Varian INOVA 600 MHz spectrometer. HR-MS data were generated in house by the Boston College Mass Spectrometry Center. Circular dichroism measurements were performed on an AVIV CD spectrometer (Aviv Biomedical Inc. Lakewood, NJ). The LogP calculations were performed on an Agilent LC-MS (Agilent Technologies, Santa Clara, CA) in house. The peptide concentrations were determined on a Nanodrop 2000c Spectrophotometer (Thermo Fisher Scientific, Waltham, MA).

II. Synthesis of Fmoc-N-2,6-difluorophenylalanine

(2S,5R)-2-(2,6-difluorobenzyl)-3,6-diethoxy-5-isopropyl-2,5-dihydropyrazine (3). In a flame dried round bottom flask equipped with a magnetic stir bar under N_2, compound **2** (630 mg, 2.97 mmol) was dissolved in dry THF (15 mL) and cooled to -78 °C. N-butyllithium (2.5 N solution in hexanes, 1.2 mL) was added dropwise and allowed to stir for 30 mins at -78 °C. A solution of 2,6-difluoro benzyl bromide (615 mg, 2.97 mmol) in THF (1 mL) was added dropwise and allowed to stir for 2hrs at -78 °C. The reaction was

quenched with saturated NH_4Cl, the organic separated and the aqueous layer extracted 3x with dichloromethane. The combined organic layers were washed with brine (3x) and dried over Na_2SO_4. The crude product was purified on a silica gel column with 4:1 hexanes: EtOAc to yield a white solid. ^{1}H-NMR (500 MHz, $CDCl_3$) δ 0.66-0.64 (d, 3H), 0.99-0.97 (d, 3H), 1.22-1.18 (t, 3H), 1.27-1.24 (t, 3H), 2.22-2.18 (m, 1H), 2.98-2.94 (m, 1H), 3.25-3.21 (m, 1H), 3.61-3.59 (t, 1H), 4.18-3.97 (m, 4H), 4.25-4.21 (m, 1H), 6.83-6.79 (dd, 2H), 7.15-7.12 (m, 1H)

(S)-ethyl 2-amino-3-(2,6-difluorophenyl)propanoate (4). Compound **3** (268 mg, 0.792 mmol) was dissolved in THF (19 mL) at 23 °C in a rb flask equipped with a magnetic stir bar and cooled to 0 °C. To this solution, 2N HCl (11 mL) was added and the solution allowed to stir for 10 mins at 10 °C while warming to 23 °C over 2 hrs. Ice was added to the mixture and the pH tuned with aqueous ammonia. The solution was extracted with dichloromethane (3x) and the combined organic layers washed with brine and dried over Na_2SO_4. The crude product was purified on a silica gel column with 1:1 EtOAc: hexanes to yield **4** as a white solid. ^{1}H-NMR (500 MHz, $CDCl_3$) δ 1.23-1.20 (t, 3H), 2.96-2.92 (dd, 1H), 3.12-3.08 (dd, 1H), 3.73-3.71 (t, 1H), 4.17-4.13 (q, 2H), 6.87-6.83 (dd, 2H), 7.19-7.15 (m, 1H)

Fmoc-N-2,6-difluorophenylalanine (6). Compound **4** (150 mg, 0.655 mmol) was dissolved in ethanol (3.3 mL) and added to a rb flask quipped with a stir bar. 1M NaOH (2.2 mL) was added and the resulting solution mixed at 50 °C for 2 hrs. The reaction was quenched with ice and the pH adjusted to 7 with 2N HCl. The resulting solution was

concentrated in vacuo and redissolved in 9% sodium carbonate (2.6 mL) and cooled to 0 °C. Fmoc-Osu (220 mg, 0.652 mmol) was dissolved in acetonitrile (2 mL) and added to the solution. The mixture was left to stir for 1 h at room temperature. The solution was diluted with water and tuned to pH 2 with concentrated HCl. The organic phase was separated and the aqueous phase extracted with ethyl acetate (6x). The combined organic layers were washed with brine (2x) and water (2x) and concentrated in vacuo. The crude product was purified by silica gel chromatography 2:1 EtOAc: hexanes (2% acetic acid) to afford **6** as a white solid. ^{1}H-NMR (500 MHz, $CDCl_3$) δ 3.15-3.10 (dd, 1H), 3.29-3.27 (dd, 1H), 4.12-4.03 (t, 1H), 4.26-4.14 (m, 2H), 4.49-4.46 (dd, 1H), 6.91-6.88 (t, 2H), 7.24-7.22 (m, 1H), 7.31-7.25 (m, 2H), 7.39-7.36 (t, 2H), 7.61-7.59 (dd, 2H), 7.78-7.77 (d, 2H)

III. Peptide Synthesis and Characterization

All peptides were synthesized via solid phase peptide synthesis (SPPS) using standard Fmoc/tBu chemistry. Syntheses were performed on a 0.05mmol scale using Fmoc-Phe-Wang resin and 5 equivalents of Fmoc-protected amino acids. The resin was treated twice with a mixture of 20% piperidine v/v in DMF for 10 mins each at room temperature. The subsequent Fmoc-protected amino acids coupled by activating the carboxylic acid with 0.05 mmol HBTU for 2.5 mins with 0.4 M N-methylmorpholine in DMF. After activation, amino acids were mixed with the resin for 30 mins at room temperature. A final Fmoc-deprotection step was incorporated on the terminal residue and the peptide was cleaved and globally deprotected with reagent K (80% TFA, 7.5% phenol, 5% thioanisole, 5% H_2O and 2.5% 1,2,ethanedithiol) for 2 hrs at room

temperature. The crude products were precipitated with cold diethyl ether (3x), centrifuged and vacuum-dried overnight.

Peptide sequence. All mutations were made at position F10.

6 10 17

WT: H_2N—LSDED**F**KAV**F**GMTRSA**F**ANLPLWKQQHLKKEKGLF--COOH

Purification. Peptides were purified by reverse-phase HPLC on a Waters PrepLC using a Phenomenex Jupiter C18 prep column (250 x 20.00 mm, 10 micron). After purification, peptides pure fractions were collected, combined and lyophilized for further analysis. Purities and identities were confirmed using LC-MS analysis.

IV. Circular Dichroism Spectroscopy

All peptides samples for CD analysis were dissolved in Native Buffer A (20 mM NaP_i. 150 mM NaCl, pH 7.4). Wavelength scans in the Far-UV region were collected using an AVIV model 202SF CD spectrometer equipped with a temperature-controlled cell holder. CD spectra were recorded at 2 °C using a 2 mm path length quartz cuvette and monitored at a wavelength between 260 nm to 190 nm. All HP35 variants displayed the characteristic α-helical structures with ellipticity minima at 222 nm and 208 nm.

V. Thermal and Thermodynamic Analysis

Thermal denaturation experiments were monitored at a wavelength of 222 nm for all samples. Peptides samples were prepared in Native Buffer A (20 mM NaP_i. 150 mM

NaCl, pH 7.4) at a concentration of 50 μM in a 2 mm path length quartz cuvette. The ellipticity data were collected at 2 °C increments with a 90 s equilibration time and signals were averaged for 30 s. All thermal denaturation curves display sigmoidal transitions, which were then tabulated to yield T_m values.

Guanidinium chloride (Gdm·Cl) denaturation experiments were carried out at 2 °C on the circular dichroism spectrometer equipped with an automated titrator. Two 10 μM peptide solutions were prepared: solution A in Native Buffer A and solution B in Native Buffer B (20 mM NaP_i. 150 mM NaCl, 7M Gdm·Cl, pH 7.4). 2.6 mL of solution A was added to a 10 mm path length quartz cuvette equipped with a magnetic stir bar. Solution B was added in fractions and before each addition, an equal volume of the solution in the cuvette was taken out. After each addition, the sample was mixed for 30 seconds, followed by a 2 min equilibration period. The ellipticity values were recorded at 225 nm and plotted against concentration to yield the denaturation curves. Thermodynamic fitting using the standard baseline extrapolation method gave the thermodynamic parameters listed in Table 2.

VI. Experimental LogP Calculations

LogP values were measured using N-terminal acetylated amino acids. Briefly, Fmoc-protected unnatural amino acids were deprotected using 20% piperidine in DCM v/v solution for 30 mins. The solvent was removed in vacuo to isolate the free amino acids, which were then re-dissolved in methanol (3 mL), Et_3N (2 equivalents) and acetic

anhydride (2 equivalents) and sonicated for 20 minutes at room temperature to yield the acetylated molecules.

LogP experiments were performed by preparing a solution of the acetyl-protected amino acid (8 mg/mL) in a Gly buffer, pH 2.0 and adding an equal volume of octanol. The solution was vortexed and left to sit for 30 mins at room temperature. The layers were separated and analyzed by LC-MS to determine their UV absorption values. The LogP value was calculated by dividing the area under the curve of the octanol layer by the aqueous layer. The experiment was repeated to confirm reproducibility.

VII. ^{19}F NMR analysis.

Samples for 1D ^{19}F NMR experiments were prepared by dissolving the peptide in a 20 mM sodium phosphate buffer, pH 5.5, H_2O:D_2O (9:1) to a concentration of 1 mM. Temperature gradient measurements were taken on an INOVA 600 MHz NMR spectrometer and an echo experiment was performed for each peptide mutant to circumnavigate the TFA signal. NMR data were processed using MestRe Nova (Mestrelab Research S. L. Spain).

References

1. Schmuck, C., *Side chain selective binding of N-acetyl-α-amino acid carboxylates by a 2-(guanidiniocarbonyl)pyrrole receptor in aqueous solvents.* Chemical Communications, **1999**, 843-844.
2. Schmuck, C., *Carboxylate binding by 2-(Guanidinocarbonyl)pyrrole receptors in aqueous solvents: improving the binding properties of guanidinium cations through additional hydrogen bonds.* Chemistry a Eurpoean Journal, **2000**, 6, 709-718.
3. Schmuck, C. Geiger, L., *Dipeptide binding in water by a de novo designed guanidinocarbonylpyrrole receptor.* Journal of the American Chemical Society, **2004**, 126, 8898-8899.
4. Jensen, K.B., Braxmeier, T. B., Demarcus, M., Frey, J. G., Kilburn, J. D., *Synthesis of guanidinium-derived receptor libraries and screening for selective peptide receptors in water.* Chemistry a Eurpoean Journal. **2002**, 8**,** 1300-1309.
5. Shepard, J., Gale, T., Jensen, K. B., Kilburn, J. D., *Synthesis of unsymmetrical tweezer receptor libraries and identification of receptors for Lys-D-Ala-D-Ala in aqueous solution.* Chemistry a Eurpoean Journal, **2006**, 12, 713-720.
6. Storer, R. I., Aciro, C., Jones, L. H., *Squaramides: physical properties, synthesis and applications.* Chemical Society Reviews, **2011**, 40, 2330-2346.
7. Garau, C., Frontera, A., Ballester, P., Quinonero, D., Costa, A., Deya, P. M., *A theoretical ab initio study of the capacity of several binding units for the*

molecular recognition of anions. European Journal of Organic Chemistry, **2005**, 179-183.

8. Prohens, R., Tomas, S., Morey, J., Deya, P. M., Ballester, P., Costa, A., *Squaramido-based receptors: molecular recognition of carboxylate anioncs in highly competitive media.* Tetrahedron Letters, **1998**, 39, 1063-1066.
9. Quinonero, D., Prohens, R., Garau, C., Frontera, A., Ballester, P., Costa, A., Deya, P.M., *A theoretical study of aromaticity in squaramide complexes with anions.* Chemical Physical Letters, **2002**, 351, 115-120.
10. Higgins, C., *Cystic fibrosis. Chloride channels revisited.* Nature, **1992**, 358, 536.
11. Busschaert, N., Kirby, I. L., Young, S., Coles, S. J., Horton, P. N., Light, M. E., Gale, P. A., *Squaramides as potent transmembrane anion transporters.* Angewandte Chemie International Edition, **2012**, 51, 4426-4430.
12. Ghose, A.K., Pritchett, A., Crippen, G. M, *Atomic physiochemical parameters for three dimensional structure directed quantitative structure-activity relationships III: modeling hydrophobic interactions.* Journal of Computational Chemistry, **1988**, 9, 80-90.
13. Young, R.C., Duran, G. J., Emmett, J. C., Ganellin, C. R., Graham, M. J., Mitchell, R. C., Prain, H. D., Roantree, M. L. , *Dipole moment in relation to H2 receptor histamine antagonist activity for cimetidine analogues.* Journal of Medicinal Chemistry, **1986**, 29, 44-49.
14. Elmes, R. B. P., Joliffe., K. A., *Amino acid-based squaramides for anion recognition.* Supramolecular Chemistry, **2015**, 27, 321-328.

15. Amerongen, A.V.N., Bolscher, J. G., Bloemena, E., Veerman, E. C., *Sulfomucins in the human body.* Biological Chemistry, **1998**, 379, 1-18.

16. Olomu, A.B., Vickers, C. R., Warring, R. H., Clements, D., Babbs, C., Warnes, T. W., Elias, E., *High incidence of poor sulfoxidation in patients with primary biliary cirrhosis.* New England Journal of Medicine, **1998**, 318, 1089-1092.

17. Mintzer, M. A., Grinstaff, M. W., *Biomedical applications of dendrimers; a tutorial.* Chemical Society Reviews, **2011**, 40, 173-190.

18. Pflugrath, J. W., Quiocho, F. A., *Sulphate sequestered in the sulphate-binding protein of Salmonella typhimurium is bound solely by hydrogen bonds.* Nature, **1985**, 314, 257-260.

19. Qin, L., Hartley, A., Turner, P., Elmes, R. B. P. and Joliffe, K. A., *Macrocyclic squaramides: anion receptors with high sulfate binding affinity and selectivity in aqueous media.* Chemical Science, **2016**, 7, 4563-4572.

20. Springsteen, G., Wang, B., *A detailed examination of boronic acid-diol complexation.* Tetrahedron, **2002**, 58, 5291-5300.

21. James, T. D., Sandanayake, K. R. A. S.; Iguchi, R.; Shinkai, S. , *Novel saccharide-photoinduced electron transfer sensors based on the interaction of boronic acid and amine* Journal of the American Chemical Society, **1995**, 117, 8982-8987.

22. Eggert, H. Frederiksen, J., Morin, C., Norrlid, J. C., *A new glucose-selective fluorescen bisboronic acid. First report of strong α-furanose complexation in aquous solution at physiological pH.* Journal of Organic Chemistry, **1999**, 64, 3846-3852.

23. Draffin, S. P., Duggan, P. J., Duggan, S. A. M., *Highly fructose selective transport promoted by boronic acids based on a pentaerythritol core.* Organic Letters, **2011,** 3, 917-920.

24. Gardiner, S., Smith, B., Duggan, P., Karpa, M., Griffin, G., *Selective fructose transport through supported liquid membranes containing diboronic acid or conjugated monoboronic acid-quaternary ammonium carriers.* Tetrahedron, **1999**, 55, 2857-2864.

25. Adamek, C. L., X.-C.; Zhang, Y. A.; Adamkova, K.; Scouten, W. H., *New aliphatic boronate ligands for affinity chromatography.* Journal of Chromatography, **1992**, 625, 91-99.

26. Malik, D. K., Baboota, S., Ahuja, A., Hasan, S., Ali, J. , *Recent advances in protein and peptide drug delivery systems.* Current Drug Delivery, **2007**, 4, 141-151.

27. Zhao, X., Li, H., Lee, R., *Targeted drug delivery via folate receptors.* Expert Opninion Drug Delivery, **2008**, 5, 309-319.

28. Gao, Y., Gao, G., He, Y., Liu, T., Qi, R., *Recent advances of dendrimers in delivery of genes and drugs.* Mini Review Medicinal Chemistry, **2008**, 8, 889-900.

29. Ellis, G. A., Palte, M. J., Raines, R. T., *Boronate-Mediated Biologic Delivery.* Journal of the American Chemical Society, **2012**, 134, 3631-3634.

30. Ishiguro, M., Hisako, T., Sakakibara, R., Yamaguchi, J., Aso, Y., *A ricin B chain-Ribonuclease A hybrid protein: a new tool for introduction of a foreign*

protein into targeted cells. Journal Faculty of Agriculture Kyushu University, **2002,** 46, 367-379.

31. Varki, A., Cummings, R. D., Esko, J. D., Freeze, H. H., Stanley, P., Bertozzi, C. R., Hart, G. W., *Essentials of Glycobiology, 2nd ed.* Cold Spring Harbor Laboratory Press: Cold Spring Harbor, NY, **2009**.

32. D'Alessio, G., Riordan, J. F., *Ribonucleases: Structures and Functions.* Academic Press: New York, **1997**.

33. Leland, P. A., Raines, R. T., *Cancer chemotherapy-ribonucleases to the rescue.* Chemistry and Biology, **2001**, 8, 405-413.

34. Dube, D. H., Bertozzi, C. R., *Glycans in cancer and inflammation—a pote*ntial for therapeutics and diagnostics, *Nat Rev Drug Discovery, **2005**,* 4, 477-488.

35. Gingrich, J. A., Caron, M. G., *Recent advances in the molecular biology of dopamine receptors.* Neuroscience, **1993**, 16, 299-321.

36. Mannnironi, C., Di Nardo, A., Fruscoloni, P., Tocchini-Valentini, G. P., *In vitro selection of dopamine RNA ligands.* Biochemistry, **1997**, 36, 9726-9734.

37. Bernardo, A. R., Stoddart, J. F., Kaifer, A. E., *Cyclobis(paraquat-p-phenylene) as a synthetic receptor for electron-rich aromatic compounds: electrochemical and spectroscopic studies of neurotransmitter binding* Journal of the American Chemical Society, **1992**, 114, 10624-10631.

38. Secor, K. E., Glass, T. E., *Selective amine recognition: development of a chemosensor for dopamine and norepinephrine.* Organic Letters, **2004**, 6, 3727-3730.

39. Wright, G. D., *Molecular mechanisms of antibitotic resistance.* Chemical Communications, **2011**, 47, 4055-4061.

40. Schafer, M., Schneider, T. R., Sheldrick, G. M., *Cystal structure of Vancomycin.* Structure, **1996**, 4, 1509-1515.

41. Boonyarattanakalin, S., Hu, J., Dykstra-Rummel, S. A., *Endocytotic delivery of vancomycin mediated by a synthetic cell surface receptor: rescue of bacterially infected mammalian cells and tissue targeting in vivo.* Journal of the American Chemical Society, **2007**, 129, 268-269.

42. Okesli, A., Cooper, L. E., Fogle, E. J. and van der Donk, W. A., *Nine post-translational modifications during the biosynthesis of cinnamycin.* Journal of the American Chemical Society, **2011**, 133, 13753-13760.

43. Hou, S., Johnson, S. E., *A one-step staining probe for phosphatidylethanolamine.* ChemBioChem, **2015**, 16, 1955-1960.

44. Behrend, R., Meyer, E. and Rusche, F., *Ueber Condensationsproducte aus Glycoluril und Formaldehyd.* Justus Liebig's Annalen der Chemie, **1905**, 339, 1-37.

45. Freeman, W. A., Mock, W. L. and Shih, N.-Y., *Cucurbituril.* Journal of the American Chemical Society, **1981**, 103, 7367-7368.

46. Cheng, X.-L. et al., *Twisted cucurbit[14]uril.* Angewandte Chemie International Edition, **2013**, 52, 7252-7255.

47. Lee, J. W., Samal, S., Selvapalam, N., Kim, H. J., Kim, K., *Cucurbituril homologues and derivatives: new opportunities in supramolecular chemistry.* Accounts of Chemical Research, **2003**, 36, 621-630.

48. Zhao, J., Kim, H.-J., Oh, J., Kim, S.-Y., Lee, J. W., Sakamoto, S., Yamaguchi, K. and Kim, K., *Cucurbit[n]uril derivatives soluble in water and organic solvents.* Angewandte Chemie International Edition, **2001**, 113, 4363-4365.

49. Li, S., Yuet-Wa Chan, J., Li, Y., Bardelang, D., Zheng, J., Wai, W., Chan, D. P. C., Lee, S. M. Y. and Wang, R., *Complexation of clofazimine by macrocyclic cucurbit[7]uril reduced its cardiotoxicity without affecting the antimycobacterial efficacy.* Organic and Biomolecular Chemistry, **2016**, 14, 7563-7569.

50. van Meer, G. Voelker, D. R., Feigenson, G. W., *Membrane lipids: where they are and how they behave.* Nature Reviews Molecular Cell Biology, **2008**, 9, 112-124.

51. Wenk, M. R., *Lipidomics: new tools and applications.* Cell, **2010**, 143, 888-895.

52. Schutters, K., Reutelingsperger, C., *Phosphatidylserine targeting for diagnosis and treatment of human diseases.* Apoptosis, **2010**, 15, 1072-1082.

53. Devaux, P. F., *Static and dynamic lipid asymmetry in cell membranes.* Biochemistry, **1991**, 30, 1163-1173.

54. Williamson, P., Schlegal, R. A., *Back and forth regulation and function of transbilayer phospholipid movement in eukaryotic cells.* Molecular Membrane Biology, **1994**, 11, 199-216.

55. Zachowski, A., Favre, E.; Cribier, S.; Herve, P. and Devaux, P. F., *Outside-inside translocation of aminophospholipids in the human erythrocyte membrane is mediated by a specific enzyme.* Biochemistry, **1986**, 25, 2285-2590.

56. Daleke, D. L., Huestis, W. H., *Incorporation and translocation of aminophospholipids in human erythrocytes.* Biochemistry, **1985**, 24, 5406-5416.

57. Verhoven, B., Schlegel, R. A., Williamson, P., *Mechanisms of phosphatidylserine exposure, a phacocyte recognition signal, on apoptotic T lymphocytes.* Journal of Experimental Medicine, **1995**, 182, 1597-1601.

58. Williamson, P., Kulick, A., Zachowski, A., Schlegal, R. A., Devaux, P. F., *Ca2+ induces transbilayer redistribution of all major phospholipids in human erythrocytes.* Biochemistry, **1992**, 31, 6355-6360.

59. Mattson, M. P., *Apoptosis in neurodegenerative disorders.* Nature Reviews Molecular Cell Biology, **2000**, 1,120-129.

60. Wong, R. S. Y., *Apoptosis in cancer: from pathogenesis to treatment.* Journal of Experimental and Clinical Cancer Research, **2011**, 30, 87.

61. van Generen, H., Kenis, H., Hofstra, L., Narula, J. Reutelingsperger, C., *Extracellular annexin A5: Functions of phsophatidylserine-binding and two-dimensional crystallization.* Biochimica et Biophysica Acta, **2008**, 1783, 953-963.

62. Fan, X., Krahling, S., Smith, D., Williamson, P. and Schlegel, R. A., *Macrophage surface expression of annexins I and II in the phagocytosis of apoptotic lymphoctyes.* Molecular Biology of the Cell, **2004**, 15, 2863-2872.

63. Hingorani, R., Deng, J., Elia, J., McIntyre, C., Mittar, D., *Detection of Apoptosis Using the BD Annexin V FITC Assay on the BD FACSVerse System.* **2011**.

64. Ntziachristos, V., Schellenberger, E. A., Ripoli, J., Yessayan, D., Graves, E., Bogdanov, A. Jr., Josephson, L., Weissleder, R., *Visualization of antitumor treatment by means of fluorescence molecular tomography with an annexin V-Cy5.5 conjugate.* Procedings of the National Academy of Sciences U.S.A, **2004**, 101, 12294-12299.

65. Belhocine, T., Steinmetz, N., Hustinx, R., Bartsch, P., Jerusalem, G., Seidel, L., Rigo, P., Green, A., *Increased uptake of the apoptosis-imaging agent (99m)Tc recombinant human Annexin V in human tumors after one course of chemothrapy as a predictor of tumor response and patient prognosis.* Clinical Cancer Research, **2002**, 8, 2766-2774.

66. Vermeersch, H., Loose, D., Lahorte, C., Merville, K., Dierckx, R., Steinmetz, N., Vanderheyden, J. L., Cuvelier, C., Slegers, G., Van de Wiele, C., *99mTc-HYNIC Annexin-V imaging of primary head and nexk carcinoma.* Nuclear Medicine Communications, **2004**, 25, 259-263.

67. Edgington, L. E., Berger, A. B., Blum, G., Albrow, V. E., Paulick, M. G., Lineberry, N., Bogyo, M., *Noninvasive optical imaging of apoptosis by caspace-targeted activity-based probes.* Nature Medicine, **2009**, 15, 967-973.

68. Hvarregaard, J., Andersen, M. H., Berglund, L., Rasmussen, J. T., Petersen, T. E., *Characterization of glycoprotein PAS-6/7 from membranes of bovide milk fat globules.* European Journal of Biochemistry, **1996**, 15, 628-636.

69. Hanayama, R., Tanaka, M., Miwa, K., Shinohara, A., Iwamatsu, A., Nagata, S., *Identification of a factor that links apoptotic cells to phagocytes.* Nature, **2002**, 9, 182-187.

70. Shi, J., Heegaard, C. W., Rasmussen, J. T., Gilbert, G. E., *Lactadherin binds selectively to membranes containing phosphatidyl-L-serine and increased curvature.* Biochimica et Biophysica Acta, **2004**, 1667, 82-90.

71. Waehrens, L. N., Heegaard, C. W., Gilbert, G. E., Rasmussen, J. T., *Bovine lactadherin as a calcium-independent imaging agent of phosphatidylserine*

expressed on the surface of apoptotic HeLa cells. Journal of Histochemistry and Cytochemistry, **2009**, 57, 907-914.

72. Shi, J., Shi, Y., Waehrens, L. N., Rasmussen, J. T., Heegaard, C. W., Gilbert, G. E., *Lactadherin detects early phosphatidylserine exposure on immortalized leukemia cells undergoing programmed cell death.* Cytometry A, **2006**, 69, 1193-1201.

73. Hou, J., Fu, Y., Zhou, J., Li, W., Xie, R., Cao, F., Gilbert, G. E., Shi, J., *Lactadherin functions as a probe for phosphatidylserine exposure and as an anticoagulant in the study of stored platelets.* Vox Sang, **2011**, 100, 187-195.

74. Lin, L., Huai, Q., Huang, M., Furie, B. C., Furie, B. C., *Crystal structure of the bovide lactadherin C2 domain, a membrane binding motif, shows similarity to the C2 domains of factor V and factor VIII.* Journal of Molecular Biology, **2007**, 371, 717-724.

75. Shao, C., Novakovic, V. A., Head, J. F., Seaton, B. A., Gilbert, G. E., *Crsytal structure of lactadherin C2 domain at 1.7A resolution with mutational and computational analyses of its membrane-binding motif.* Journal of Biological Chemistry, **2007**, 283.

76. Zheng, H., Wang, F., Wang, Q., Gao, J., *Cofactor-free detection of phosphatidylserine with cyclic peptides mimicking lactadherin.* Journal of the American Chemical Society, **2011**, 133, 15280-15283.

77. Xiao, Q., Pei, D., *High-Throughput Synthesis and Screening of Cyclic Peptide Antibiotics.* Journal of Medicinal Chemistry, **2007**, 50, 3132-3137.

78. Joo, S. H., Xiao, Q., Ling, Y., Gopishetty, B., Pei, D., *High-Throughput Sequence Determination of Cyclic Peptide Lobrary Members by Partial Edman Degradation/Mass Spectrometry.* Journal of the American Chemical Society, **2006**, 128, 13000-13009.

79. Hosseini, A. S., Zheng, H., Gao, J., *Understanding Lipid Recognition by Protein-Mimicking Cyclic Peptides.* Tetrahedron, **2014**, 70, 7632-7638.

80. Horswill, A. R., Savinov, S. N., Benkovic, S. J., *A systematic method for identifying small-molecule modulators of protein-protein interactions.* Procedings of the National Academy of Sciences U.S.A, **2004**, 101, 15591-15596.

81. Kritzer, J. A., Hamamichi, S., McCaffrey, J. M., Santagata, S., Naumann, T. A., Caldwell, K. A., Caldwell, G. A., Lindquist, S., *Rapid selectrion of cyclic peptides that reduce α-synuclein toxicity in yeast and animal models.* Nature Chemical Biology, **2009**, 5, 655-663.

82. Dawson, P. E., Kent, S. B. H., *Synthesis of Native Protines by Chemical Ligation.* Annual Review of Biochemistry, **2000**, 69, 923-960.

83. Machaidze, G., Seelig, J., *Specific binding of cinnamycin (Ro 09-0198) to phosphatidylethanolamine. Comparisson between micellar and membrane environments.* Biochemistry, **2003**, 42, 12570-12576.

84. Hosoda, K., Ohya, M., Kohno, T., Maeda, T., Endo, S., Wakamatsu, K., *Structure determination of an immunopotentiator peptide, cinnamycin, complexed with lysophosphatidylethanolamine by H-1-NMR.* Journal of Biochemistry, **1996**, 119, 226-230.

85. *Use and applications of Dbz resins in native chemical ligation. Novabiochem*

Innovations:3/11.

86. Fasman, G. D., *Handbook of Biochemistry and Molecular Biology, 3rd Edition.* Proteins, **1976**, 1, 183-203.

87. Butterfield, S. M., Patel, P. R., Waters, M. L., *Contribution of Aromatic Interactions to α-Helix Stability.* Journal of the American Chemical Society, **2002**, 124, 9751-9755.

88. Cornell, B. A. B.-M., *U.S. patent.* **1995,** 5(433), 955.

89. Stewart, J. C. M., *Colorimetric determination of phospholipids with ammonium ferrothiocyanate.* Analytical Biochemistry, **1980**, 104, 10-14.

90. Ross, N. T., Katt, W. P., Hamilton, A. D., *Synthetic mimetics of protein secondary structure domains.* Philosophical transactions Series A, Mathematical, physical and engineering sciences, **2010**, 368, 989-1008.

91. Fosgerau, K., Hoffman, T., *Peptide therapeutics: current status and future directions.* Drug Discovery Today, **2015**, 20, 122-128.

92. Lau, Y. H., de Andrade, P., Wu, Y., Spring, D. R., *Peptide stapling techniques based on different macrocyclisation chemistries.* Chemical Society Reviews, **2015**, 44, 91-102.

93. Walensky, L. D., Bird, G. H., *Hydrocarbon-stapled peptides: principles, practice, and progress.* Journal of Medicinal Chemistry, **2014**, 57, 6275-6288.

94. Gisin, B. F., Merrifield, R. B., Tosteson, D. C., *Solid-phase synthesis of the cyclododecadepsipeptide.* Journal of the American Chemical Society, **1969**, 91, 2691-2695.

95. Karle, I. L., Flippen-Anderson, J. L., *New conformation exhibiting near-threefold symmetry for uncomplexes valinomycin in crystals from dimethyl sulfoxide.* Journal of the American Chemical Society, **1988**, 11, 3253-3257.

96. Pinkerton, M., Steinrauf, L. K., Dawkins, P., *The molecular structure and some transport properties of valinomycin.* Biochemical and Biophysical Research Communications, **1969**, 35, 512-518.

97. Gisin, B. F., Merrifield, R. B., *Synthesis of a hydrophobic potassium binding peptide.* Journal of the American Chemical Society, **1972**, 94, 6165-6170.

98. Hamilton, J. A., Sabesan, M. N., Steinrauf, L. K., *The structure of prolinomycin-a synthetic peptide analogue of valinomycin.* Acta Crystal, **1980**, B36, 1052-1057.

99. Hamilton, J. A., Sabesan, M. N., Gisin, B. F., Steinrauf, L. K., *Crystal structure of peptide cyclo-(D-val-L-pro-L-val-D-pro)3.* Biochemical and Biophysical Research Communications, **1978**, 80, 949-954.

100. Davis, D. G., Gisin, B. F., Tosteson, D. C., *Conformational studies of peptide cyclo-[D-Val-L-Pro-L-Val-D-Pro]3, a cation-binding analog of valinomycin.* Biochemistry, **1976**, 15, 768-774.

101. Shang, S., Tan, Z., Dong, S., Danishefsky, S. J., *An advance in proline ligation.* Journal of the American Chemical Society, **2011**, 133, 10784-10786.

102. Townsend, S. D., Tan, Z., Dong, S., Shang, S., Brailsford, J. A. and Danishefsky, S. J., *Advances in proline ligation.* Journal of the American Chemical Society, **2012**, 134, 3912-3916.

103. Carter, P. J., *Introduction to current and future protein therapeutics: A protein engineering perspective.* Experimental Cell Research, **2011**, 317, 1261-1269.

104. Leader, B., Baca, Q. J., Golan, D. E., *Protein therapeutics: a summary and pharmacological classification.* Nature Reviews Drug Discovery, **2008**, 7, 21-39.

105. Burley, S. K., Petsko, G. A., *Aromatic-aromatic interaction: a mechanism of protein structure stabilization.* Science, **1985**, 229, 23-28.

106. Jackel, C., Koksch, B., *Fluorine in peptide design and protein engineering.* Journal of Organic Chemistry, **2005**, 4483-4503.

107. Buer, B. C., Marsh, E. N. G., *Fluorine: A new element in protein design.* Protein Science, **2012**, 21, 453-462.

108. Bilgicer, B., Kumar, K., *De novo design of defined helical bundles in membrane environments.* Procedings of the National Academy of Sciences U.S.A, **2004**, 43, 15324-15329.

109. Li, C. G., Wang, G. F., Wang, Y. Q., Creager-Allen, R., Lutz, E. A., Scronce, H., Slade, K. M., Ruf, R. A. S., Mehl, R A., Pielak, G. J., *Protein F-19 NMR in Escheria coli.* Journal of the American Chemical Society, **2010**, 132, 321-327.

110. Afonin, S., Dur, U. H. N., Glaser, R. W., Ulrich, A. S., *'Boomerand'-like insetion of a fusogenic peptide in a lipid membrane revealed by solid-state F-19 NMR.* Magnetic Resonance in Chemistry, **2004**, 42, 195-203.

111. Gaye, B., Adejare, A., *Fluorinated molecules in the diagnosis and treatment of neurodegenrative diseases.* Future Medicinal Chemistry, **2009**, 1, 821-833.

112. Salonen, L. M., Ellermann, M., Diederich, F., *Aromatic Rings in Chemical and Biological Recognition: Energetics and Structures.* Angewandte Chemie International Edition, **2011**, 50, 4808-4842.

113. Tatko, C. D., Waters, M. L., *Selective aromatic interactions in beta-hairpin peptides.* Journal of the American Chemical Society, **2002**, 124, 9372-9373.

114. Chung, D. M., Dou, Y., Baldi, P., Nowick, J. S., *The absence of favorable aromatic interactions between beta-sheet peptides.* Journal of the American Chemical Society, **2005**, 127, 9998-9999.

115. Wouters, M. A., Curmi., P. M. G, *An analysis of side chain interactions and pair correlations within antiparallel β-sheets: The differences between backbone hydrogen-bonded and non-hydrogen-bonded residue pairs.* Proteins: Structure, Function, and Bioinformatics, **1995**, 22, 119-131.

116. Hutchinson, E. G., Sessions, R. B., Thornton, J. M., Woolsfson, D. N., *Determinants of strand register in antiparallel beta-sheets of proteins.* Protein Science, **1998**, 7, 2287-2300.

117. Zheng, H., Comeforo, K., Gao, J., *Expanding the fluorous arsenal: tetrafluorinated phenylalanines for protein design.* Journal of the American Chemical Society, **2009**, 131, 18-19.

118. Woll, M. G., Hadley, E. B., Mecozzi, S., Gellman, S. H., *Stabilizing and destabilziign effects of phenylalanine--> F5-phenylalanine mutations on the folding of a small proteins.* Journal of the American Chemical Society, **2006**, 128, 15932-15933.

119. Pace, C. J., Zheng, H., Mylvaganam, R., Kim, D. and Gao, J., *Stacked fluoroaromatics as supramolecular synthons for programming protein dimerization specificity.* Angewandte Chemie International Edition, **2012**, 51, 103-107.